

KATHOLIEKE UNIVERSITEIT LEUVEN
INGENIEURSWETENSCHAPPEN
DEPARTEMENT ELEKTROTECHNIEK
Kasteelpark Arenberg 10, 3001 Leuven (Heverlee)

ADVANCED PREPROCESSING TECHNIQUES AND NONLINEAR SIGNAL ANALYSIS APPLIED TO SCALP ELECTROENCEPHALOGRAMS FOR THE PREDICTION OF EPILEPTIC SEIZURES

Promotoren:
Prof. dr. ir. S. Van Huffel
Prof. dr. W. Van Paesschen

Proefschrift voorgedragen tot
het behalen van het doctoraat
in de ingenieurswetenschappen

door

Wim DE CLERCQ

Mei 2005



KATHOLIEKE UNIVERSITEIT LEUVEN
INGENIEURSWETENSCHAPPEN
DEPARTEMENT ELEKTROTECHNIEK
Kasteelpark Arenberg 10, 3001 Leuven (Heverlee)

ADVANCED PREPROCESSING TECHNIQUES AND NONLINEAR SIGNAL ANALYSIS APPLIED TO SCALP ELECTROENCEPHALOGRAMS FOR THE PREDICTION OF EPILEPTIC SEIZURES

Jury:
Prof. dr. ir. P. Van Houtte, voorzitter
Prof. dr. ir. S. Van Huffel, promotor
Prof. dr. W. Van Paesschen, co-promotor
Prof. dr. ir. A. Barbé
Prof. dr. P. Dupont
Prof. dr. ir. I. Lemahieu (Universiteit Gent)
Prof. dr. ir. D. Lowe (Aston University)
Prof. dr. ir. R. Sepulchre (Université de Liège)
Prof. dr. ir. D. Vandermeulen

Proefschrift voorgedragen tot
het behalen van het doctoraat
in de ingenieurswetenschappen

door

Wim DE CLERCQ

U.D.C. 616.831.2:616.853 Mei 2005

©Katholieke Universiteit Leuven – Faculteit Ingenieurswetenschappen
Arenbergkasteel, B-3001 Heverlee (Belgium)

Alle rechten voorbehouden. Niets uit deze uitgave mag vermenigvuldigd en/of openbaar gemaakt worden door middel van druk, fotocopie, microfilm, elektronisch of op welke andere wijze ook zonder voorafgaande schriftelijke toestemming van de uitgever.

All rights reserved. No part of the publication may be reproduced in any form by print, photoprint, microfilm or any other means without written permission from the publisher.

D/2005/7515/36

ISBN 90-5682-601-8

Voorwoord

Dit proefschrift zou niet tot stand zijn gekomen zonder de steun, medewerking en hulp van een aantal personen. Bij het begin van dit proefschrift zou ik dan ook graag deze personen willen bedanken.

Op de eerste plaats gaat mijn oprechte dank uit naar mijn promotoren Prof. Sabine Van Huffel en Prof. Wim Van Paesschen. Graag zou ik jullie willen bedanken voor de kansen die jullie me geboden hebben en het vertrouwen dat jullie in me stelden, ook al kwam ik uit een ander nest en had ik geen ervaring met typische ingenieurszaken. Ik wil hen in het bijzonder bedanken voor de vrijheid die ze me gegeven hebben om het onderzoek naar eigen goeddunken in te richten.

Verder wil ik ook de leden van de begeleidingscommissie, Prof. André Barbé, Prof. Patrick Dupont, Prof. Rodolphe Sepulchre en Prof. Dirk Vandermeulen bedanken voor het nalezen van het proefschrift en de waardevolle suggesties en aanvullingen. Ik bedank ook Prof. Ignace Lemahieu en Prof. David Lowe voor hun onmiddellijke bereidheid om deel uit te maken van de jury. Tenslotte wil ik Prof. Paul Van Houtte bedanken voor het waarnemen van het voorzitterschap van de examencommissie.

Guido Van Driel wil ik bedanken voor de goede samenwerking met de epilepsiemonitoringeenheid van het UZ Gasthuisberg. Zonder de metingen die je me bezorgde was dit werk niet mogelijk geweest. Ook de verhelderende uitleg die je gaf bij het lezen van de EEG's heb ik steeds gewaardeerd. Tevens bedank ik Prof. Johan Van Hees en Prof. André Palmini voor hun medewerking.

Natuurlijk zou de voorliggende tekst niet tot stand zijn gekomen zonder de interactie en hulp van de andere medewerkers van de BIOMED groep en SCD. Vooreerst wil ik de post-docs bedanken: Dr. Philippe Lemmerling om me in te leiden in de wereld van biomedische signaalverwerking en Dr. Bart Vanrumste voor de vele suggesties die mijn onderzoek op een hoger niveau gebracht hebben. Verder dank ik ook collega Anneleen Vergult voor de productieve samenwerking gedurende het laatste jaar van mijn doctoraat. Mijn verschillende bureaugenoten Pieter, Geert, Jean-Michel, Jean-Baptiste, Anneleen, Magnolis en Bart worden

bedankt voor de aangename werksfeer. Daarnaast bedank ik Ida, Bart, Lut en Ilse voor de vlotte afhandeling van alle administratieve en financiële zaken.

Ik ben het F.W.O.-Vlaanderen en de K.U.Leuven erkentelijk voor de financiering van dit onderzoek.

Ook buiten het werk hebben familie en vrienden op een iets minder directe, maar daarom niet minder belangrijke manier, bijgedragen aan het totstandkomen van dit proefschrift. De leden van KMNS Footbalos, de vroegere fysica-studiegenoten en alle andere vrienden worden bedankt voor het leveren van de nodige ontspanning op tijd en stond.

Tot slot wil ik nog een speciaal woordje van dank richten aan de mensen die me het nauwst aan het hart liggen. Mijn ouders en broer bedank ik voor de goede zorgen, warmte en de onvoorwaardelijke steun waarop ik iedere dag kan rekenen. En als laatste, maar niet in het minst: dank je, Liesbet, om het zonnetje in mijn leven te willen zijn!

Wim De Clercq
Mei 2005

Abstract

This thesis is focused on the signal processing of scalp electroencephalographic signals of patients with epilepsy. By measuring the potential differences between electrodes placed on the scalp, the ElectroEncephaloGram (EEG) represents the electrical activity of the brain. The EEG is a valuable tool for diagnosis of neurological disorders or diseases and to study human brain functioning. One of the many application areas is the diagnosis of epilepsy.

Epilepsy affects more than 50 million individuals worldwide -about 1% of the world's population. In about 25% of individuals with epilepsy, seizures cannot be controlled by any available therapy. One of the most devastating features of epilepsy is the apparent unpredictable nature of seizures. Every day activities are impaired and can become dangerous for patients.

The prediction of epileptic seizures by quantitative analysis methods applied to EEG has been a focus of much interest in recent years. This resurgence of interest has been motivated by several factors, including the proliferation of powerful new methods for analyzing nonlinear system dynamics, as well as the interest in developing epilepsy control devices. We reported on the low ability of one of the nonlinear measures used for seizure prediction to predict seizures on scalp EEG signals. We were the first research group reporting on negative findings in the research area of seizure prediction. Later on, many other studies confirmed our results, showing that nonlinear methods have a very low predictive ability not only on scalp EEG signals but also on intracranial EEGs. The obtained results are far from sufficient for clinical application.

Unfortunately, as scalp EEG measurements are noninvasive, potentials that are generated by (physiological or non-physiological) sources other than the brain are picked up by scalp electrodes and recorded together with the EEG. These potentials are referred to as artifacts and often obscure the epileptiform activity in the EEG recording. In this thesis we illustrate that if we want to have any success in predicting seizures from scalp EEG electrodes, we first need to remove the artifacts contaminating it. Two newly developed methods for artifact removal are presented.

A new subspace-based method for modelling the common dynamics is introduced in the biomedical signal processing world in general and EEG signal processing world in particular. The method can be applied for the removal of artifacts and background EEG from multichannel interictal and ictal EEG.

Also the problem of muscle artifact removal is concerned. The EEG is frequently contaminated by electrophysiological potentials associated with muscle contraction due to biting, chewing and frowning. We present a new method for muscle artifact removal. The method does not have the adverse effects of the existing filtering methods and removes the muscle artifact without altering the underlying brain activity (and thus without removing the interesting information). The first preliminary results of a clinical study of patients with refractory epilepsy show that the removal of muscle artifact results in a better interpretation of the ictal EEG, leading to an earlier detection of the seizure onset and a better localization of the seizures onset zone. These findings make the current method indispensable for every Epilepsy Monitoring Unit.

Korte Inhoud

Deze thesis is gericht op de signaalverwerking van scalp elektro-encefalogram (EEG) signalen van patiënten met epilepsie. Door het opmeten van potentiaalverschillen tussen elektrodes die geplaatst zijn op de hoofdhuid meet het elektro-encefalogram de elektrische activiteit van de hersenen. Het EEG is waardevol in de diagnose van talrijke neurologische afwijkingen en in het bestuderen van de werking van de hersenen. Eén van de vele toepassingen is de diagnose van epilepsie.

Epilepsie komt wereldwijd voor bij meer dan 50 miljoen mensen -ongeveer 1% van de wereldpopulatie. In ongeveer 25% van deze individuen kunnen de epileptische aanvallen niet gecontroleerd worden door beschikbare therapieën. Eén van de meest problematische eigenschappen van epilepsie is het onvoorspelbare karakter van de aanvallen. Dagdagelijkse activiteiten worden hierdoor beperkt en kunnen gevaarlijk worden voor de patiënt.

Een gebied dat veel interesse opwekt de laatste jaren is de voorspelling van epileptische aanvallen aan de hand van kwantitatieve analysemethodes toegepast op EEG signalen. Dit is te wijten aan verschillende factoren waaronder de ontwikkeling van krachtige nieuwe methodes om niet-lineaire systemen te bestuderen, en de interesse om een epilepsie-monitoringtoestel te ontwikkelen. In dit doctoraatswerk rapporteren we over de lage performantie van één van de niet-lineaire methodes om epileptische aanvallen te voorspellen. We waren de eerste onderzoeksgroep die rapporteerde over negatieve bevindingen in het onderzoeksdomein van aanvalsvoorspelling. Later bevestigden vele andere onderzoeksgroepen onze resultaten. De resultaten zijn onvoldoende voor de klinische praktijk.

Daar scalp EEG opnames niet-invasief zijn, worden potentialen gegenereerd door andere bronnen (fysiologisch en niet-fysiologisch) ook opgenomen door de scalp elektrodes. Deze potentialen noemt men artefactsignalen en deze signalen verduisteren dikwijls de epileptische activiteit in het EEG. In deze thesis tonen we aan dat we eerst de artefacten moeten verwijderen indien we ooit enig succes willen hebben in het voorspellen van epileptische aanvallen. Er werden twee nieuwe methodes ontwikkeld voor het verwijderen van artefacten in scalp EEG signalen.

Een nieuwe deelruimte gebaseerde methode werd ontwikkeld voor de modellering van de gemeenschappelijke dynamica in de verschillende EEG kanalen. Deze methode verwijdert succesvol artefacten en achtergrond EEG van epileptiforme EEG en doet dit beter dan principale componenten analyse (PCA). Met deze bevindingen illustreren we dat het modelleren van de gemeenschappelijke dynamica in meerkanaals-EEG opnames nieuwe perspectieven opent voor het verwijderen van artefacten en achtergrond EEG.

Daarnaast wordt ook het probleem van spierartefactverwijdering behandeld. Het EEG is vaak bevuild met elektrofysiologische potentialen geassocieerd met spiersamentrekkingen ten gevolge van bijten, kauwen en fronsen. We stellen een nieuwe methode voor om deze spierartefacten te verwijderen. De voorgestelde methode heeft niet het nadelige effect van de huidige filtertechnieken en verwijdert de spierartefacten zonder de onderliggende opgenomen hersenactiviteit aan te tasten (en dus zonder klinisch relevante informatie te verwijderen). De eerste voorlopige resultaten van een klinische studie van patiënten met refractaire epilepsie tonen aan dat de verwijdering van spierartefact resulteert in een betere interpretatie van het aanvals-EEG. Dit leidt tot een vroegere detectie van de start van de epileptische aanval en een betere lokalisatie van de epileptische focus. Deze bevindingen maken de huidige methode onmisbaar voor elke epilepsie-monitoringeenheid.

Glossary

Used Symbols and Notation

$C(x, y)$	cross-correlation sum of x and y
I_n	length of n-th time interval between two successive positive going zero crossings
K	model order
N	number of data points
a_k	amplitude of signal pole k
c_k	complex amplitude of signal pole k
d_k	damping of signal pole k
$e(n)$	error of signal at time n
f	frequency
f_k	frequency of signal pole k
m	embedding dimension
$x(k)$	observed signal at time k
$\bar{x}(k)$	modelled signal at time k
$\hat{x}$	estimate of x
z_k	signal pole k
$\mathbf{x}$	vector
$\mathbf{x}(n)$	n-th element of vector $\mathbf{x}$
$\mathbf{C_{xx}}$	within-sets covariance matrix of x
$\mathbf{C_{xy}}$	between-sets covariance matrix of x and y
$\mathbf{X}$	data matrix
$\mathbf{X}^T$	transpose of matrix $\mathbf{X}$
$\mathbf{X}^H$	Hermitian transpose of matrix $\mathbf{X}$
$\mathbf{X}^{-1}$	inverse of matrix $\mathbf{X}$
$\mathbf{X}(m, n)$	element on the m-th row and n-th column of matrix $\mathbf{X}$
Δt	sampling interval
Θ	Heaviside step function
ϕ_k	phase of signal pole k
$\rho(x, y)$	correlation between x and y
σ	singular value

τ	time delay
$max_k(\mathbf{x}(\mathbf{k}))$	maximum element of vector $\mathbf{x}$
$\|\| \cdot \|\|$	Euclidian norm

Acronyms and Abbreviations

BSS	Blind Source Separation
CCA	Canonical Correlation Analysis
cf.	confer : compare with
cICA	constrained Independent Component Analysis
Cl^-	Chloride
CPS	Complex Partial Seizure
CT	Computed Tomography
ECoG	ElectroCorticoGram
ECD	Ethyl Cysteinate Dimer
EDS	Exponentially Damped Sinusoidal
EEG	ElectroEncephaloGram
e.g.	exempli gratia : for example
EMG	ElectroMyoGram
ERP	Event Related Potential
EOG	ElectroOculoGram
EP	Evoked Potential
EPSP	Excitatory PostSynaptic Potential
FFT	Fast Fourier Transform
FIR	Finite Impulse Respons
fMRI	functional Magnetic Resonance Imaging
GS	Generalized Seizure
GUI	Graphical User Interface
HTLS	Hankel Total Least Squares
ICA	Independent Component Analysis
ICEEG	IntraCranial ElectroEncephaloGraphy
i.e.	id est : that is
ILAE	International League Against Epilepsy
IPSP	Inhibitory PostSynaptic Potential
JADE	Joint Approximate Diagonalization of Eigen-matrices
K^+	Potassium
MASP	Most Active Signal Pole
MEG	MagnetoEncephaloGram
MRI	Magnetic Resonance Imaging
mTLCPS	mesial Temporal Lobe Complex Partial Seizure
MTLE	Mesial Temporal Lobe Epilepsy

Na^+	Sodium
nl	noise level
NPS	Neocortical Partial Seizure
NSP	Number of Signal Poles
PCA	Principal Component Analysis
PET	Positron Emission Tomography
PSP	PostSynaptic Potential
RMS	Root Mean Square
RMSE	Root Mean Square Error
RRMSE	Relative Root Mean Square Error
SGS	Secondarily Generalized Seizures
SNR	Signal-to-Noise Ratio
SOBI	Second-Order Blind Identification
SPECT	Single Photon Emission Computed Tomography
SVD	Singular Value Decomposition
TLE	Temporal Lobe Epilepsy
TLS	Total Least Squares
vs.	versus

Contents

Voorwoord **i**

Abstract **iii**

Korte Inhoud **v**

Glossary **vii**

Contents **x**

Samenvatting **1**

1 Introduction **25**
1.1 Biomedical signal processing 25
1.2 Topic of thesis 26
1.3 Chapter by chapter overview 27

2 Electrical brain activity and epilepsy **31**
2.1 Introduction 31
2.2 The brain 31
2.2.1 Anatomy 31
2.2.2 Electrical brain activity 32
2.3 Electroencephalography 35
2.3.1 Scalp EEG 37
2.3.2 Intracranial electrodes 39
2.3.3 The limitations of scalp/intracranial EEG recordings 40
2.3.4 Artifacts 41
2.3.5 Application areas of EEG 44
2.4 Epilepsy 44
2.4.1 Epileptic seizures 45
2.4.2 Epileptiform activity in the EEG 47
2.4.3 Presurgical evaluation 47
2.4.4 Contribution of presented work to the presurgical evaluation 51
2.5 Conclusion 52

3 Epileptic seizure prediction **55**
3.1 Introduction . . . 55
3.2 Detecting pre-ictal states by nonlinear EEG analysis . . . 56
3.2.1 State space reconstruction of the observed dynamical system by the method of delays . . . 56
3.2.2 Nonlinear measures for the characterization of the dynamical behavior of a system . . . 57
3.2.3 Nonlinear measures and the detection of a pre-ictal state . 59
3.2.4 Prediction of epileptic seizures from scalp EEG recordings . 60
3.3 Prediction of epileptic seizures from scalp EEG recordings: a study on the similarity index . . . 61
3.3.1 Method: similarity index . . . 61
3.3.2 Materials . . . 64
3.3.3 Results of study . . . 65
3.3.4 Robustness to artifacts . . . 67
3.3.5 Conclusion . . . 71
3.4 Critical comments on nonlinear measures and seizure prediction . . 73
3.5 Conclusion . . . 74

4 Modelling common dynamics in multichannel signals with applications to artifact and background removal in EEG recordings **77**
4.1 Introduction . . . 77
4.2 Methods . . . 79
4.2.1 EDS model . . . 79
4.2.2 Common dynamics . . . 79
4.3 Simulation study . . . 83
4.3.1 Simulation . . . 83
4.3.2 Results of simulation study . . . 86
4.4 Method applied to real life data . . . 89
4.4.1 Method applied to interictal activity . . . 89
4.4.2 Method applied to ictal activity . . . 89
4.5 Discussion . . . 92
4.6 Conclusion . . . 95

5 Canonical Correlation Analysis applied to remove muscle artifacts from the scalp EEG **97**
5.1 Introduction . . . 97
5.2 Blind source separation by CCA for artifact removal . . . 99
5.2.1 Blind source separation by canonical correlation analysis . . 99
5.2.2 Applying BSS-CCA to EEG for artifact correction . . . 101
5.3 Materials and Methods . . . 102
5.3.1 Construction of the synthetic data . . . 102
5.3.2 Methods for comparison . . . 104
5.3.3 Ictal EEG recording . . . 105
5.4 Results . . . 105

5.4.1 Results on the synthetic data . . . 105
5.4.2 Results on the ictal EEG recording . . . 106
5.5 Discussion . . . 112
5.6 Semi-automatic removal of muscle artifacts . . . 119
5.7 Clinical validation: improving the interpretation of the ictal scalp EEG . . . 120
5.7.1 Methods . . . 120
5.7.2 Results . . . 120
5.7.3 Conclusion . . . 124
5.8 Conclusion . . . 124

6 Conclusions and further research 127

Appendices 131

A Parameter settings of the similarity index 131
A.1 Standard parameter settings . . . 131
A.2 Distance . . . 131
A.3 Dimension reduction by SVD truncation . . . 133
A.4 Embedding dimension . . . 134
A.5 Delay time . . . 135

B Mean phase coherence as a measure for phase synchronization and its application to the scalp EEG of patients with MTLE 139
B.1 Hilbert transform . . . 139
B.2 Mean phase coherence . . . 140
B.3 Synchronization analysis of the scalp EEG of patients with MTLE 141

C Analyzing multichannel scalp EEG signals of patients with epilepsy using exponential data modelling 145
C.1 Materials . . . 146
C.2 Methods . . . 146
C.2.1 Subspace based pole estimation methods . . . 146
C.2.2 Measures based on the energy distribution of the common signal poles . . . 149
C.3 Results . . . 151
C.3.1 Case studies . . . 152
C.3.2 Long term EEG recordings . . . 154
C.4 Discussion and Conclusion . . . 154

Bibliography 157

List of publications 169

Curriculum Vitae 173

Samenvatting

Gevorderde voorbewerkingstechnieken en niet-lineaire signaalanalyse toegepast op scalp EEG signalen voor de voorspelling van epileptische aanvallen

Hoofdstuk 1: Inleiding

Het menselijk lichaam is opgebouwd uit verschillende systemen. Elk systeem is onderverdeeld in verschillende deelsystemen die elk hun eigen fysiologische processen hebben. De meeste fysiologische processen zijn vergezeld van signalen die de activiteit van het systeem weergeven. Ziektes of storingen in een biologisch systeem veroorzaken veranderingen in de normale fysiologische processen en zijn typisch geassocieerd met signalen afwijkend van de normale signalen. In vele gevallen is het mogelijk om de signalen verbonden met een biologisch systeem op te meten en de toestand van het systeem te karakteriseren aan de hand van de opgemeten signalen.

Het doel van de biomedische signaalverwerking kan algemeen omschreven wor-

den als het duidelijker maken van de informatie die bevat is in de biomedische signalen voor een waarnemer. Concreet kan dit gaan om:

- het filteren van de signalen om ruis of artefacten te verwijderen;
- het nauwkeurig bepalen van klinisch relevante parameters;
- classificatie voor diagnostische doeleinden;
- ...

Deze thesis is gericht op de signaalverwerking van scalp elektro-encefalogram (EEG) signalen van patiënten met epilepsie. Door het opmeten van potentiaalverschillen tussen elektrodes die geplaatst zijn op de hoofdhuid meet het elektro-encefalogram de elektrische activiteit van de hersenen. Het EEG is waardevol in de diagnose van talrijke neurologische afwijkingen en in het bestuderen van de werking van de hersenen. Eén van de vele toepassingen is de diagnose van epilepsie.

Hoofdstuk 2: Elektrische activiteit van de hersenen en epilepsie

De werking van de hersenen gaat gepaard met zwakke elektrische activiteit van de hersencellen. Ten gevolge hiervan kunnen op het hoofdoppervlak in de tijd variërende potentiaalverschillen gemeten worden. Elektro-encefalografie, d.i. de registratie van deze potentiaalverschillen m.b.v. elektroden op de hoofdhuid, is bij uitstek geschikt als onderzoek bij patiënten die lijden aan epilepsie. Bij deze patiënten veroorzaakt abnormaal sterke elektrische activiteit in bepaalde hersenzones immers epileptische aanvallen, die het normaal functioneren van een persoon in het dagelijkse leven sterk kan hinderen. Elektro-encefalografie kan aangewend worden om de verschillende types epilepsie van elkaar te onderscheiden en om de hersenzones te identificeren die een rol spelen bij het ontstaan van de aanvallen. Met dit doel kunnen epilepsiepatiënten opgenomen worden in een epilepsie-monitoringeenheid waar een elektro-encefalogram gedurende enkele dagen continu wordt geregistreerd.

Tijdens de preheelkundige evaluatie van epilepsiepatiënten wordt onderzocht of de mogelijkheid bestaat de patiënt aanvalsvrij te laten worden door het uitvoeren van een heelkundige ingreep aan de hersenen. Deze preheelkundige evaluatie omvat naast medische beeldvorming van de hersenen o.m. ook een video-EEG registratie in een epilepsie-monitoringeenheid.

Deze thesis is van belang voor twee modaliteiten van de preheelkundige evaluatie. De voorspelling van een epileptische aanval kan leiden tot een betere ictale-SPECT beeldvorming. Daarnaast leidt de verwijdering van artefacten tot een betere interpretatie van het ictale EEG.

Hoofdstuk 3: Voorspelling van epileptische aanvallen

De detectie van een pre-ictale toestand met behulp van niet-linaire analysetechnieken

Epilepsie komt wereldwijd voor bij meer dan 50 miljoen mensen -ongeveer 1% van de wereldpopulatie. In ongeveer 25% van deze individuen kunnen de epileptische aanvallen niet gecontroleerd worden door beschikbare therapieën. Eén van de meest problematische eigenschappen van epilepsie is het onvoorspelbare karakter van de aanvallen. Dagdagelijkse activiteiten worden hierdoor beperkt en kunnen gevaarlijk worden voor de patiënt.

Een pre-ictale toestand wordt gedefinieerd als de toestand van de epileptische hersenen die onvermijdelijk leidt tot een epileptische aanval. De detectie van deze toestand, en de bijhorende voorspelling van de epileptische aanval, m.b.v. niet-lineaire methodes toegepast op EEG signalen is een onderzoeksdomein dat heden ten dage veel interesse opwekt. Dit is te wijten aan verschillende factoren waaronder de ontwikkeling van krachtige nieuwe methodes om niet-lineaire systemen te bestuderen, en de interesse om een epilepsie-monitoringsysteem te ontwikkelen.

Diverse studies tonen aan dat niet-lineaire analysetechnieken het potentieel hebben om eigenschappen aan het EEG signaal te onttrekken die kunnen aanzien worden als voortekenen van een aankomende epileptische aanval ([79, 80, 57, 58, 59, 89, 100, 62, 109, 122]; voor recente overzichten zie [78, 84, 83, 75]). De meeste studies in dit onderzoeksdomein concentreren zich op de analyse van intracraniële EEG signalen. Op lange termijn echter, is de toepassing op scalp EEG opnames essentieel voor de bruikbaarheid van methodes in 'real-life' omstandigheden. Een monitoringsysteem gebaseerd op niet-invasieve elektrodes zal veel gemakkelijker aanvaard en onderhouden worden dan een systeem dat gebaseerd is op operatief ingebrachte elektrodes.

De voorspelling van een epileptische aanval met behulp van scalp EEG opnames: de similariteitsindex

Le Van Quyen rapporteerde de voorspelling van epileptische aanvallen door de similariteitsindex (*Similarity index*) methode toe te passen op scalp EEG signalen. Een pre-ictale toestand werd gedetecteerd in 25 van de 26 onderzochte scalp EEG opnames van patiënten met mesiale temporale kwab epilepsie (MTLE).

Omdat scalp EEG opnames niet-invasief zijn, worden potentialen gegenereerd door andere bronnen (fysiologisch en niet-fysiologisch) ook opgenomen door de scalp elektrodes. Deze potentialen noemt men artefactsignalen en deze signalen verduisteren dikwijls de hersenactiviteit in het EEG. Daarenboven zijn scalp EEG

signalen onderhevig aan signaalverzwakking en hebben ze een slechte spatiale resolutie vergeleken met invasief ingebrachte elektrodes. Als we deze factoren in rekening brengen lijkt het resultaat van Le van Quyen verrassend. Onze groep probeerde deze resultaten te reproduceren en een pre-ictale toestand te detecteren door de similariteitsindex toe te passen op de scalp EEG opnames van 12 patiënten met MTLE.

Methode: de similariteitsindex

De similariteitsindex methode wordt volledig beschreven in [73] en kan kort samengevat worden als volgt:

- een referentie EEG signaal van 5 min wordt geselecteerd; dit referentiesignaal bevat normale interictale hersenactiviteit en bevindt zich minstens één uur voor de aanval;
- de dynamica van het referentiesignaal wordt opgebouwd;
- deze referentiedynamica wordt vergeleken met de dynamica van opeenvolgende EEG vensters van 30 s.

Een pre-ictale toestand wordt gedefinieerd wanneer de similariteitsindex onder de drempelwaarde van 5 standaardafwijkingen blijft tot aan de start van de aanval.

Metingen

De scalp EEG opnames van 13 patiënten die opgenomen werden in de epilepsiemonitoringeenheid werden gebruikt in deze studie. Twaalf patiënten hadden complex partiële aanvallen van mesiale temporale kwab oorsprong en één patiënt had neocorticale aanvallen. De data van deze patiënt was afkomstig van de onderzoeksgroep van Le Van Quyen.

Resultaten

Fig. 1 toont de analyse van de $O1$ scalp elektrode voor de neocorticale aanval. Tussen vensternummer 186-211 gebeurden verschillende aanvallen. De referentietoestand werd gekozen van vensternummer 1 tot 10. Een aanhoudende zakking van de similariteitsindex onder de statistische drempel (horizontale lijn) tot aan de start van de aanval werd waargenomen. Een pre-ictale toestand werd gedefinieerd en deze toestand begon 21 minuten vóór de aanval. De grote afwijking van de similariteitsindex tussen vensternummer 60 en 70 werd veroorzaakt door artefacten.

De similariteitsindex was niet in staat om een pre-ictale toestand te detecteren in de scalp EEG opnames van de 12 patiënten met MTLE. Fig. 2 toont het resultaat van de analyse van de $F4$ elektrode voor de aanval van patiënt 2. De aanval duurde van venster 146 tot venster 153. De referentietoestand werd gekozen van vensternummer 1 tot 10. De similariteitsindex blijft hoog tot aan de start

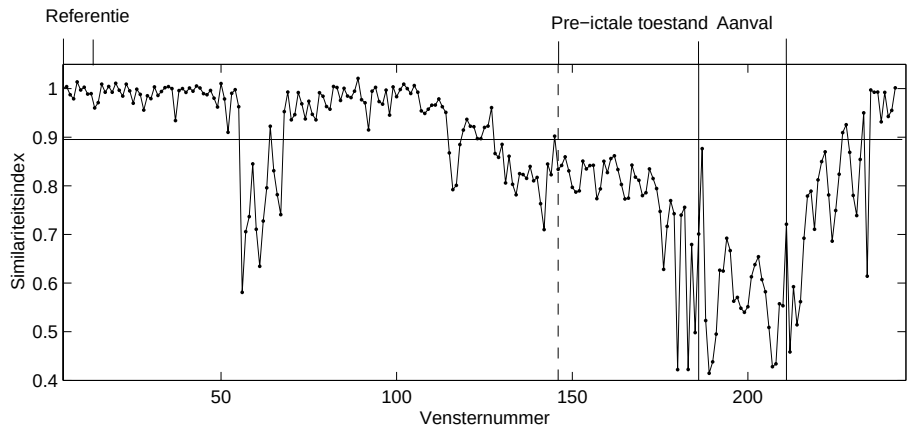

Figuur 1: *Het tijdsverloop van de similariteitsindex van de O2 scalp elektrode van de patiënt met neocorticale aanvallen (patiënt 13). De referentietoestand werd gekozen van venster 1 tot 10. Verschillende aanvallen gebeurden tussen vensternummer 186 en 211. Een pre-ictale toestand kon gedefinieerd worden. Deze toestand begon 21 minuten voor de start van de aanval. De grote afwijking van de similariteitsindex tussen vensternummer 60 en 70 werd veroorzaakt door artefacten.*

van de aanval. De zakkingen van de similariteitsindex onder de drempelwaarde worden veroorzaakt door artefacten in het geanalyseerde venster. Bij de start van de epileptische aanval treed er een sterke zakking van de similariteitsindex op. Er werd echter geen aanhoudende zakking van de similariteitsindex onder de drempelwaarde (horizontale lijn) tot aan de start van de aanval waargenomen. Bijgevolg kon er geen pre-ictale toestand gedefinieerd worden. Vergelijkbare resultaten werden bekomen voor alle andere elektrodes en alle andere scalp EEG signalen opgenomen in de studie.

Aangezien artefacten aanleiding geven tot zakkingen van de similariteitsindex tot onder de statistische drempelwaarde, bestuderen we de robuustheid van de similariteitsindex voor artefacten in de volgende paragraaf.

Robuustheid voor artefacten

In een simulatiestudie wordt de sensitiviteit van de similariteitsindex aangetoond t.o.v. spier- en oogartefacten. In deze studie wordt het artefactsignaal bij het referentiesignaal opgeteld en wordt de similarteitsindex berekend tussen het gesommeerde signaal en het referentiesignaal. Indien de similariteitsindex robuust is voor artefacten dan zou de similariteitsindex gelijk moeten zijn aan 1. Fig. 3 toont de similariteitsindex als functie van het ruisniveau. Hoe hoger het ruisniveau hoe groter de bijdrage van het artefactsignaal in het gesommeerde signaal.

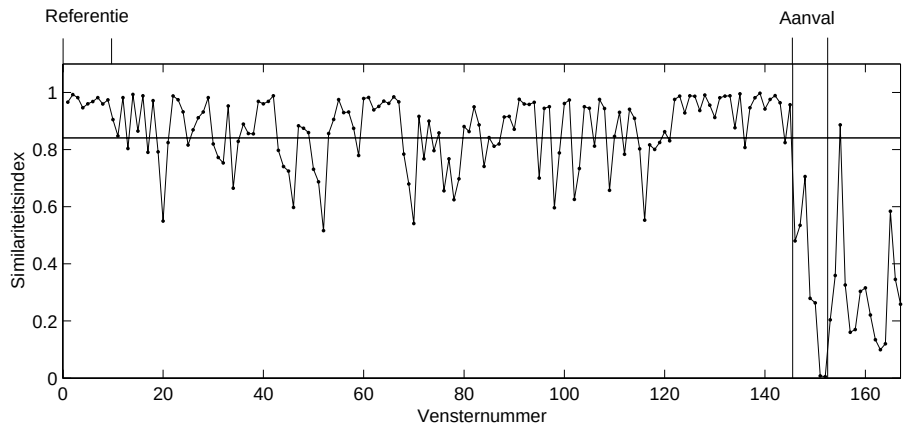

Figuur 2: *Het tijdsverloop van de similariteitsindex van de F4 scalp elektrode van patiënt 2. De referentietoestand werd gekozen van venster 1 tot 10. De epileptische aanval duurde van venster 146 tot 153. Er werd geen pre-ictale toestand waargenomen.*

Deze figuur toont aan dat de similariteitsindex gevoelig is voor spierartefact, zelfs wanneer het spierartefact een lage amplitude heeft in vergelijking met het EEG signaal. Daarenboven toonden we ook aan dat de similariteitsindex gevoelig is voor oogartefacten.

Besluit

In deze studie probeerden we de bevindingen van Le Van Quyen te reproduceren en een pre-ictale toestand te detecteren met behulp van de similariteitsindex toegepast op scalp EEG signalen van 12 patiënten met MTLE. We waren niet in staat de bevindingen te reproduceren. De similariteitsindex was niet in staat pre-ictale veranderingen waar te nemen in de scalp EEG opnames. Een pre-ictale toestand kon gedefinieerd worden in de scalp EEG opname van een patiënt met neocorticale aanvallen. Dit resultaat verzekert ons er van dat de similariteitsindex correct geïmplementeerd is en dat de methode het potentieel heeft om aanvallen te voorspellen.
Daarenboven toonden we aan dat de similariteitsindex gevoelig is voor spier- en oogartefacten. Bijgevolg kan de analyse van de scalp EEG signalen verbeterd worden door een extra voorbewerking van de signalen, waarin de artefacten verwijderd worden; en dit om twee redenen. Ten eerste zal de similariteitsindex minder zakkingen hebben ten gevolge van artefacten, hetgeen de interpretatie van de similariteitsindex analyse eenvoudiger maakt. Op deze manier worden valse voorspellingen vermeden. Ten tweede kunnen artefacten de hersenactiviteit, die gerelateerd is aan de pre-ictale toestand, verduisteren. Indien we ooit enig succes willen hebben met het voorspellen van epileptische aanvallen aan de hand

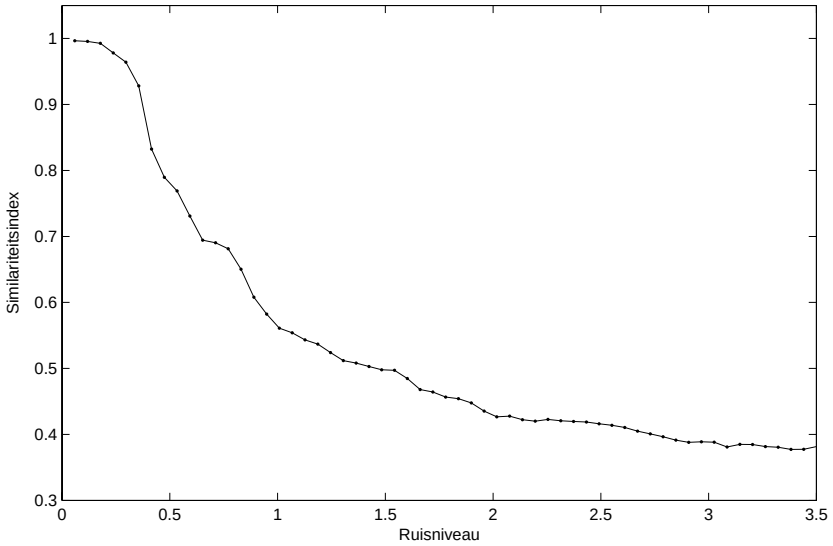

Figuur 3: *De similariteitsindex als functie van het ruisniveau. De bijdrage van het spierartefact wordt groter bij hogere ruisniveaus.*

van scalp EEG signalen zullen we eerst de artefacten moeten verwijderen. Deze bevindingen werden gepubliceerd in o.a. The Lancet [21, 19]. Met deze publicaties was onze onderzoeksgroep de eerste groep die rapporteerde over negatieve bevindingen in dit onderzoeksdomein. Na het verschijnen van deze publicaties bevestigden vele andere groepen onze bevindingen. Verschillende studies trekken het nut van de niet-lineaire methodes in vraag [90, 91, 62]. Andere studies waren niet in staat om de bevindingen van eerdere studies te reproduceren en trekken het voorspellend karakter van de niet-lineaire methodes in vraag [2, 87, 72, 71, 111].

Hoofdstuk 4: Het modelleren van de gemeenschappelijke dynamica in meerkanaalssignalen met toepassing in het verwijderen van artefacten en achtergrond EEG in scalp EEG signalen

Het verwijderen van artefacten en achtergrond EEG van interictale en ictale EEG opnames is een belangrijk onderzoeksdomein geworden in de EEG signaalverwerking. In dit hoofdstuk wordt een nieuwe deelruimte gebaseerde methode ontwikkeld voor de modellering van de gemeenschappelijke dynamica in de verschillende EEG kanalen. De methode kan gebruikt worden om artefacten te verwijderen wanneer de epileptische activiteit gemeenschappelijk is in de meeste kanalen en

de artefacten aanwezig zijn in enkele kanalen. De performantie van de methode werd getest op gesimuleerde data voor verschillende ruisniveaus. Daarnaast werd de methode uitgetest op 'real life' interictale en ictale EEG opnames die bevuild waren met spierartefact. De methode verwijderde succesvol artefacten en achtergrond EEG van de epileptiforme EEG en doet dit beter dan principale componenten analyse (PCA). Met deze bevindingen illustreren we dat het modelleren van de gemeenschappelijke dynamica in meerkanaals-EEG opnames nieuwe perspectieven opent voor het verwijderen van artefacten en achtergrond EEG.

Methode

Eerst introduceren we het EDS (exponentieel gedempte sinusoïden) model [114]. Dit model voorziet een geschikt kader om de gemeenschappelijke dynamica in een set signalen te definiëren. Vervolgens wordt de methode om de gemeenschappelijke dynamica te modelleren beschreven.

EDS model

We gebruikten het parametrische EDS model waarin het signaal gemodelleerd wordt als een eindige som van exponentieel gedempte sinusoïden:

$$\begin{aligned} x(n) &= \sum_{k=1}^{K} a_k \exp(j\phi_k) \exp\left((-d_k + j2\pi f_k) n\Delta t\right) + e(n), \qquad (1) \\ n &= 0, 1, \ldots, N-1; \end{aligned}$$

waarin $j = \sqrt{-1}$, $n\Delta t$ het tijdsverschil tussen de oorsprong en het punt $x(n)$ voorstelt, Δt het bemonsteringinterval, en $e(n)$ witte ruis. De parameters van het model zijn de amplitude a_k, de fase ϕ_k, de demping d_k en de frequentie f_k. De modelfunctie (1) kan herschreven worden als een som van complexe amplitudes $c_k = a_k \exp(j\phi_k)$ en signaalpolen $z_k = \exp\left((-d_k + j2\pi f_k)\Delta t\right)$:

$$\begin{aligned} x(n) &= \sum_{k=1}^{K} c_k z_k^n + e(n), \qquad (2) \\ n &= 0, 1, \ldots, N-1. \end{aligned}$$

Gemeenschappelijke dynamica

In verschillende toepassing is het van groot belang om de gemeenschappelijke dynamica uit een gegeven set signalen te extraheren. Dit wordt mogelijk door over te gaan naar een deelruimterepresentatie van de signalen en vervolgens de gemeenschappelijke deelruimte te bepalen. In wat volgt introduceren we een nieuwe methode die deze gemeenschappelijke deelruimte bepaalt [112]. De methode kan onderverdeeld worden in twee delen; in het eerste deel wordt voor elk kanaal afzonderlijk de relevante signaaldeelruimte bepaald. In het tweede deel wordt de

gemeenschappelijke deelruimte vastgelegd en worden vervolgens de parameters van de gemeenschappelijke signaalpolen bepaald. Allereerst wordt een beschrijving van het wiskundig probleem gegeven.

Beschrijving wiskundig probleem Gegeven S kanalen $x_s(n),\ s = 1, \ldots, S;\ n = 0, \ldots, N-1$ die gemodelleerd kunnen worden als een som van exponentieel gedempte sinusoïden. Veronderstel dat deze S kanalen K_c gemeenschappelijke polen $z_k,\ k = 1, \ldots, K_c$ hebben:

$$\begin{aligned} x_1(n) &= \sum_{k=1}^{K_1-K_c} c'_{1,k} z_{1,k}^n + \sum_{k=1}^{K_c} c_{1,k} z_k^n + e_1(n), \\ &\vdots \\ x_s(n) &= \sum_{k=1}^{K_s-K_c} c'_{s,k} z_{s,k}^n + \sum_{k=1}^{K_c} c_{s,k} z_k^n + e_s(n), \\ &\vdots \\ x_S(n) &= \sum_{k=1}^{K_S-K_c} c'_{S,k} z_{S,k}^n + \sum_{k=1}^{K_c} c_{S,k} z_k^n + e_S(n), \end{aligned} \tag{3}$$

met $z_{s,k},\ k = 1, \ldots, (K_s - K_c)$ de overblijvende signaalpolen in kanaal s. De gemeenschappelijke dynamica wordt dan beschreven door de gemeenschappelijke signaalpolen. De overeenkomstige amplitude en fase kan verschillen van kanaal tot kanaal.

Algoritme deel 1 (Eénkanaalsvoorbewerking) In dit deel wordt elk kanaal afzonderlijk voorbewerkt. Dit gebeurt door over te gaan naar een deelruimterepresentatie van het kanaal en vervolgens de relevante deelruimte te selecteren [112, 131]. De geselecteerde deelruimte dient dan als invoer voor het tweede deel van het algoritme . De voorbewerkingsstap wordt als volgt samengevat:

- **invoer:** S kanalen bestaande uit de datapunten $x_s(n),\ n = 0, \ldots, N-1;\ s = 1, \ldots, S.$; de individuele modelorde K_s voor elk kanaal s.
- **uitkomst:** een basis $\mathbf{U_{s_{K_s}}}$ van de signaaldeelruimte van elk kanaal $s = 1, \ldots, S$ en de voorbewerkte data $x'_s(n)$.
- ***Stap 1***. Schik voor elk kanaal $s, s = 1, \ldots, S$ de data $x_s(n), n = 0, \ldots, N-1$ in een Hankel matrix $\mathbf{H_s}$ met dimensie $L \times M$ als volgt:

$$\mathbf{H}(x_s) = \mathbf{H_s} = \begin{bmatrix} x_s(0) & x_s(1) & x_s(2) & \cdots & x_s(M-1) \\ x_s(1) & x_s(2) & \iddots & \cdots & \vdots \\ x_s(2) & \iddots & \iddots & \cdots & \vdots \\ \vdots & \vdots & \vdots & \vdots & x_s(N-2) \\ x_s(L-1) & \cdots & \cdots & x_s(N-2) & x_s(N-1) \end{bmatrix}, \tag{4}$$

waarin $N = L + M - 1$.

- ***Stap 2***. Berken de singuliere waarden ontbinding (SVD) [51, 52] van elke Hankel matrix $\mathbf{H_s}$:

$$\mathbf{H_s} = \mathbf{U_s}\mathbf{\Sigma_s}\mathbf{V_s^H}, \tag{5}$$

waarin het superscript H staat voor de hermitiaanse toegevoegde. Volgens [131] reduceert de SVD van $\mathbf{H_s}$ in afwezigheid van ruis tot het product:

$$\mathbf{H_{s_{K_s}}} = \mathbf{U_{s_{K_s}}}\mathbf{\Sigma_{s_{K_s}}}\mathbf{V^H_{s_{K_s}}}, \tag{6}$$

waarin $\mathbf{U_{s_{K_s}}}$, $\mathbf{V_{s_{K_s}}}$ respectievelijk de eerste K_s kolommen zijn van $\mathbf{U_s}$, $\mathbf{V_s}$ en $\mathbf{\Sigma_{s_{K_s}}}$ $(K_s \times K_s)$ deelmatrix is van $\mathbf{\Sigma_s}$. In de aanwezigheid van ruis is $\mathbf{H_s}$ een volle rang matrix. In dit geval is de afgesneden SVD, $\mathbf{H_{s_{K_s}}}$, van $\mathbf{H_s}$ de beste rang-K_s benadering van $\mathbf{H_s}$ en brengen de kolomvectoren van de afgesneden matrix $\mathbf{U_{s_{K_s}}}$ de signaalruimte voort [131]. Deze matrix zal dienen als invoer voor het tweede deel van het algoritme. Door uit te middelen over de antidiagonalen van de matrix $\mathbf{H_{s_{K_s}}}$ kunnen we de Hankel structuur herstellen en kunnen we de gefilterde tijdreeks $x'_s(n)$ extraheren [10, 31, 54]:

$$x'_s(n) \quad = \quad \frac{1}{a} \sum_{i+j=n+2} \mathbf{H_{s_{K_s}}}(i,j), \tag{7}$$

met $a = (n+1)$ voor $n = 0, \ldots, M-1$ en $a = (N-n)$ voor $n = M, \ldots, N-1$.

In de praktijk is de modelorde K_s niet op voorhand gekend. Daarom introduceren we de volgende regel om de $\mathbf{U_s}$ matrices af te snijden in stap 2. De $\mathbf{U_s}$ matrices worden afgesneden wanneer:

$$\sigma_s^2(K_s) \geq \; d \cdot \sigma_s^2(1) \sigma_s^2(K_s + 1) < \; d \cdot \sigma_s^2(1) \tag{8}$$

met $\sigma_s(k)$ de k^{de} grootste singuliere waarde die overeenstemt met de k^{de} linker singuliere vector in $\mathbf{U_s}$. De parameter d, die ingesteld wordt door de gebruiker, bepaalt welke linkersinguliere vectoren tot de signaaldeelruimte behoren. Op deze manier worden de individuele modelordes K_s vervangen door d in de invoer van het eerste deel van het algoritme.

Algoritme deel 2 (Extractie van de gemeenschappelijke dynamica) Eerst tonen we hoe we het aantal gemeenschappelijke signaalpolen bepalen van een gegeven set signalen. Eénmaal de gemeenschappelijke deelruimte vastgelegd is, worden de parameters van de gemeenschappelijke polen geschat in een tweede stap. Finaal worden de overeenkomstige schattingen van de amplitudes en fases van de gemeenschappelijke signaalpolen voor elk kanaal afzonderlijk bepaald. Het algoritme wordt als volgt samengevat:

- **invoer:** een basis $\mathbf{U_{s_{K_s}}}$ van de signaaldeelruimte voor elk kanaal $s = 1, \ldots, S$ en de voorbewerkte data $x'_s(n)$.

- **uitkomst:** de schatting van de parameters $d_k,\ f_k,\ k = 1, \ldots, K_c$ van de gemeenschappelijke signaalpolen en de overeenkomstige amplitudes en fases $a_{s,k},\ \phi_{s,k};\ k = 1, \ldots, K_c,\ s = 1, \ldots, S$.

- ***Stap 1***. Schik de afgesneden $\mathbf{U_{s_{K_s}}},\ s = 1, \ldots, S$ matrices in een $L \times \sum_{s=1}^{S} K_s$ matrix als volgt:

$$\mathbf{U_{stacked}} = [\mathbf{U_{1_{K_1}}} | \mathbf{U_{2_{K_2}}} | \ldots | \mathbf{U_{S_{K_S}}}]. \tag{9}$$

en bereken de SVD van deze matrix

$$\mathbf{U_{stacked}} = \mathbf{U_c \Sigma_c V_c^H}. \tag{10}$$

In [112] wordt uitgelegd waarom de SVD van $\mathbf{U_{stacked}}$ onmiddellijk informatie geeft over het aantal gemeenschappelijke signaalpolen en de gemeenschappelijke deelruimte. Indien er K_c polen gemeenschappelijk zijn in S kanalen, dan bevat de kerndiagonaalmatrix $\mathbf{\Sigma_c}$ een eerste set van K_c singuliere waarden gelijk aan $\sqrt{S}$. De K_c eerste vectoren van de linkersinguliere vector matrix $\mathbf{U_{c_{K_c}}}$ brengen de gemeenschappelijke deelruimte voort. We selecteren deze vectoren door $\mathbf{U_c}$ af te kappen tot een matrix van rang K_c, $\mathbf{U_{c_{K_c}}}$.

- ***Stap 2***. De parameterschatting van de gemeenschappelijke signaalpolen wordt volledig beschreven in [112]. Een overzicht van de verschillende stappen van de parameterschatting wordt hieronder gegeven.
Vorm de volgende set overgedetermineerde lineaire vergelijkingen:

$$\mathbf{U^{\uparrow}_{c_{K_c}}} \approx \mathbf{U^{\downarrow}_{c_{K_c}} Z}, \tag{11}$$

waarin de pijlen $\uparrow$ en $\downarrow$ respectievelijk de operatoren voorstellen waarin de laatste, eerste rij verwijderd wordt. De totaal kleinste kwadraten (TLS) oplossing van deze set vergelijkingen wordt gegeven door:

$$\mathbf{\tilde{Z}} = -\mathbf{W_{12} W_{22}^{-1}}, \tag{12}$$

waarin

$$\mathbf{W} = \begin{bmatrix} \mathbf{W_{11_{K_c \times K_c}}} & \mathbf{W_{12_{K_c \times K_c}}} \\ \mathbf{W_{21_{K_c \times K_c}}} & \mathbf{W_{22_{K_c \times K_c}}} \end{bmatrix}, \tag{13}$$

bekomen wordt uit de SVD van de matrix $[\mathbf{U^{\uparrow}_{c_{K_c}}}\ \mathbf{U^{\downarrow}_{c_{K_c}}}]$:

$$[\mathbf{U^{\uparrow}_{c_{K_c}}}\ \mathbf{U^{\downarrow}_{c_{K_c}}}] = \mathbf{Y_{(L-1)\times(L-1)} \Gamma W^H_{2K_c \times 2K_c}}. \tag{14}$$

Eénmaal $\tilde{\mathbf{Z}}$ geschat is, geven de K_c eigenwaarden λ_k een schatting van de gemeenschappelijke signaalpolen [131]:

$$\lambda_k = \hat{z}_k = \exp\{(-\hat{d}_k + j2\pi\hat{f}_k)\Delta t\}, k = 1, \ldots, K_c. \tag{15}$$

De frequentie en demping van deze signaalpolen worden hieruit gemakkelijk bepaald.

- ***Stap 3***. De overeenkomstige schattingen voor de amplitudes $a_{s,k}$ en fases $\phi_{s,k}$, $s = 1, \ldots, S; k = 1, \ldots, K_c$ van de gemeenschappelijke signaalpolen worden bepaald voor elk kanaal afzonderlijk door de bekomen signaalpolen in te vullen in de modelfunctie (3) en de volgende vergelijkingen op te lossen

$$x'_s(n) \approx \sum_{k=1}^{K_c} c_{s,k}\hat{z}_k^n, n = 0, 1, \ldots, N-1. \tag{16}$$

De $x_s(n)$ in (3) worden vervangen door de voorbewerkte $x'_s(n)$ (7) voor een betere schatting van de amplitudes en fases.

Simulatiestudie

In een simulatiestudie wordt een ruismatrix $\mathbf{B}$ gesommeerd met een signaalmatrix $\mathbf{A}$:

$$\mathbf{X}(\lambda) = \mathbf{A} + \lambda \cdot \mathbf{B}, \tag{17}$$

met $\lambda \in \mathbb{R}$. De ruismatrix $\mathbf{B}$ bevat achtergrond EEG, spierartefact en ruis afkomstig van het elektriciteitsnet. De signaalmatrix $\mathbf{A}$ bevat 4 Hz epileptiforme activiteit die gemeenschappelijk is in alle kanalen. De waarde van de wortel uit het gemiddelde van de kwadraten (RMS-waarde) van het signaal wordt gegeven door:

$$RMS(\mathbf{A}) = \sqrt{\frac{1}{S \cdot N}\sum_{s=1}^{S}\sum_{n=0}^{N-1}\mathbf{A}^2(n,s)}, \tag{18}$$

en de RMS-waarde van de ruis is gelijk aan

$$RMS(\lambda \cdot \mathbf{B}) = \sqrt{\frac{1}{S \cdot N}\sum_{s=1}^{S}\sum_{n=0}^{N-1}(\lambda \cdot \mathbf{B}(n,s))^2}. \tag{19}$$

Een belangrijke maat is het ruisniveau (nl), gedefinieerd als,

$$nl = \frac{RMS(\lambda \cdot \mathbf{B})}{RMS(\mathbf{A})}. \tag{20}$$

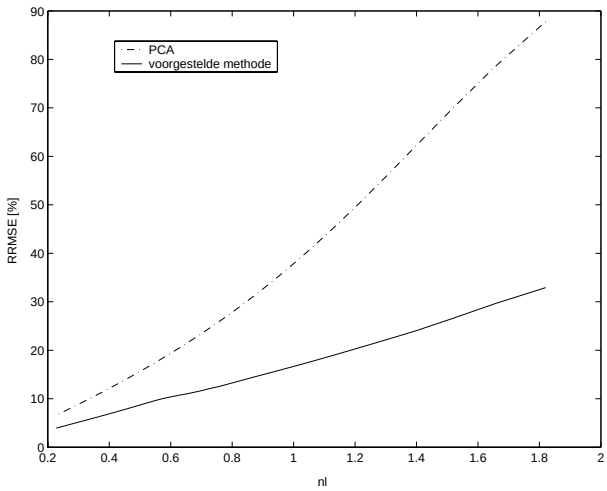

Figuur 4: *De RRMSE-waarde in functie van het ruisniveau (nl) wordt getoond voor de voorgestelde methode en PCA.*

Door de λ parameter te wijzigen, verandert het ruisniveau van het gesimuleerde signaal.

Het doel van deze studie was om de performantie van de methode na te gaan voor het modelleren van de gemeenschappelijke 4 Hz epileptische activiteit. We voerden verscheidene simulaties uit met verschillende ruisniveaus. De performatie werd uitgedrukt in termen van de RRMSE-waarde (Relative Root Mean Squared Error), gedefinieerd als:

$$RRMSE = \frac{RMS(\mathbf{A} - \hat{\mathbf{A}})}{RMS(\mathbf{A})} \cdot 100[\%], \tag{21}$$

waarin $\hat{A}$ een schatting is van de gemeenschappelijke dynamica.

Resultaten van de simulatiestudie

De RRMSE-waarde in functie van het ruisniveau wordt getoond in Fig. 4. In deze figuur wordt een vergelijking gemaakt tussen de voorgestelde methode en principale componenten analyse (PCA). De methode werkt beter dan PCA voor alle ruisniveaus en het verschil in performantie wordt groter bij hogere ruisniveaus.

Interictaal en ictaal EEG

Fig. 5 (a) toont een scalp EEG opname van 4 s. Dit EEG bevat ictale activiteit, voornamelijk op de *T2* en *F8* elektrodes. De EEG opname is bevuild met spierartefact. Fig. 5 (b) toont het gereconstrueerde EEG bekomen door de modellering van de gemeenschappelijke dynamica. Het spierartefact is verwijderd terwijl de epileptische activiteit behouden is. Naast de epileptische activiteit is er ook een tragere activiteit aanwezig in alle kanalen die behouden is door de methode. Deze activiteit is voornamelijk zichtbaar op de elektrodes *F3, F7* and *Fz*.
Ter vergelijking werd het resultaat van de ruisverwijdering door middel van de afgesneden SVD van de datamatrix bepaald voor verschillende afsnijdingsniveaus. Fig. 5 (c) toont het resultaat bekomen met de drie meest energetische principale componenten. In Fig. 5 (d) werd enkel de eerste principale component geselecteerd voor reconstructie. Opnieuw is het resultaat van de voorgestelde methode beter dan de PCA filtering. Vergelijkbare resultaten werden bekomen op een EEG opname met interictale activiteit.

Besluit

Het modelleren van de gemeenschappelijke dynamica in meerkanaals-EEG opnames opent nieuwe perspectieven voor het verwijderen van artefacten en achtergrond EEG in ictale en intericale EEG opnames. In dit hoofdstuk werd een deelruimte gebaseerde methode voorgeteld voor het modelleren van de gemeenschappelijke dynamica. Deze methode werd toegepast op gesimuleerde data en op interictale en ictale EEG. In alle gevallen verwijderde de voorgestelde methode de artefacten en het achtergrond EEG en was de performantie beter dan de performantie van PCA. Verder onderzoek is nodig om de methode te vergelijken met andere artefactverwijderingstechnieken en om het potentieel en de beperkingen van deze nieuwe methode te bepalen.

Hoofdstuk 5: Canonieke correlatie analyse toegepast om spierartefacten te verwijderen in scalp EEG signalen

In dit hoofdstuk wordt het probleem van spierartefactverwijdering behandeld. Het EEG is vaak bevuild met elektrofysiologische potentialen geassocieerd met spiersamentrekkingen ten gevolge van bijten, kauwen en fronsen. We stellen een nieuwe methode voor om deze spierartefacten te verwijderen. De methode is gebaseerd op Canonieke Correlatie Analyse (CCA) toegepast als een blinde bronscheidingstechniek (BSS).

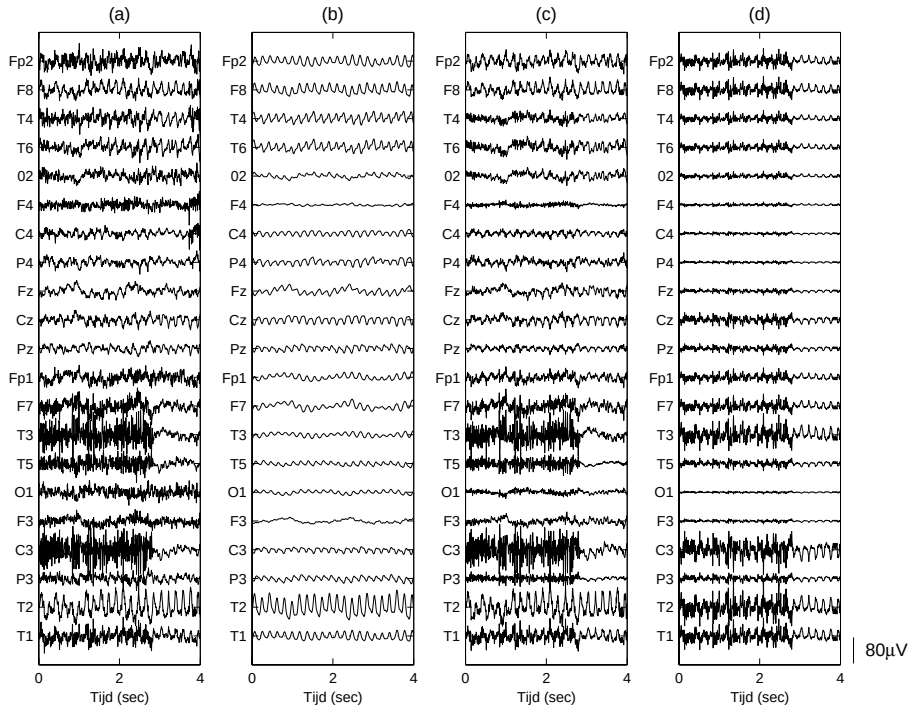

Figuur 5: *(a) Ictale EEG opname van 4 s. (b) Het gereconstrueerde EEG aan de hand van de modellering van de gemeenschappelijke dynamica. (c) Het gereconstrueerde EEG aan de hand van de drie meest energetische principale componenten. (d) Het gereconstrueerde EEG aan de hand van de eerste principale component.*

Blinde bronscheiding door canonieke correlatie analyse

In het blinde bronscheidingsprobleem is het geobserveerde signaal $\mathbf{x}(t) = [x_1(t), x_2(t), ..., x_K(t)]^T$, met $t = 1, ..., N$, met N het aantal tijdspunten en K het aantal elektrodes, het resultaat van een onbekende lineaire combinatie van een set onbekende bronsignalen $\mathbf{s}(t) = [s_1(t), s_2(t), ..., s_K(t)]^T$:

$$\mathbf{x}(t) = \mathbf{A}\mathbf{s}(t), \tag{22}$$

waarin $\mathbf{A}$ een onbekende matrix is. Het doel is deze matrix te bepalen en de originele bronsignalen $\mathbf{s}(t)$ te reconstrueren. Dit wordt uitgevoerd door het introduceren van de matrix $\mathbf{W}$ zodat

$$\mathbf{z}(t) = \mathbf{W}\mathbf{x}(t), \tag{23}$$

de onbekende bronsignalen $\mathbf{s}(t)$, op een schalingsfactor na, benadert. De canonieke correlatie analyse lost dit probleem op door op te leggen dat de bronnnen onderling ongecorreleerd zijn en maximaal gecorreleerd zijn met een gedefinieerde functie [7, 46].
Stel dat $\mathbf{x}(t)$ de geobserveerde datamatrix is met K mengingen en N tijdspunten, dan definiëren we de functie $\mathbf{y}(t)$ als een tijdsvertraagde versie van de originele datamatrix, om op die manier op te leggen dat de bronnen maximaal autogecorreleerd zijn [7, 46]:

$$\mathbf{y}(t) = \mathbf{x}(t-1). \tag{24}$$

Voor het vervolg van dit hoofdstuk refereren we met BSS-CCA naar deze autocorrelatieversie.
Wanneer het gemiddelde van elke rij van de datamatrices $\mathbf{x}(t)$ en $\mathbf{y}(t)$ verwijderd is, bekomt CCA twee sets van basisvectoren, één voor $\mathbf{x}$ en de andere voor $\mathbf{y}$, zodat de correlaties tussen de projecties van de variablen op deze basissen onderling maximaal zijn. Beschouw de lineaire combinaties van de componenten in $\mathbf{x}$ en $\mathbf{y}$:

$$\begin{aligned} x &= w_{x_1}x_1 + ... + w_{x_K}x_K = \mathbf{w_x}^T\mathbf{x}, \\ y &= w_{y_1}y_1 + ... + w_{y_K}y_K = \mathbf{w_y}^T\mathbf{y}, \end{aligned} \tag{25}$$

CCA vindt de vectoren $\mathbf{w_x} = [w_{x_1}, ..., w_{x_K}]^T$ en $\mathbf{w_y} = [w_{y_1}, ..., w_{y_K}]^T$ die de correltatie ρ maximaliseert tussen x en y door het volgende maximalisatieprobleem op te lossen:

$$\begin{aligned} \max_{\mathbf{w_x},\mathbf{w_y}} \rho(x,y) &= \frac{E[xy]}{\sqrt{E[x^2]E[y^2]}} \\ &= \frac{E[(\mathbf{w_x}^T\mathbf{x})(\mathbf{w_y}^T\mathbf{y})]}{\sqrt{E[(\mathbf{w_x}^T\mathbf{x})(\mathbf{w_x}^T\mathbf{x})]E[(\mathbf{w_y}^T\mathbf{y})(\mathbf{w_y}^T\mathbf{y})]}} \\ &= \frac{\mathbf{w_x}^T\mathbf{C_{xy}}\mathbf{w_y}}{\sqrt{(\mathbf{w_x}^T\mathbf{C_{xx}}\mathbf{w_x})(\mathbf{w_y}^T\mathbf{C_{yy}}\mathbf{w_y})}}, \end{aligned} \tag{26}$$

met $\mathbf{C_{xx}}$ en $\mathbf{C_{yy}}$ de covariantiematrices van $\mathbf{x}$ en $\mathbf{y}$, respectievelijk, en $\mathbf{C_{xy}}$ de covariantiematrix tussen $\mathbf{x}$ en $\mathbf{y}$. Dit maximalisatieprobleem kan opgelost worden door de afgeleiden van vgl. (26) naar $\mathbf{w_x}$ en $\mathbf{w_y}$ gelijk te stellen aan nul. Dit leidt tot de volgende twee eigenwaardeproblemen [48, 46]:

$$\begin{cases} \mathbf{C}_{xx}^{-1}\mathbf{C}_{xy}\mathbf{C}_{yy}^{-1}\mathbf{C}_{yx}\hat{\mathbf{w}}_{\mathbf{x}} &= \rho^2\hat{\mathbf{w}}_{\mathbf{x}}, \\ \mathbf{C}_{yy}^{-1}\mathbf{C}_{yx}\mathbf{C}_{xx}^{-1}\mathbf{C}_{xy}\hat{\mathbf{w}}_{\mathbf{y}} &= \rho^2\hat{\mathbf{w}}_{\mathbf{y}}. \end{cases} \tag{27}$$

In de BSS-CCA versie is het voldoende om vgl. (27) op te lossen voor $\hat{\mathbf{w}}_{\mathbf{x}}$. Dit resulteert in K oplossingen $\{\rho_i, \hat{\mathbf{w}}_{\mathbf{x_i}}\}$, $i = 1...K$, gerangschikt volgens autocorrelatie ρ_i. De K schattingen van de bronsignalen $\mathbf{s}_i(t)$ worden dan gegeven door $\mathbf{z}_i(t) = \hat{\mathbf{w}}_{\mathbf{x_i}}^T\mathbf{x}(t)$.
De canonieke correlaties, die in de BSS-CCA versie gelijk zijn aan de autocorrelaties van de bronnen, worden ook gegeven door de cosinussen van de principale hoeken tussen de rijruimtes van $\mathbf{x}^T$ en $\mathbf{y}^T$ [52]. De principale richtingen in de rijruimte van $\mathbf{x}^T$ stemmen overeen met de bronsignalen $\mathbf{s}_i(t)$ [52].

BSS-CCA toepassen voor spierartefactverwijdering in EEG signalen

Wanneer BSS-CCA toegepast wordt op het EEG en de bronnen die bijdragen tot dit EEG bepaald zijn, kan men de bronnen die gerelateerd zijn aan het spierartefact verwijderen door de kolommen die overeenstemmen met de activatie van deze bronnen gelijk te stellen aan nul in de reconstructie $\mathbf{x}_{clean}(t)$ van het EEG:

$$\mathbf{x}_{clean}(t) = \mathbf{A}_{clean}\mathbf{z}(t), \tag{28}$$

met $\mathbf{z}(t)$ de bronsignalen die we bekomen hebben door middel van BSS-CCA, en $\mathbf{A}_{clean}$ de mengmatrix waarin de kolommen die overeenkomen met de artefactbronsignalen gelijk gesteld zijn aan nul.
We observeerden dat de spierartefactcomponenten goed gescheiden zijn van de componenten die gerelateerd zijn met de hersenactiviteit en dat deze componenten zich in de laagst autogecorreleerde componenten bevinden. Deze observaties werden uitgebuit om een semi-automatische methode te ontwikkelen die de spierartefacten één voor één verwijdert door middel van een scroller.

Simulatiestudie

Het doel van de simulatiestudie was het evalueren van de performantie van de voorgestelde methode om spierartefact te verwijderen. Verscheidene simulaties werden uitgevoerd met verschillende signaal-ruisverhoudingen.

Data en maten om de performantie te testen

In de simulatiestudie werd een spierartefactsignaal $\mathbf{M}$ gesommeerd op een EEG signaal $\mathbf{B}$ dat uitsluitend hersenactiviteit bevat:

$$\mathbf{X}(\lambda) = \mathbf{B} + \lambda \cdot \mathbf{M}, \tag{29}$$

met $\lambda \in \mathbb{R}$. De RMS-waarde van het hersensignaal is gelijk aan

$$RMS(\mathbf{B}) = \sqrt{\frac{1}{K \cdot N} \sum_{k=1}^{K} \sum_{n=1}^{N} \mathbf{B}^2(k,n)}, \tag{30}$$

met N gelijk aan het aantal tijdspunten en K gelijk aan het aantal EEG kanalen. De RMS-waarde van het spierartefactsignaal is gelijk aan

$$RMS(\lambda \cdot \mathbf{M}) = \sqrt{\frac{1}{K \cdot N} \sum_{k=1}^{K} \sum_{n=1}^{N} (\lambda \cdot \mathbf{M}(k,n))^2}. \tag{31}$$

Een belangrijke maat is de signaal-ruisverhouding, gedefinieerd als,

$$SNR = \frac{RMS(\mathbf{B})}{RMS(\lambda \cdot \mathbf{M})}. \tag{32}$$

Door de λ parameter te wijzigen, veranderen we de signaal-ruisverhouding van ons simulatiesignaal. Verscheidene simulaties werden uitgevoerd met verschillende signaal-ruisverhoudingen. De performantie wordt uitgedrukt in termen van de RRMSE-waarde, gedefinieerd als:

$$RRMSE = \frac{RMS(\mathbf{B} - \hat{\mathbf{B}})}{RMS(\mathbf{B})}, \tag{33}$$

waarin $\hat{B}$ het gefilterde signaal voorstelt. De simulaties werden uitgevoerd voor drie verschillende hersensignalen $\mathbf{B_1}$, $\mathbf{B_2}$ en $\mathbf{B_3}$, die respectievelijk delta, alfa en bèta activiteit bevatten. De performantie van de methode wordt vergeleken met de performantie van een laagdoorlaatfilter met verschillende doorlaatfrequenties en onafhankelijke componenten analyse (ICA).

Resultaten van de simulatiestudie

De RRMSE-waarde in functie van de signaal-ruisverhouding voor de simulatiestudie met het $\mathbf{B_2}$ hersensignaal voor verschillende artefactverwijdertechnieken (BSS-CCA, ICA(JADE) en een laagdoorlaatfilter met doorlaatfrequentie gelijk aan 10Hz, 15Hz, 20Hz en 30Hz) wordt getoond in Fig. 6. De BSS-CCA methode werkt beter voor alle SNRs. De resultaten van de simulatiestudie met de $\mathbf{B_1}$ en $\mathbf{B_3}$ hersensignalen zijn vergelijkbaar met de resultaten bekomen voor het $\mathbf{B_2}$ hersensignaal.

Ictaal EEG

Omdat ictale EEG's vaak bevuild zijn met spierartefact, hetgeen de bepaling en lokalisatie van de ictale start bemoeilijkt, is deze studie gericht op het verwijderen van spierartefacten in ictale EEG's. Fig. 7 (a) toont een ictaal EEG van 10 s. De

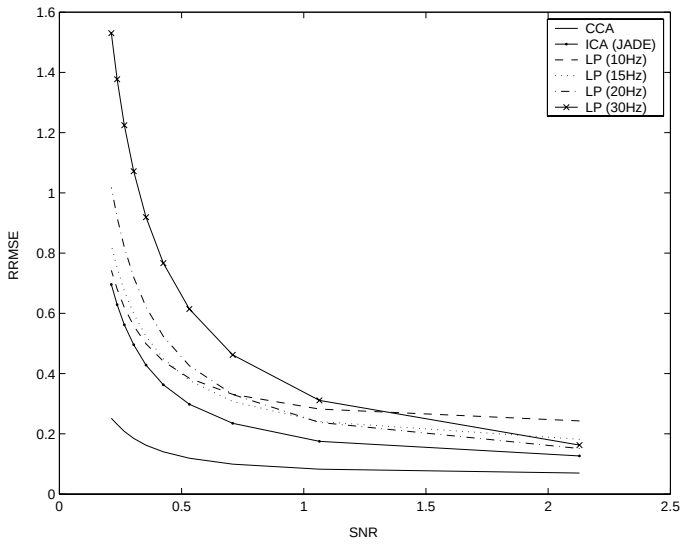

Figuur 6: *De RRMSE-waarde in functie van de signaal-ruisverhouding (SNR) voor de simulatiestudie met het* $\mathbf{B_2}$ *signaal (alfa (8-13Hz) activiteit) voor de verschillende spierartefactverwijdertechnieken.*

epileptische activiteit is voornamelijk aanwezig op de $T2$, $F8$ en $T4$ elektrodes. Het EEG is sterk bevuild met spierartefact. Figuur. 7 (b) toont het gereconstrueerde EEG na het verwijderen van de laatste 11 CCA componenten. (9-21). Merk op dat het spierartefact volledig verwijderd is, terwijl de scherpe kwaliteit van de ictale theta activiteit in de rechts temporale kwab ($T2$, $F8$, en in mindere mate $T4$ en $T6$) behouden is.

Klinische validatie

De eerste voorlopige resultaten van een klinische studie van 26 ictale EEG's van patiënten met refractaire epilepsie tonen aan dat de verwijdering van spierartefact resulteert in een beter interpretatie van het aanvals-EEG. Dit leidt tot een vroegere detectie van de start van de epileptische aanval en een betere lokalisatie van de epileptische focus. Deze bevindingen maken de huidige methode onmisbaar voor elke epilepsie-monitoringeenheid. De resultaten van de studie worden samengevat in Tabel 1.

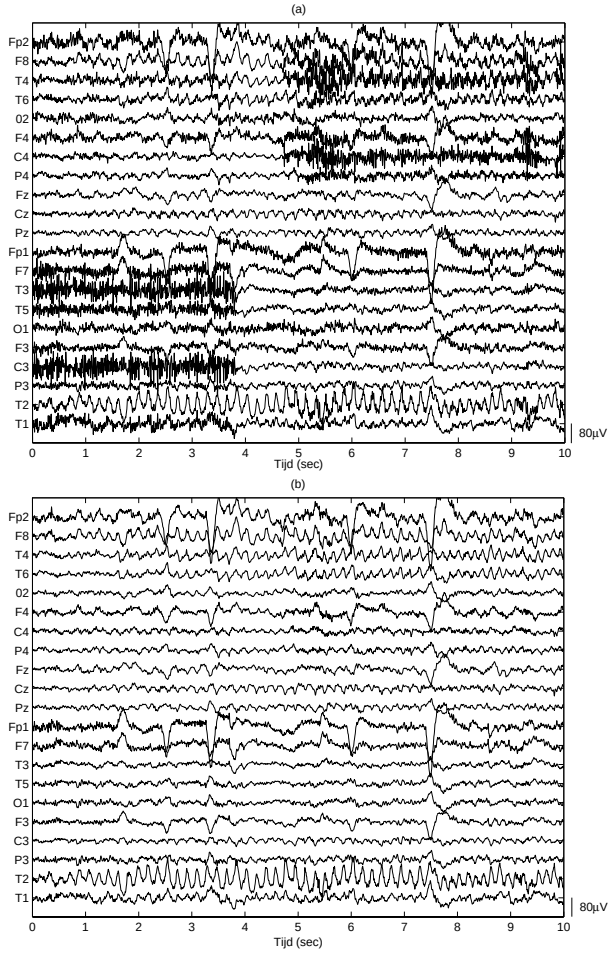

Figuur 7: *(a) Ictaal EEG van 10 s dat bevuild is met spierartefact ; (b) EEG reconstructie na het verwijderen de 11 laatste CCA componenten. Merk op dat het spierartefact volledig verwijderd is, terwijl de scherpe kwaliteit van de ictale theta activiteit in de rechts temporale kwab (*$T2$*, *$F8$*, en in mindere mate *$T4$* en *$T6$*) behouden is.*

Bevuiling met spierartefact	24/26 (92%)
Gemakkelijkere interpreatatie	24/24 (100%)
Verbeterde interpretatie	11/24 (42%)
Vroegere detectie van de ictale start in het EEG	9/26 (35%)
Betere lokalisatie van de ictale start	7/26 (27%)
Ictaal startpatroon met een hogere frequentie	8/26 (31%)
Gelokaliseerde beta activiteit enkel na verwijdering van spierartefact	5/26 (19%)
Degradatie van het ictale EEG door de methode	0/26 (0%)

Tabel 1: Voorlopige resultaten van de klinische studie.

Besluit

In dit hoofdstuk werd een nieuwe methode voorgesteld voor artefactverwijdering gebaseerd op CCA. De voorgestelde methode werd getest op gesimuleerde data en op ictaal EEG dat bevuild is met spierartefact. De methode werkt beter dan de huidige laagdoorlaatfilters en onafhankelijke componenten analyse (ICA) gebaseerde technieken. Daarenboven heeft de voorgestelde methode niet het nadelige effect van de huidige filtertechnieken en verwijdert de spierartefacten zonder de onderliggende opgenomen hersenactiviteit aan te tasten (en dus zonder klinisch relevante informatie te verwijderen). EEG opnames die zwaar bevuild zijn met spierartefact en die bijgevolg niet kunnen geïnterpreteerd worden met de huidig filtertechnieken, kunnen correct geïnterpreteerd worden met onze methode. De eerste voorlopige resultaten van een klinische studie van patiënten met refractaire epilepsie tonen aan dat de verwijdering van spierartefact resulteert in een betere interpretatie van het aanvals-EEG. Dit leidt tot een vroegere detectie van de start van de epileptische aanval en een betere lokalisatie van de epileptische focus. Deze bevindingen maken de huidige methode onmisbaar voor elke epilepsie-monitoringeenheid.

Hoofdstuk 6: Conclusies en verder onderzoek

Voorspelling van epileptische aanvallen met behulp van scalp EEG signalen

We probeerden de bevindingen van Le Van Quyen te reproduceren en een pre-ictale toestand te detecteren met behulp van de similariteitsindex toegepast op scalp EEG signalen van 12 patiënten met MTLE. We waren niet in staat de bevindingen te reproduceren. De similariteitsindex was niet in staat pre-ictale veranderingen waar te nemen in de scalp EEG opnames van de 12 patiënten. Deze bevindingen werden gepubliceerd in o.a. The Lancet [21, 19]. Met deze publicaties was onze onderzoeksgroep de eerste groep die rapporteerde over negatieve bevindingen in dit onderzoeksdomein. Na het verschijnen van deze publicaties bevestigden vele andere groepen onze bevindingen.

Daarenboven toonden we aan dat we eerst de artefacten zullen moeten verwijderen indien we ooit enig succes willen hebben met het voorspellen van epileptische aanvallen aan de hand van scalp EEG signalen. Verder onderzoek op dit onderwerp omvat de similariteitsindex analyse van de EEG signalen na verwijdering van artefacten. De volgende stappen zullen moeten ondernomen worden om deze analyse uit te kunnen voeren:

- Automatiseren van de in dit werk voorgestelde artefactverwijdertechnieken voor de voorbewerking van langdurige EEG signalen.
- Het ontwikkelen van een automatische techniek voor oogartefactverwijdering.

Modelleren van de gemeenschappelijke dynamica

Een nieuwe deelruimte gebaseerde methode werd ontwikkeld voor de modellering van de gemeenschappelijke dynamica in de verschillende EEG kanalen. Deze methode verwijdert succesvol artefacten en achtergrond EEG van epileptiforme EEG en doet dit beter dan principale componenten analyse (PCA). Met deze bevindingen illustreren we dat het modelleren van de gemeenschappelijke dynamica in meerkanaals-EEG opnames nieuwe perspectieven opent voor het verwijderen van artefacten en achtergrond EEG. Verder onderzoek is vereist om de volgende zaken vast te leggen:

- De methode moet gevalideerd worden op een groot aantal EEG opnames.
- Verder onderzoek is nodig om de methode te vergelijken met andere artefactverwijderingstechnieken om het potentieel en de beperkingen van deze nieuwe methode te bepalen.
- Een adaptieve segmentatie kan ontwikkeld worden om de methode te automatiseren.
- De methode kan toegepast worden op andere biomedische signalen waar er nood is om de gemeenschappelijke dynamica te modelleren.

Spierartefactverwijdering

Een nieuwe methode werd voorgesteld voor artefactverwijdering gebaseerd op CCA. De voorgetelde methode werd getest op gesimuleerde data en op ictaal EEG dat bevuild is met spierartefact. De methode werkt beter dan de huidige laagdoorlaatfilters en ICA gebaseerde technieken. Daarenboven heeft de voorgestelde methode niet het nadelige effect van de huidige filtertechnieken en verwijdert de spierartefacten zonder de onderliggende opgenomen hersenactiviteit aan te tasten (en dus zonder klinisch relevante informatie te verwijderen). EEG opnames die zwaar bevuild zijn met spierartefact en die bijgevolg niet kunnen geïnterpreteerd worden met de huidig filtertechnieken, kunnen correct geïnterpreteerd worden

met onze methode. De eerste voorlopige resultaten van een klinische studie van patiënten met refractaire epilepsie tonen aan dat de verwijdering van spierartefact resulteert in een betere interpretatie van het aanvals-EEG. Dit leidt tot een vroegere detectie van de start van de epileptische aanval en een betere lokalisatie van de epileptische focus. Deze bevindingen maken de huidige methode onmisbaar voor elke epilepsie-monitoringeenheid. Verder onderzoek kan gedaan worden op de volgende onderwerpen:

- Verder onderzoek is vereist om een volledig automatische methode te ontwikkelen voor spierartefactverwijdering.
- De techniek kan gebruikt worden als voorbewerkingtechniek om de verdere signaalverwerking te verbeteren.
- De methode kan ook toegepast worden om spierartefact te verwijderen in MEG opnames.
- Het is nog niet duidelijk of CCA geschikt is voor het verwijderen van oogartefacten. Een studie waarin de performantie van CCA vergeleken wordt met de performantie van ICA op een grote dataset van EEG's met oogartefacten kan dit bepalen. Het is bovendien nog niet duidelijk of CCA hersenactiviteit kan scheiden in zijn onderliggende bronnen.

Chapter 1

Introduction

In this chapter the presented work is situated in the research area of biomedical signal processing, and a chapter by chapter overview of the thesis is presented.

1.1 Biomedical signal processing

The human body is made up of many component *systems*, including the nervous system, the cardiovascular system, and the musculoskeletal system, among others. Each system is made up of several subsystems that carry on many *physiological processes*. Most physiological processes are accompanied by or manifest themselves as *signals* that reflect their nature and activities. Such signals could be of many types, including biochemical in the form of hormones and neurotransmitters, electrical in the form of potential or current, and physical in the form of pressure or temperature. Diseases or defects in a biological system cause alterations in its normal physiological processes, typically associated with signals that are different in some respects from the corresponding normal signals. If we possess a good understanding of a system of interest, it becomes possible to observe the corresponding signals and assess the state of the system.

All treatments of signals that occur between the data acquisition of the signals and the interpretation of an observer is considered as *signal processing*. In general the aim of biomedical signal processing is to enhance/extract the relevant information in/from the measured signal. Depending on the application this could be: reduction of noise and artifacts, accurate quantification of clinical parameters, detection of physiological events or states, classification for diagnosis, ...
Usually four steps can be discriminated in the processing of biomedical signals, which are shown in figure 1.1 [94]. The *data acquisition* includes both the data acquisition at the sensor level and the analog to digital conversion. In the *preprocessing* step, the digital signals are transformed to improve the parameter estimation or feature extraction in the next step. The *parameter estimation* con-

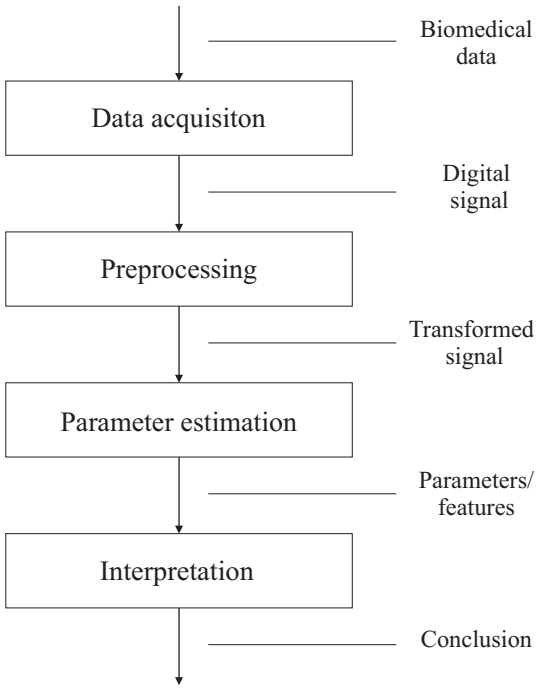

Figure 1.1: *General biomedical signal processing scheme.*

sists of the extraction of clinically relevant features or parameters from the transformed signals. In the *interpretation* step, these parameters are used for human or computer-aided decision making.

1.2 Topic of thesis

This thesis is focused on the preprocessing and parameter estimation for a specific biomedical application, namely the processing of scalp electroencephalographic signals of patients with epilepsy. By measuring the potential differences between electrodes placed on the skull of the scalp, the ElectroEncephaloGram (EEG) represents the electrical activity of the brain. The EEG is a valuable tool for diagnosis of neurological disorders or diseases and to study human brain functioning. One of the many application areas is the diagnosis of epilepsy.
Unfortunately, as scalp EEG measurements are noninvasive, potentials that are generated by (physiological or non-physiological) sources other than the brain are picked up by scalp electrodes and recorded together with the EEG. These potentials are referred to as artifacts and often obscure the epileptiform activity in the EEG recording. As a result, these artifacts often give rise to misinterpretation or

false decision making. Consequently, a preprocessing step, in which the artifacts are removed, is essential for accurate parameter estimation or correct interpretation. In chapter 3 we illustrate how artifacts can hamper the feature extraction of scalp EEG signals when seizure prediction is the aim. In chapter 4 and 5, two newly developed artifact removal techniques are proposed. Depending on the application the presented artifact removal techniques can become preprocessing techniques (when the artifact removal is followed by a parameter estimation) or processing techniques (when visual interpretation of the EEG is the aim). In the next section a detailed chapter by chapter overview is given.

1.3 Chapter by chapter overview

In chapter 2 an introduction is given to both electroencephalography and epilepsy. First, the neurophysiological phenomena responsible for generating the EEG, the acquisition, and the different application areas of EEG are briefly described. In the second part of this chapter we focus on the application of EEG in the diagnosis of epilepsy and the contribution of the presented work to the presurgical evaluation of patients with refractory epilepsy is highlighted.

Chapter 3 deals with the prediction of epileptic seizures from EEG recordings. One of the most devastating features of epilepsy is the apparent unpredictable nature of seizures. Every day activities are impaired and can become dangerous for patients [16]. The unpredictability of seizure onset is one of the most important causes of morbidity and stress in patients with epilepsy [98, 9]. Being able to predict the onset of seizures would render the implementation of alarm systems and novel therapeutic approaches possible; e.g. automated interventional measures like the application of anticonvulsant drugs or electrical brain stimulation. The prediction of epileptic seizures by quantitative analysis methods applied to EEG has been a focus of much interest in recent years. This resurgence of interest has been motivated by several factors, including the proliferation of powerful new methods for analyzing nonlinear system dynamics, as well as the interest in developing epilepsy control devices. In this chapter a literature overview of state-of-the-art nonlinear seizure prediction methods is given. It turns out that many of the earlier studies reporting on seizure prediction are incomplete and the predictive ability of the nonlinear measures is very low. We report on the low ability of the similarity index to predict seizures on scalp EEG recordings. These negative findings were published in The Lancet [21], and with this publication we were the first research group reporting on a low predictive ability of a nonlinear measure. Later on, many other studies confirmed our results, showing that nonlinear measures have a very low ability to predict epileptic seizures both on scalp EEG signals and intracranial EEGs. Furthermore, by illustrating the sensitivity of the similarity index to artifacts, we propose an additional preprocessing step for scalp EEG recordings in which artifacts like eye blinks and muscle artifacts are removed. The presence of artifacts might mask the brain activity related to

the pre-ictal state in the scalp EEG recordings. If we want to have any success in predicting seizures from scalp EEG electrodes, we first will need to remove the artifacts contaminating it. In the following chapters two newly developed methods for artifact removal are presented.

In chapter 4 a new technique for artifact and background EEG removal is proposed. Removing artifacts and background EEG from multichannel interictal and ictal EEG has become a major research topic in EEG signal processing in recent years. We applied for this purpose a recently developed subspace-based method for modelling the common dynamics in multichannel signals. When the epileptiform activity is common in the majority of channels and the artifacts appear only in a few channels the proposed method can be used to remove the latter. The performance of the method was tested on simulated data for different noise levels. For high noise levels the method was still able to identify the common dynamics. In addition, the method was applied to real life EEG recordings containing interictal and ictal activity contaminated with muscle artifact. The muscle artifacts were removed successfully. For both the synthetic data and the analyzed real life data the results were compared with the results obtained with Principal Component Analysis (PCA). In both cases the proposed method performed better than PCA. The results are published in [24, 23].

Chapter 5 deals with the removal of muscle artifacts in scalp EEG signals. The EEG is frequently contaminated by electrophysiological potentials associated with muscle contraction due to biting, chewing and frowning. These muscle artifacts obscure the EEG and complicate the interpretation of the EEG or even make the interpretation unfeasible. In the domain of Event Related Potentials (ERP), epochs heavily contaminated with muscle artifacts are typically rejected. When a small number of epochs is available, for instance in complex memory tasks, each rejected epoch will reduce the interpretability of the ERP [126]. In automated epileptic seizure detection, muscle artifacts considerably reduce the selectivity of the method [119]. In the field of seizure prediction, muscle artifacts obscure the interpretation of the nonlinear measures when looking for a pre-ictal state in scalp EEG recordings (Chapter 2). Hence, there is a clear need to remove these artifacts from the EEG. In this chapter a new method for muscle artifact removal in EEG is presented, based on Canonical Correlation Analysis (CCA) as a Blind Source Separation (BSS) technique. This method is demonstrated on a synthetic data set and on a real ictal EEG recording contaminated with muscle artifacts. The proposed method removed successfully the muscle artifact. The method outperformed a low pass filter with different cut-off frequencies and an Independent Component Analysis (ICA) based technique for muscle artifact removal. Moreover, the fast computational time and the ordering of the CCA components make the proposed method applicable in clinical practice. Furthermore, the method does not have the adverse effects of the existing filtering methods and removes the muscle artifact without altering the underlying brain activity (and thus with-

out removing the interesting information). Heavily contaminated recordings, that could not be interpreted with the existing filtering methods, can be correctly interpreted with the current method. Since the muscle artifact is one of the most common artifacts in scalp EEG recordings, every digital EEG acquisition station could benefit from incorporating this method. The first preliminary results of a clinical study on 26 ictal EEGs of patients with refractory epilepsy showed that the removal of muscle artifact results in a better interpretation of the ictal EEG, leading to an earlier detection of the seizure onset and a better localization of the seizures onset zone. These findings make the current method indispensable for every Epilepsy Monitoring Unit. The material of this chapter has been submitted for publication [28, 27, 135, 26] and has been patented [25].

In chapter 6 findings and conclusions of the presented work are summarized and some directions for further research are pointed out.

Chapter 2

Electrical brain activity and epilepsy

2.1 Introduction

In this chapter an introduction is given to both electroencephalography and epilepsy. First, we briefly describe the neurophysiological phenomena responsible for generating the EEG, the acquisition, and the different application areas of EEG. Next, we focus on the application of EEG in the diagnosis of epilepsy. Based on the ictal EEG findings and clinical manifestations, epileptic seizures are classified according to the classification of the International League Against Epilepsy. Furthermore, the EEG is utilized in localizing the surgical seizure focus, i.e. that part of the brain that has to be removed in order to render a patient seizure free. In section 2.4.4 the contribution of the presented work to the presurgical evaluation of patients with refractory epilepsy is highlighted.

2.2 The brain

Based on [3, 105, 41] an introduction to the brain anatomy and electrical brain activity is given.

2.2.1 Anatomy

The brain consists of about 10^{10} nerve cells or neurons. The neurons are more diverse in size and shape than cells in any other tissue of the body. Nevertheless they have certain features in common: they usually possess dendrites, a cell body, an axon and synaptic terminals, as illustrated in Fig. 2.1. Dendrites extend from the cell body and share with it the function of receiving information from synaptic connections with adjoining neurons. The cell body, also known as soma, contains

the nucleus, which synthesizes proteins for export to the axon. The axon is a slender tube ranging in length from a few hundred micrometers to more than a meter. Axons are usually longer than dendrites and at their ends they branch to form terminals which make contact with other cells at synapses. Synaptic terminals are the sites of release chemicals (neurotransmitters) and are usually in close proximity to another neuron.

Brain tissue is divided into two types: gray matter and white matter. These names derive very simply from their appearance to the naked eye. Gray matter is made up of the cell bodies and dendrites of nerve cells. The gray matter can be found at the outermost surface of the brain, the cortex, and in some deeper structures. The thickness of the cortex varies between 1 mm and 4 mm. The larger inner part of the brain contains the white matter, which is made up of only the axons of the nerve cells. Fig. 2.2 presents a horizontal slice in the brain. The white matter and gray matter are easily distinguished. The brain is divided into two hemispheres and in each hemisphere, the cortex is subdivided into four lobes, i.e the frontal, parietal, occipital and temporal lobe, as illustrated in Fig. 2.3. Each of these lobes contains many distinct areas that control different functions.

2.2.2 Electrical brain activity

Neurons, like other cells, are electrically polarized so that their interior is negatively charged with respect to the outside of the cell. This potential difference, called the resting potential, is due to an unequal distribution of Na^+, K^+ and Cl^- ions across the cell membrane. Typical resting values for neurons are about -70 mV.

Cells communicate with one another by chemical and electrical signals. The arrival of an action potential in the presynaptic region is followed by the release of chemical transmitters, called neurotransmitters, which diffuse across the synaptic cleft. The neurotransmitters interact with receptors on the postsynaptic membrane and produce a change in membrane conductance; this causes a local change in the resting potential or a postsynaptic potential (PSP). Depending on the conductance change the membrane may be either depolarized or hyperpolarized. An excitatory postsynaptic potential (EPSP) is a transient partial reduction in membrane potential which is usually due to increased local permeability to sodium (Na^+) ions. Because sodium is a positively charged ion on the outside of the cell, its entry into the cell makes the negative intracellular resting potential less negative. (i.e. partially depolarizes the cell). In contrast, an inhibitory postsynaptic potentials (IPSP) is a transient increase in intracellular negativity produced by the entry of negatively charged chloride (Cl^-) ions into the cell. The postsynaptic potentials alter the neuronal membrane potential by several millivolts and last over $\sim$10 ms. When the neuronal membrane is depolarized beyond a critical level or threshold an action potential is generated that proliferates along the axon to

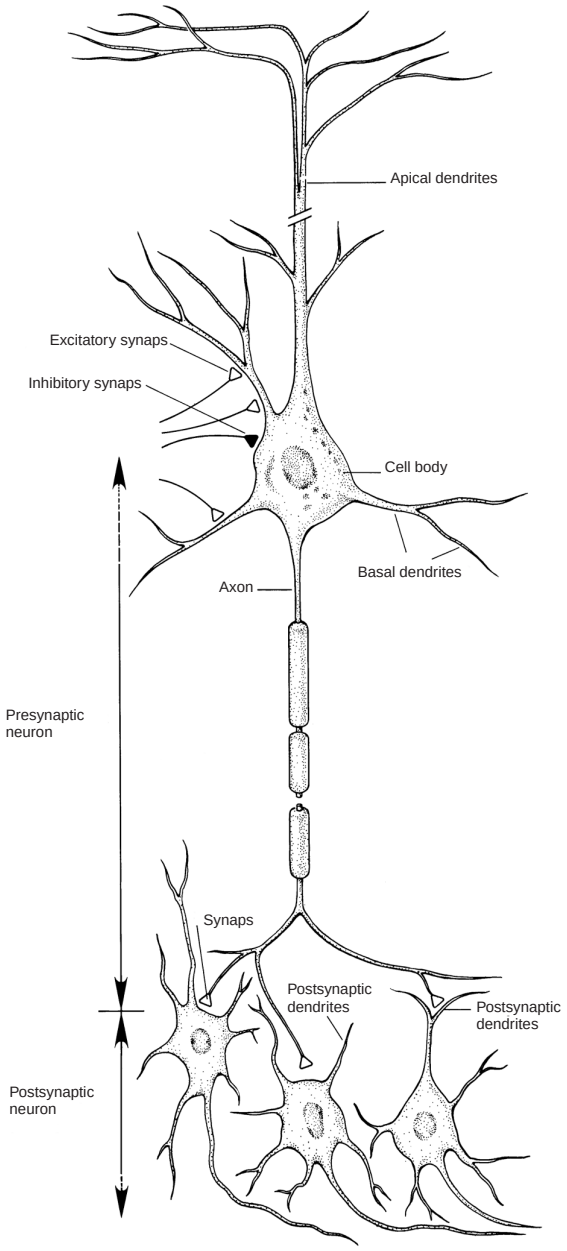

Figure 2.1: *The basic parts of a neuron: cell body, dendrites, axon and synaptic terminals.*

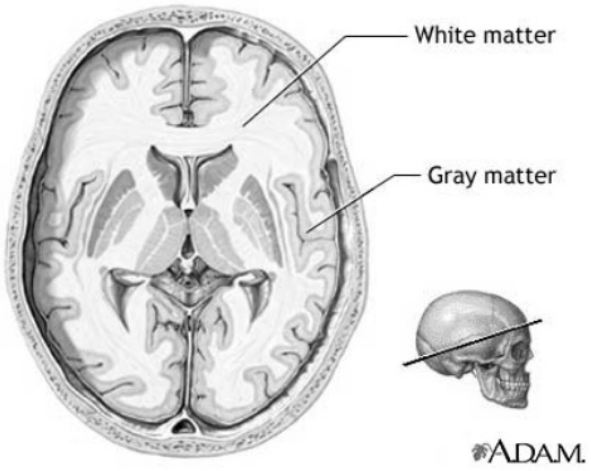

Figure 2.2: *A horizontal slice of the brain. The gray matter, which is made up of the cell bodies and dendrites, can be found at the outmost surface of the brain (the cortex) and in some deeper structures. The larger inner part of the brain contains the white matter, which is made up of only the axons of the nerve cells.*

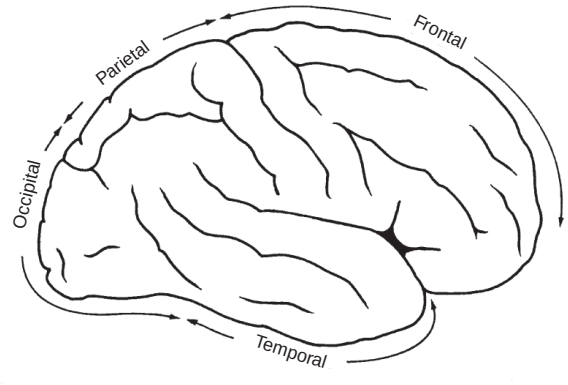

Figure 2.3: *The four different lobes.*

other neurons. This threshold can be obtained by spatial or temporal summation of the postsynaptic potentials. Fig. 2.4 illustrates the summation of excitatory and inhibitory postsynaptic potentials. If the potential is excitatory, action potentials may be initiated in the postsynaptic cell but if inhibitory, action potential generation will be suppressed.

2.3 Electroencephalography

Summation of the electrical potential changes in the cortex occurs mainly at the vertical oriented large pyramidal cells of the cortex. The spatial properties of these neurons is so that they amplify each other's extracellular field [41]. The currents generated by these neurons summate in the extracellular space and a small fraction penetrates through the meningeal coverings, spinal fluid and skull to the scalp where it causes different parts of the scalp to be at different potential levels. These potential differences, of usually only 10 to 100 μV, can be recorded between two electrodes and constitute the EEG. It is believed that the synchronized pyramidal cell postsynaptic potentials are the generators of the potential fields recorded on the scalp. Although their amplitude (0.1-10 mV) is much smaller than the amplitude of action potentials (70-110 mV), their time interval of 10-20 ms enables summed activity of neighboring neurons. The action potentials have a small interval of time (0.3 ms), which makes a synchronous firing of action potentials unlikely. The electrical field generated by a group of pyramidal cells can be approximated sufficiently by a single dipole [29].

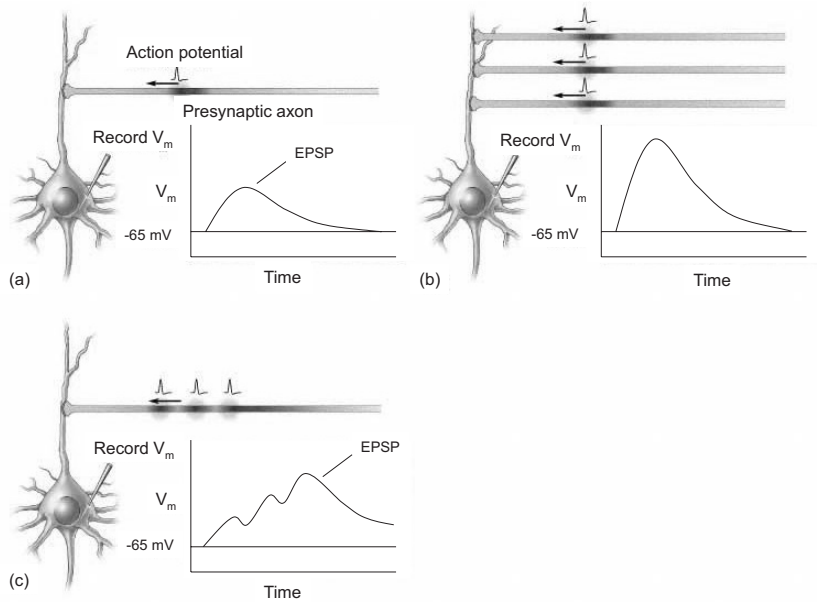

Figure 2.4: *(a) A presynaptic action potentials triggers a small EPSP in a postsynaptic neuron. (b) Spatial summation of EPSPs: when two ore more presynaptic inputs are active at the same time, their individual EPSPs add together. (c) Temporal summation of EPSPs: when the same presynaptic fiber fires action potentials in quick succession, the individual EPSPs add together. Figure from [3].*

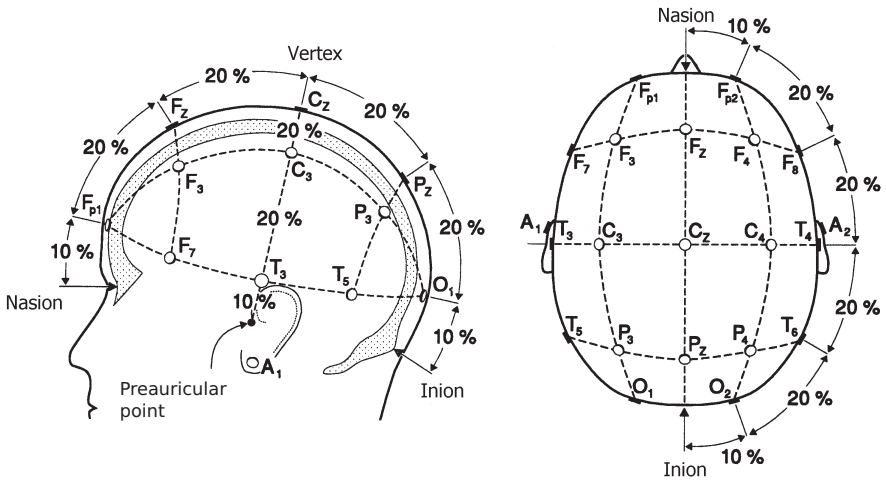

Figure 2.5: *A representation of the 10-20 international system electrode placement: side view and top view of the head. Figure from [88].*

2.3.1 Scalp EEG

As mentioned in the previous section, when cortical neurons are simultaneously active, potential difference are generated between electrodes positioned on the scalp. An electroencephalogram measures these potential differences as a function of time. The electrodes are placed at standard positions on the head according to the international 10-20 system [107]. This electrode placement provides for uniform coverage of the entire scalp. It uses the distances between bony landmarks of the head to generate a system of lines which run across the head and intersect at intervals of 10 or 20% of their total length. Electrodes are placed at the intersections. Fig. 2.5 presents the 10-20 international system; the nasion, inion and preauricular points are used as landmarks. In this work we used the 10-20 international system with two additional electrodes $T1$ and $T2$ on the temporal regions. A total of 21 electrodes was used. Each electrode is given a label as illustrated in Fig. 2.6.

The electroencephalogram displays the time course of potential differences between electrodes. The selection of electrodes in inputs 1 and 2 of any one amplifier channel is referred to as derivation. A montage consists of a combination of derivations using multiple channels of recording. There are currently 5 basic kinds of montages: bipolar, common electrode reference, average reference, weighted average reference and Laplacian (source derivation) [42]. Montages perform the function of spatial filtering. Some montages (e.g. bipolar or Laplacian) are best suited for viewing highly localized activity over a limited area of the scalp and

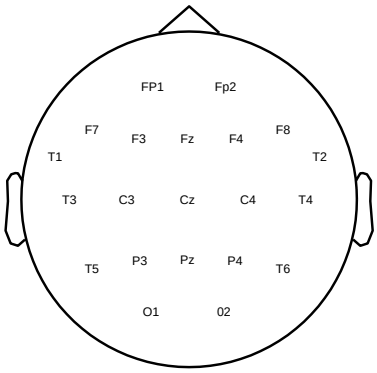

Figure 2.6: *Electrode setup used in the epilepsy monitoring unit. This setup is used in the presented work.*

filtering out widespread waveforms that are coherent (i.e., occur with similar amplitude and phase). Others (e.g. common reference, average reference, weighted average reference) are better for viewing widespread coherent waveforms than localized waveforms.

Modern acquisition equipment, samples the EEG and stores it digitally. The sample rate varies between 100 Hz and 1 kHz. There are a number of compelling reasons to abandon the analog technology [35]. One of the important tools for analyzing the spatial distribution of EEG over the scalp is montage reformatting. In contrast to analog EEG instruments, digital montage reformatting becomes possible and is surprisingly simple if it is recalled that the EEG signal from each channel is simply the subtraction of the activity in the electrode in input 2 from input 1. Moreover, the digital EEG recorders allow for digital signal (pre)processing of the EEG signals.

The normal EEG of an adult may show various types of activity alone or in combination. The commonly used terms of EEG frequency f bands are:

- Delta: $0.5 \leq f < 4$Hz;
- Theta: $4 \leq f < 8$Hz;
- Alpha: $8 \leq f < 13$Hz; and
- Beta: $13 \leq f < 30$Hz.

Fig. 2.7 illustrates traces of EEG signals with the rhythms listed above. EEG rhythms are associated with various physiological and mental processes [38, 39]. The alpha rhythm is the principle resting rhythm of the brain, and is common in wakeful, resting adults with closed eyes, especially in the occipital area with

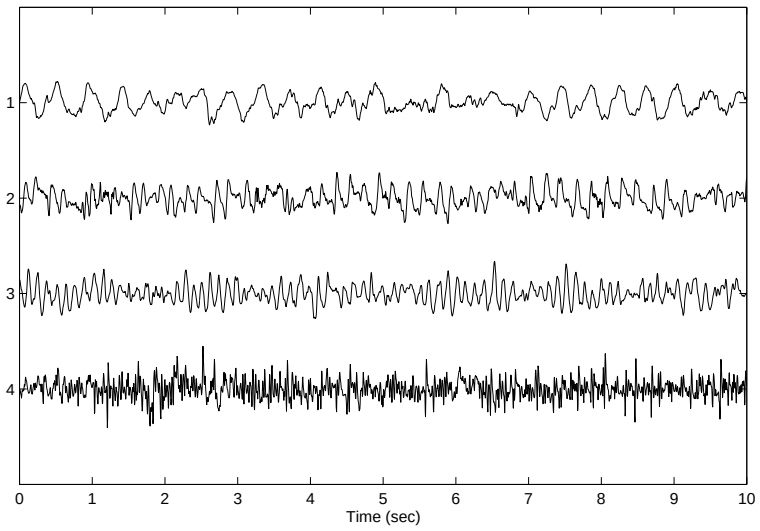

Figure 2.7: *From top to bottom: (1) delta rhythm (0.5-4Hz); (2) theta rhythm (4-8Hz); (3) alpha rhythm (8-13Hz); (4) beta rhythm (13-30Hz).*

bilateral synchrony. The alpha wave is replaced by slower rhythms at various stages of sleep. Theta waves appear at the beginning stages of sleep; delta waves appear at deep-sleep stages. High frequency beta waves appear in frontal areas when concentrating and as background activity in tense and anxious subjects.

2.3.2 Intracranial electrodes

Besides placing electrodes on the scalp, invasive electrodes can be placed in the vicinity of brain areas that are suspected to cause a disorder. The EEG recordings obtained from these electrodes are referred to as intracranial EEG recordings. Different types of electrodes are used depending on the clinical situation and application [40, 102]. Subdural electrodes are used to localize epileptiform activity and to map cortical function. They consist of sheets or single column strips embedded in a thin layer of flexible translucent Silastic rubber. The sheets are inserted through craniotomy opening. Once the electrodes are in place the underlying cortical activity can be recorded.
Depth electrodes are used for EEG recording to define the targets for surgical removal, and for placement as stimulating electrodes for the treatment of movement disorders. The depth electrodes consist usually of a bundle of fine wires that terminate at different cylindrical contacts along the length of the depth electrode and thus allow for recordings from different depths (Fig. 2.8).

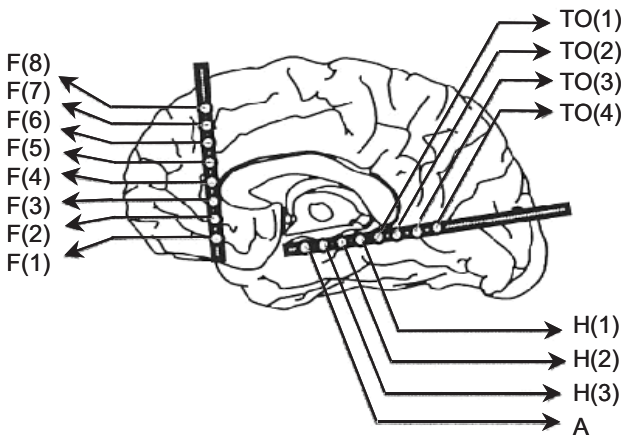

Figure 2.8: *Intracranial depth electrodes. From [73].*

2.3.3 The limitations of scalp/intracranial EEG recordings

One must keep in mind that scalp EEG recordings detect only a portion of the underlying brain electrical activity. The mechanisms by which the cortical activity is altered at the scalp level are not fully understood. From a practical point of view, however, some general principles can be recognized [116, 41]. At a very basic level, it is known that the amplitude of a recorded electrical signal is inversely proportional to the square of the distance from the signal origin to the recording electrode [49]. This simplistic concept illustrates that scalp electrodes will be less sensitive to discharges that originate from deep brain structures. It is also obvious that the scalp EEG is attenuated to a certain degree by the electrical conductive properties of the intervening brain tissue, meninges, skull and scalp. It appears that the coverings of the brain act as "low-pass" filter [30]. The principles of volume conduction provide further explanation for the alteration of scalp recorded signals. Volume conductor theory predicts that the ability of any electrode to record the potential produced by a dipole generator at some distance is critically dependent upon the geometric orientation of the recording electrode to the dipole layer of interest [49]. Dipole orientations which are 'aimed' towards the electrode are favorable.

Intracranial recording technique can overcome some of the limitations of surface technique. With optimal intracranial electrode placement, it is obviously possible to shorten the distance between a potential generator and the electrode. The

selective attenuation of fast frequencies noted with scalp technique should not be a problem. The problem of geometric orientation is still present with intracranial technique, although with different ramifications.
In summary, when a focal intracranial EEG potential of interest is not detected by surface recording technique, various factors may be responsible: (a) the scalp electrode may be simply too far away, (b) the potential of interest may be fast enough to be averaged out by the intervening layers, (c) the scalp recording electrode may have such a geometric orientation to the dipole generator that the electrical signal is not recorded.
As a consequence, intracranial EEG may be superior to the scalp EEG, as it is possible to record the localized, low amplitude and fast frequency discharges that originate from deep brain structures. Moreover, as scalp electrodes are non-invasive, potentials that are generated by sources other than the brain are picked up by scalp electrodes and recorded together with the EEG. These potentials are referred to as artifacts and will be discussed in the next section. However, intracranial EEG has also important limiting factors [116]. Only a small part of the cortex is investigated by intracranial electrodes. This restriction is a major limiting factor with intracranial recording technique. Moreover, the electrodes must be placed accurately and cover all suspicious areas for successful monitoring. Furthermore, invasive examinations carry a risk of complications such as bleedings and infections in 2% of the patients.
This limited discussion does not constitute an adequate explanation for all discrepancies between surface and intracranial recordings, nor is intended to do so. The point to be made is that EEG at the scalp level is altered and may not provide a sufficient assessment of underlying brain electrical activity.

2.3.4 Artifacts

Potentials that are generated by sources other than the brain that are picked up by scalp electrodes and recorded together with the EEG are referred to as artifacts. Artifacts may be divided into two categories depending on their origin: physiological artifacts or non-physiological artifacts [33]. For instance scalp electrodes located over muscle frequently record muscle fibre activity. Movements of the eyes, tongue and other large and electrically charged structures also generate changing electrical fields, which are recorded by scalp electrodes. Heart muscle contraction can induce potential changes at scalp electrodes similar to the potential changes recorded in the ElectroCardioGram (ECG). Strong sources of alternating current near the recording site may interfere with the recording. Below, the two most common artifacts, ocular artifacts and muscle artifacts, are discussed in detail, followed by a brief overview of the other artifacts found in scalp EEG recordings.

Ocular artifacts

There are three artifacts originating from the eye: eye blinks, and vertical and horizontal eye movements [33].

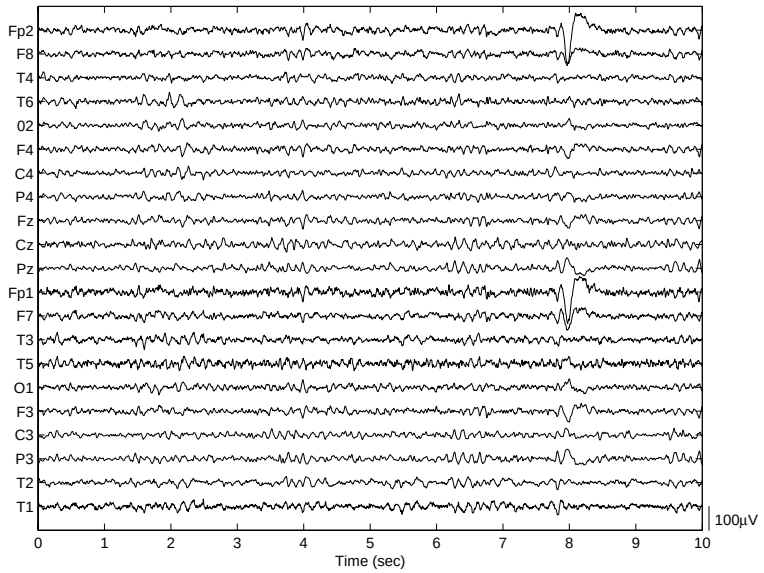

Figure 2.9: *10 s EEG epoch containing an eye blink at t = 8 s. An average reference montage was used.*

Eye blink artifacts originate from alterations in ocular conductance arising from contact of the eyelid with the corona. The alterations produce a short high amplitude signal, often many times larger than the EEG signals of interest. Their contribution is largest in the frontal $Fp1$ and $Fp2$ electrodes and decreases rapidly with distance from the eyes. Fig. 2.9 shows a 10 s EEG epoch containing an eye blink at t = 8 s.

Movements of the eye cause potential changes that are picked up mainly by frontal electrodes, although they may extend into central and temporal electrodes. A simple way of understanding eye movement artifact is to picture the front of the eye as a positive charge that either moves towards or away from the recording electrodes. The electrodes that record the largest potential changes with vertical eye movement are $Fp1$ and $Fp2$ because they are placed above the eye. The electrodes that record the largest potential changes with horizontal eye movements are $F7$ and $F8$ because they are approximately lateral to the eyes. Eye movements artifact in the EEG can usually be identified by their frontal distribution, their symmetry and characteristic shape.

Eye blinks and movements may be monitored by electrodes placed near the eyes and linked so that ocular activity can be distinguished from cerebral activity. This recording, also called ElectroOculoGram (EOG), is often displayed simultaneously with the EEG. Comparison of these recordings allows clear identification of the ocular artifacts. However, in our setup no EOG signals were available.

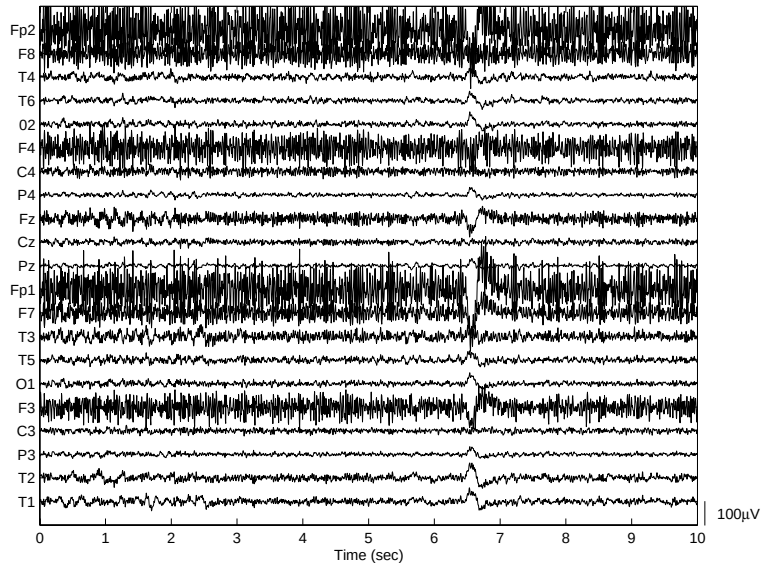

Figure 2.10: *EEG recording contaminated with muscle artifact. An average reference montage was used.*

Muscle artifact

The EEG is frequently contaminated by electrophysiological potentials associated with muscle contraction due to biting, chewing and frowning. These muscle artifacts, also known as ElectroMyoGram (EMG) artifacts, obscure the EEG and complicate the interpretation of the EEG or even make the interpretation unfeasible [125]. Muscles are composed out of different motor units, each comprising a motor neuron and a group of innervated muscle fibres. The recruitment of several motor units when contracting a muscle, leads therefore to a complex electrical activity, which is recorded by the EEG. Muscle activity causes very short duration potentials that usually occur in clusters or periodic runs. If they recur in rapid bursts of discharges, they can produce several types of potentials that can merge and obscure the recording of cerebral activity. It is known that EMG artifacts have a broad frequency distribution from 0 to > 200Hz, which overlaps with the frequency distribution of cerebral activity [53]. Muscle artifacts from scalp and face muscles occur mainly in frontal and temporal regions but may be recorded by electrodes nearly anywhere on the head. A muscle artifact is usually easily identified by its shape and repetition. It can be reduced by asking the patient to relax, drop the jaw or open the mouth slightly, or change position. As an example, Fig. 2.10 shows an EEG recording contaminated with muscle artifact.

Other artifacts

We order the remaining artifacts according to their origin: physiological or non-physiological [33].
Physiological artifacts arise from a large variety of body activities that are either due to (1) movements of the head, body or scalp, (2) moving electrical potentials within the body or (3) skin resistance changes due to sweating.
Non-physiological artifacts arise from two main sources: (1) external electrical interference from other power sources such as power lines or electrical equipment, and (2) internal electrical malfunctioning of the recording system, arising from recording electrodes, electrode positioning, cables or amplifiers.

2.3.5 Application areas of EEG

The scalp EEG remains the simplest method to examine brain activity and provides the best temporal resolution. It is a valuable tool for diagnosis of neurological disorders or diseases and to study human brain functioning. Three main research application areas can be distinguished: analysis of sleep disorders, event related potentials and epilepsy diagnosis [105].
Overnight EEG recordings are used in sleep laboratory to evaluate patients with sleep disorders. The sleep EEG can be divided into different sleep stages, based on typical EEG patterns. Abnormalities in the sleep EEG may be found when compared with normal sleep EEG [104, 8].
Electroencephalography is also used as a method to study human brain functioning. Small EEG changes related to particular events are investigated. The research field dedicated to the detection, quantification, and physiological analysis of those slight EEG changes that are related to particular events has been of growing interest in recent years. These EEG changes may be treated globally under the common title "event-related potentials"(ERP) [85]; a subset of ERPs is sensory evoked potentials (EPs) [14, 15, 32]. The basic problem of analysis is detecting ERP activity within the often much larger background activity. By superposition of time locked responses, this problem is solved as the response is enhanced in contrast to the background activity.
Finally, electroencephalography fiends clinical use in the diagnosis of epilepsy. Since the techniques presented in this work are related to this research field, a separate section is dedicated to it. Some aspects of the present work, however, can be applied also in the analysis of sleep EEG and ERPs.

2.4 Epilepsy

Epilepsy is a neurological disorder characterized by abnormal discharges in the brain. An epileptic seizure is the clinical manifestation of epilepsy, characterized by a disturbance of mental, motor, sensory or autonomic activity. Several causes of epilepsy can be found, e.g., brain damage due to head trauma, a lack of oxygen

at birth, infection of the brain, presence of brain tumors, intoxication or brain malfunction. But in most cases the cause of epilepsy is not known.

2.4.1 Epileptic seizures

The character of an epileptic seizure is more or less strongly determined by the cerebral area involved. The site and origin of epileptic seizures in the brain is of great interest in that those of focal origin may be treatable surgically. Both cortical and subcortical foci have been found but in many patients there are no signs or symptoms indicative of a focus. The most widely used and generally accepted classification of seizures is that proposed by the Commission on Classification and Terminology of the International League Against Epilepsy (ILAE) (table 2.1) [103, 34]. It defines seizure types in terms of clinical manifestations and EEG findings. It differs from previous classifications because it is based on the study of videotape recordings of simultaneous recorded EEG and clinical epileptic seizures. Seizures can be classified clinically into two categories: partial and generalized (table 2.1). Partial seizures, the first major category, originate in a small group of neurons that constitute a seizure focus. These seizures produce symptoms involving body parts or mental functions which are most affected by the area of seizure involvement. Partial seizures can be either simple partial (without alteration of consciousness) or complex partial (with alteration of consciousness). A third subgroup of partial seizures are partial seizures evolving to secondarily generalized seizures. These seizure begin like other partial seizures and they then evolve into a generalized seizure either suddenly or after gradually spreading to larger areas of the brain.
Generalized seizures involve both hemispheres from the onset. Most generalized seizures begin and remain associated with loss of consciousness. Generalized seizures can be associated with impairment of consciousness without loss of muscle tone (absence), rhythmical movements (clonic), muscle contractions (tonic) or sudden loss of muscle tone (atonic).
A third category, unclassified epileptic seizures, is included because certain kinds of seizures cannot yet be properly characterized due to either a lack of data or a consensus of opinion among investigators.

In the category of partial seizures different types of epilepsy are defined according to the location of the epileptic focus. Temporal lobe epilepsy (TLE) was defined in 1985 by the International League Against Epilepsy as a condition characterized by recurrent unprovoked seizures originating from the medial or lateral temporal lobe. The seizures associated with TLE consist of simple partial seizures without loss of awareness and complex partial seizures (i.e., with loss of awareness). The individual loses awareness during a complex partial seizure because the seizure spreads to involve both temporal lobes, which causes impairment of memory. After temporal lobe epilepsy, frontal lobe epilepsy is the next most common type of epilepsy featuring partial seizures.

1. Partial (focal) seizures
   (a) Simple partial seizures (with motor, sensory, autonomic, or psychological symptoms)
   (b) Complex partial seizures
   (c) Complex partial seizures evolving to secondarily generalized seizures
2. Generalized seizures
   (a) Absence
      i. Typical (petit mal)
      ii. Atypical
   (b) Myclonic
   (c) Clonic
   (d) Tonic
   (e) Tonic-clonic (grand mal)
   (f) Atonic
3. Unclassified

Table 2.1: *International Classification of Seizures*

2.4.2 Epileptiform activity in the EEG

Typical waveforms appear in the EEG of patients with epilepsy. Ictal activity, epileptiform discharges during a seizure, and interictal activity, epileptic discharges between seizures can be distinguished [101, 37, 36].
The wave shape of interictal activity consists of spikes or sharp waves which may combine with slow waves to form a spike-and-wave complex; these discharges are usually intermittent but may repeat briefly with little or no variation of shape. Fig. 2.11 shows a 10 s EEG recording containing an epileptic spike at t = 4.5 s. This activity has a high amplitude for the EEG signals $Fp1 - F7$, $T3 - T5$ and $T9 - TP9$.
In contrast, ictal activity consists of rhythmical waves that continue to change in shape, frequency, amplitude and distribution as the discharge progresses. Many ictal discharges begin with low amplitude rhythmical activity which increases in amplitude and decreases in frequency. As an example, Fig. 2.12 shows a 10 sec scalp EEG recording from a long-term Epilepsy monitoring unit. This recording contains ictal activity from a patient with Mesial Temporal Lobe Epilepsy (MTLE). The epileptic activity is mainly present on the $T2$, $F8$ and $T4$ electrodes. The seizure EEG is contaminated with eye blinks and muscle artifact. The potential differences between electrodes located close to the onset zone typically have a higher amplitude than the potential differences further away from this zone. By inspecting the amplitude of the EEG we are then able to roughly localize the active brain area.
Although the shape of interictal and ictal patterns has a large variety between patients, most adult patients have only one or a few interictal and ictal patterns. Both interictal and ictal activity may be seen in the same recording, but interictal activity is usually seen much more commonly.

2.4.3 Presurgical evaluation

Epilepsy is the most common serious primary neurological disease affecting 1/200 persons. The incidence is 50/100.000 persons per year. In Belgium, therefore, around 5000 persons per year develop epilepsy. In around 30% of these patients, the epilepsy will not be controlled despite optimal regimes of antiepileptic drugs. This is called refractory epilepsy. Three to five percent of these patients, i.e. 150-250 per year, are candidates for epilepsy surgery, which renders around 60-70% seizure free, and gives a reduction in seizures of more than 90% in an additional 20% of the patients.
The aim of a presurgical evaluation is the delineation of the epileptogenic zone, i.e. that part of the brain that has to be removed in order to render a patient seizure free. The success of focal epilepsy surgery strongly depends on accurate identification of the seizure focus. Several technical examinations need to be performed to localize this zone. Modern technological modalities now utilized in localizing the surgical seizure focus include electrophysiology (Video-EEG monitoring), cerebral structural imaging (MRI and CT), cerebral function imaging (SPECT and

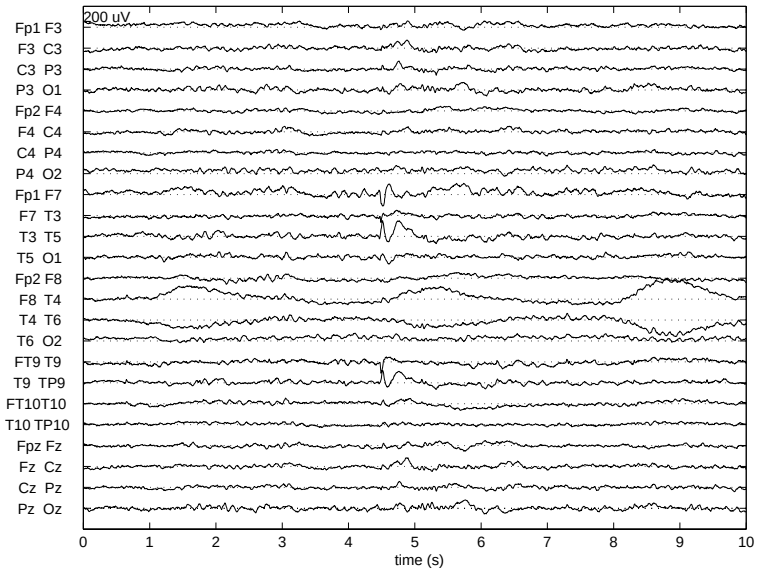

Figure 2.11: *Epoch of 10 s interictal EEG containing an epileptic spike at $t = 4.5$ s. A bipolar montage was used. This activity has a high amplitude for the EEG signals $Fp1 - F7$, $T3 - T5$ and $T9 - TP9$.*

PET) and magnetoencephalography (MEG) [124, 118, 123, 13, 12, 116]. When the findings of the different examinations lead to the same area, surgery can be considered.
The putative beneficial effect of surgery is an improvement in the quality of life that allow the individuals to become a participating member of society [129].

Fig. 2.13 shows a flowchart of the presurgical evaluation. After a thorough physical and neurological examination a series of non-invasive examinations is carried out. Long term (3-5 days) Video-EEG monitoring is essential in determining the localization of the epileptogenic zone. Surgical candidates are monitored continuously until (preferably) 3 typical seizures are recorded. The anti-epileptic treatment is decreased or stopped to precipitate a habitual seizure. The analysis of the behavioral changes and the ictal EEG is of major importance to localize the epileptogenic zone.

Structural abnormalities or lesions associated with partial epilepsy may be detected by neuroimaging techniques such as Magnetic Resonance Imaging (MRI) and Computed Tomography (CT). MRI has been shown to be superior in sensitivity and specificity to CT in identifying the structural abnormalities associated with partial epilepsy [45], and as a consequence, MRI is the structural neuroimaging procedure of choice.
A new and promising technique to identify the epileptogenic zone non-invasively

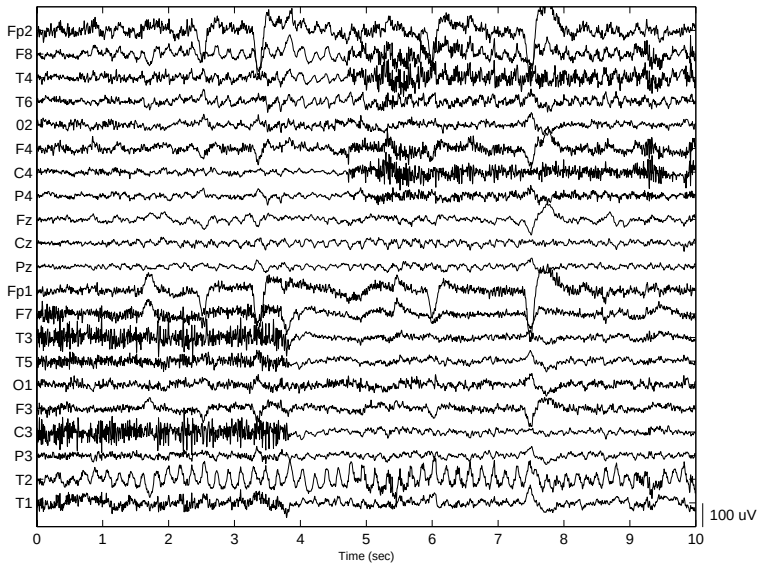

Figure 2.12: *10 sec scalp EEG recording from a long-term Epilepsy monitoring unit. This recording contains ictal activity from a patient with Mesial Temporal Lobe Epilepsy (MTLE). The epileptic activity is mainly present on the $T2$, $F8$ and $T4$ electrodes. The seizure EEG is contaminated with eye blinks and muscle artifact. An average reference montage was used.*

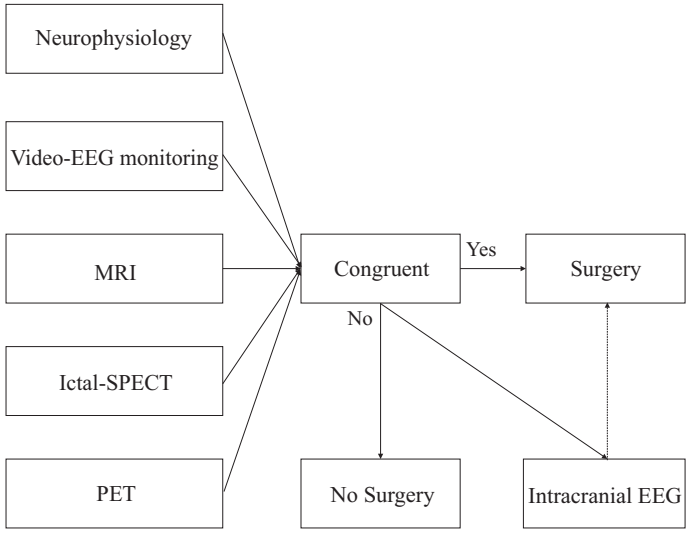

Figure 2.13: *Flowchart of the presurgical evaluation.*

is ictal single photon emission computerized tomography (SPECT). A SPECT scan is obtained by injecting a radioligand ECD (Ethyl Cysteinate Dimer) which travels with the blood to the brain, where it is taken up by the neurons and remains captured in the brain for up to three hours. The SPECT scan, which is obtained after the injection, shows the cerebral perfusion at the time of injection. The localizing value of ictal SPECT, i.e. with injection during an epileptic seizure, is based on cerebro-vascular coupling, i.e. an increase in neural activity is associated with an increase in cerebral blood flow.
Positron Emission Tomography (PET) detects changes in the regional blood flow and glucose and oxygen metabolism within the brain. Areas of glucose hypometabolism are often associated with epileptogenic zone.
The spatial relationship of the abnormal foci identified by the different modalities can be determined by coregistering all the foci to the MRI. When the different investigations indicate the same epileptogenic zone and when no major neurological deficit is expected by removal of this area, a multidisciplinary team decides to perform resective surgery. Psychological tests are carried out before the surgery to avoid the loss of cognitive functions like memory and speech.
However, when the foci determined by different tests are incongruent, further evaluation with other tests including a long term intracranial (invasive) Video-EEG monitoring may be considered. Subdural or depth electrodes are placed in the vicinity of the suspicious brain areas and the EEG recorded by these electrodes is monitored until at least 3 seizures are recorded. The invasive recordings may be superior to the scalp recordings as no artifact contaminate the measurements

and deep structures can be observed. As a consequence, intracranial EEG recordings may reveal more information that can be used for the localization of the epileptogenic zone. Furthermore, the relationship between the ictal onset zone and functional cerebral cortex can be explored in more detail. However, there are limiting factors. Only a small part of the cortex is investigated by intracranial electrodes. As a consequence, the electrodes must be placed accurately and cover all suspicious epileptogenic area for successful monitoring. Furthermore, invasive examinations carry a risk of complications such as bleedings and infections in 2% of the patients.

Some patients who are unsuitable for resective surgery may benefit from vagus nerve stimulation [121, 5]. Through an implanted device and electrode, electrical pulses are administrated to the left vagus nerve in the neck. Clinical trails indicate that this procedure is well tolerated, has no serious side effects, and reduces seizure frequency by 50% or more in a third of patients.

2.4.4 Contribution of presented work to the presurgical evaluation

This thesis focusses on the signal preprocessing and processing of scalp EEG signals. The presented work can be of importance in two modalities of the presurgical evaluation of patients with refractory epilepsy; namely ictal-SPECT and Video-EEG monitoring.

1. *Ictal-SPECT: Detection of pre-ictal state*
   Injections for ictal SPECT are performed by medical personnel who witness the seizure, which results in a delay between seizure onset and injection. During this time, seizure activity may spread and result in false lateralization or localization on ictal SPECT. This delay between seizure onset and injection of the ligand could be shortened if we could determine the pre-ictal state, i.e. the period immediately preceding the epileptic seizure. Moreover, there is some preliminary evidence to suggest that SPECT scan with injection in the pre-ictal state may provide localizing information. The detection of a pre-ictal state based on scalp EEG recordings is the research topic of chapter 3. In this chapter a nonlinear analysis technique used for seizure prediction on scalp EEG recordings is evaluated.

2. *Visual interpretation of ictal EEG: Removal of artifacts*
   The potential disadvantages of Video-EEG recordings include the inherent cost of hospitalization and the need for special resources and personnel. Also the ictal scalp-EEG patterns may be difficult to interpret because of muscle and ocular artifacts [125]. The presence of a subtle epileptiform discharge may be difficult to distinguish from the background. For example, Fig. 2.14 shows a 10 s ictal EEG recording which is difficult to interpret. The EEG

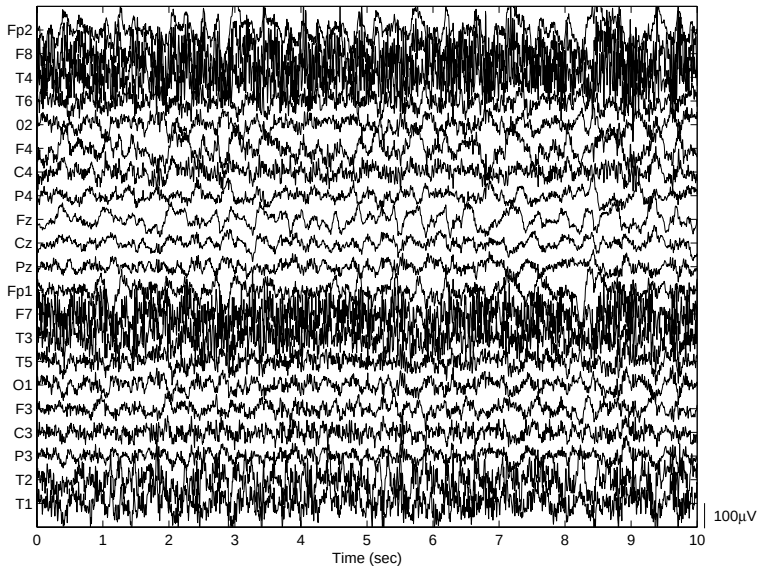

Figure 2.14: *Ictal EEG recording contaminated with muscle artifact. An average reference montage was used.*

recording is severely contaminated with muscle artifacts which masks the ictal EEG. In chapter 4 and 5 of this thesis, two newly developed artifact removal techniques are presented. These techniques can be used to obtain a clean and artifact free EEG which is easier to interpret. In chapter 4, a technique is presented which removes artifactual and background activity and enhances epileptiform interictal and ictal activity. Chapter 5 describes a semi-automatic muscle artifact removal technique which is already used in clinical practice.

However, it should be noted that the methods presented in this work have also application in other EEG research areas such as sleep EEG and ERPs, and in research areas other than EEG. These applications will be highlighted in the separate chapters.

2.5 Conclusion

In this chapter an introduction was given to both electroencephalography and epilepsy. First, the neurophysiological phenomena responsible for generating the EEG, the acquisition, and the different application areas of EEG were briefly described. Next, we focused on the application of EEG in the diagnosis of epilepsy. Based on the ictal EEG findings and clinical manifestations, epileptic seizures are classified according to the classification of the International League Against

Epilepsy. Furthermore, the EEG is utilized in localizing the seizure focus. In section 2.4.4 the contribution of this thesis to the presurgical evaluation of patients with refractory epilepsy was highlighted.

Chapter 3

Epileptic seizure prediction

3.1 Introduction

Epilepsy affects more than 50 million individuals worldwide -about 1% of the world's population. Two-thirds of affected individuals have seizures that are controlled by anti-epileptic drugs. Another 7-8% can be cured by epilepsy surgery. Thus, in about 25% of individuals with epilepsy, seizures cannot be controlled by any available therapy. One of the most devastating features of epilepsy is the apparent unpredictable nature of seizures. Every day activities are impaired and can become dangerous for patients [16]. The unpredictability of seizure onset is one of the most important causes of morbidity and stress in patients with epilepsy [98, 9]. Being able to predict the onset of seizures would render the implementation of alarm systems and novel therapeutic approaches possible; e.g. automated interventional measures like the application of anticonvulsant drugs or electrical brain stimulation [127, 50]. Implementing a bedside system of seizure anticipation in a Video-EEG unit would be of considerable help for efficient seizure monitoring and for the injection of the radioactive tracer in ictal SPECT examinations. Optimally, the tracer must be injected at seizure onset as soon as possible. Often this procedure is not informative enough due to a late injection, tens of seconds after the onset, which marks the areas of propagation more than the actual epileptogenic zone. In addition, the identification of a pre-ictal state could contribute to the investigation of the pathological mechanisms causing seizures.

A pre-ictal state may be defined as a condition of the epileptic brain and its functioning that inevitably evolve into a seizure unless some kind of intervention takes place. Given the *a posteriori* knowledge of a seizure occurrence, it appears rather trivial to postulate the existence of such a state. However, its unequivocal *a priori* definition, and with it the possibility to anticipate an impending seizure, is obviously far from being trivial. Whether this pre-ictal state can be detected by quantitative analysis methods applied to EEG has been a focus of much in-

terest in recent years. This resurgence of interest has been motivated by several factors, including the proliferation of powerful new methods for analyzing nonlinear system dynamics, as well as the interest in developing epilepsy control devices.

This chapter is organized as follows: in section 3.2 a literature overview is given of state-of-the-art nonlinear seizure prediction methods. It turns out that many of the earlier studies reporting on seizure prediction are incomplete and the predictive ability of the nonlinear measures is very low. In section 3.3 we report on the low ability of the similarity index to predict seizures on scalp EEG recordings. We were the first research group reporting on these negative findings in the Lancet [21]. Later on, many other studies confirmed our results, showing that nonlinear methods have a very low predictive ability not only on scalp EEG signal but also on intracranial EEGs. An overview of these studies will be given in section 3.4. Furthermore, by illustrating the sensitivity of the similarity index to artifacts, we propose an additional preprocessing step for scalp EEG recordings in which artifacts like eye blinks and muscle artifacts are removed. In section 3.5 we end up with a summary of conclusions which we can draw from this chapter.

3.2 Detecting pre-ictal states by nonlinear EEG analysis

Several studies indicate that nonlinear time series analysis bears potential capabilities to extract features from EEG activity that can be regarded as precursors of impending seizures ([79, 80, 57, 58, 59, 89, 100, 62, 109, 122]; for recent reviews see [78, 84, 83, 75]). In this section, the basic principles of nonlinear time series analysis will be introduced and a literature overview will be given of the different studies reporting on seizure prediction. Next to the studies based on nonlinear methods, other studies reported on the detection of a pre-ictal state based on measuring the synchronization between different brain regions using intracranial electrodes [93, 92, 70, 76, 77]. In Appendix B, the concept of synchronization is discussed in more detail.

First, the concept of a state space representation is introduced. Rather than a time or frequency domain approach, the state space representation is the hallmark of nonlinear dynamical time series analysis.

3.2.1 State space reconstruction of the observed dynamical system by the method of delays

In mathematical models of dynamical systems the dynamics is described in their state space, whose integer dimension is given by the number of variables of the model. In experiments, however, usually one variable is measured as a function of time, and the state space is not known. Given that a complex dynamic system

(e.g. the brain) can involve an enormous number of interrelated dependent variables that are impossible to measure directly, the main problem is how to analyze a multidimensional dynamic system knowing that only a few variables can be measured. Although an unknown system may well be dependent on a large-and for the EEG often unknown-number of variables, the mathematical theorem of Takens [128] states that it is possible to make quantitatively meaningful inferences about the underlying dynamical structure of the system from the behavior of a single observed variable (e.g. one channel EEG). He proved that it is possible to reconstruct, from a scalar time series only, a new state space that is diffeomorphically equivalent to the (in general unknown) original state space of the experimental system. The reconstruction of the observed system dynamics in a so-called state space is the basic principle of almost all nonlinear time series analysis techniques. A well established implementation of this state space reconstruction of the dynamical structure from one observable is through the method of delays [65]. A state space can be constructed by taking successive points of the original time series separated by a fixed time delay τ. Let $V(t)$ be the EEG recording recorded at time t and let m delayed amplitudes be recorded on an individual channel. At each time t, the state of the neuronal activity is represented as a point A_t in an m-dimensional space:

$$A_t = [V(t), V(t+\tau), \ldots, V(t+(m-1)\tau)]. \tag{3.1}$$

A sequence of such states followed in time defines a trajectory. The geometrical properties of the trajectories evolving in state space can be expressed quantitatively using nonlinear measures. Fig. 3.1 illustrates the method of delays; a close-up is shown of a brief segment of EEG and a plot of the trajectory of the EEG made by the method of delays with an embedding dimension of three and a time delay equal to one. The vectors A_t are called delay vectors.

3.2.2 Nonlinear measures for the characterization of the dynamical behavior of a system

Based on the reconstructed states the time series can be analyzed from the point of view of nonlinear dynamics. A variety of new concepts and measures have been developed that allow one to characterize fully the dynamical behavior of an unknown system in a theoretic sense: Lyapunov exponents characterize the system's stability under some small perturbation, and thus are measures of how chaotic a system behaves; dimension estimates are closely related to the number of degrees of freedom of a system; and entropies measure the degree of order/disorder. Dimension estimates and entropies can thus be regarded as an estimate of the system's complexity. For a full description of these measures we refer to [65]. These concepts allow one to describe sufficiently a nonlinear dynamical system as shown for well-known model systems that can be used to produce arbitrarily long and stationary time series at almost infinite precision. In contrast, a bulk of literature indicates a reduced importance of nonlinear time series analysis tech-

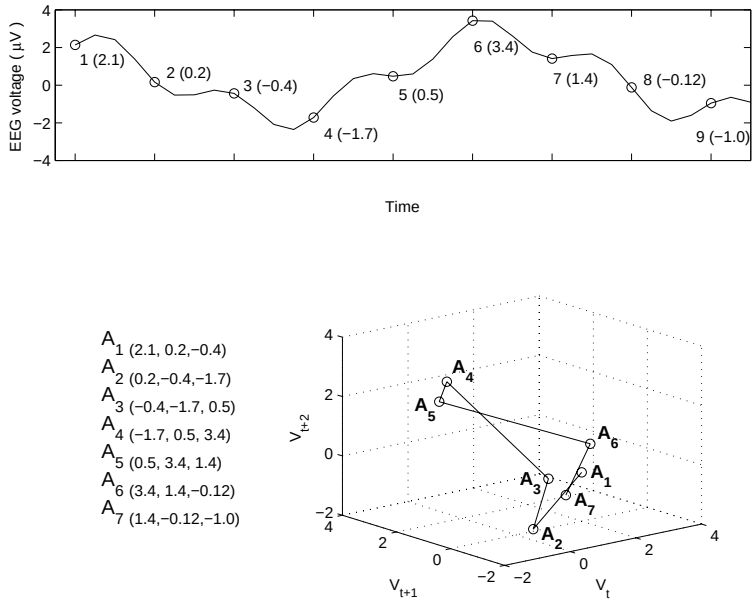

Figure 3.1: *A demonstration of the method of delays applied to a brief segment of analogue EEG sampled at nine points along the waveform. The upper part of the figure shows a one channel EEG trace sampled at individual points 1−9, with the voltage measurement at each point written beside each sampled point. The lower part shows the coordinates of each delay vector A_t. The trajectory connecting the delay vectors in the 3-dimensional state space is also given.*

niques when applied to, short, noisy, and nonstationary time series like the EEG-generated from a system with an almost unknown structure. Despite these shortcomings, it is commonly accepted today that nonlinear analysis is nonetheless able to provide new and relevant information as long as the limitations of the techniques are taken into consideration and the results are interpreted carefully.

3.2.3 Nonlinear measures and the detection of a pre-ictal state

Attempts to detect seizures automatically from EEG are not new. Initial attempts at anticipating seizure onset before the first intracranial electrical changes relied on conventional EEG analysis both in time and frequency domain [115, 117, 110, 66]. The prediction of seizure onset does not exceed more than a few seconds before visual detection of the seizure.
In recent years, following the renaissance of nonlinear dynamics and the realization that processes in the brain embodied nonlinearities in their dynamics, several studies based on nonlinear analysis of EEG recordings have provided evidence that the interictal-ictal state transition is not always an abrupt phenomenon. Historically, Babloyantz and Destexhe (1986) were the first to demonstrate that the nonlinear analysis of EEG recordings from patients with epilepsy can provide new perspectives regarding epileptogenesis. They showed that the correlation dimension for seizure activity is of lower value than for the normal activity. These findings support the hypothesis that generation of ictal activity in the brain correspond with a specific dynamic state that is different from normal, ongoing activity. A decreased level of complexity in neuronal networks is involved in the epileptic process.
Using an estimate of the largest Lyapunov exponent of the EEG, Iasemidis and Sackelares (1990) showed that the transition between normal and ictal EEG is characterized by a drop of this exponent, the earliest changes being detectable minutes before the onset of the seizure [57]. They were the first to show that nonlinear analysis can reveal pre-ictal changes in the EEG. However, this study was based on a few recordings and had no statistical validation of the significance of the nonlinear measure. From this study, it was not clear whether similar variations of the largest Lyapunov exponent can even be observed during the interictal state. This made it difficult to draw definite conclusions.
In 1998, within a few months of each other, Lehnertz et al. (1998) [79] and Martinerie et al. (1998) [89] reported that epileptic seizures could be predicted by applying nonlinear analysis to intracranial EEG recordings. These studies reported that the evolution to a seizure involves not just two states −interictal and ictal−, but also a pre-ictal transitional phase of several minutes that differs dynamically from the other two. Lehnertz et al. estimated an effective correlation dimension from intracranial EEG data of 16 patients with MTLE. They showed that, in all but one patient, changes towards long-lasting (up to 25 min) and lower dimensional states occurred before the seizure and were more pronounced

as compared to maximum changes occurring during interictal state, thus enabling to define a pre-ictal state. Martinerie et al. reported similar findings in a comparable group of patients.
Nonlinear EEG analysis and seizure prediction became hot issues after the appearance of these two papers. Since then many laboratories have tried to replicate and improve these results ([80, 59, 100, 62, 109, 122, 78, 84, 83, 75]). Significant advances were made when a newly developed measure of non-linear analysis −the similarity index− which improves the robustness and increases calculation speed has shown that seizure prediction is also possible with scalp EEG recordings and with extra temporal seizures [74, 100]. Prediction from surface electrodes will be discussed in more detail the next subsection.
All these findings indicate that nonlinear measures are able to detect a pre-seizure state of several minutes, anticipating the electroclinical onset of a seizure. This pre-ictal state could become the basis to anticipate seizures in clinical applications. However, all these studies were based only on low number of seizures per patient and short interictal data segments. Moreover, one of the major shortcomings for all studies reporting on seizure prediction is the lack of attention to the sensitivity and specificity of the nonlinear method used. The acceptance of seizure-preceding changes as predictive depends critically on the variability of the changes during the interictal periods evaluated. As Litt and Lehnertz (2002) pointed out [84], seizure prediction methods should be assessed based on long-term EEG recordings.

3.2.4 Prediction of epileptic seizures from scalp EEG recordings

Most of the work in seizure prediction has concentrated on analysis of intracranial EEG (ICEEG). Over the long term, however, the application to scalp EEG recordings is fundamental for the applicability of seizure prediction methods in real life. An important goal of nonlinear studies in epilepsy is to develop ambulatory monitoring methods with a view to being able to predict seizures. Clearly, an ambulatory monitor that relies on recordings from scalp electrodes is likely to be much more easily tolerated and maintained than one that relies on ICEEG. Moreover, as noninvasive methods of determining a seizure focus improved, the number of ICEEG studies decreased, limiting the available database.
Unfortunately scalp EEG recordings have some disadvantages compared to ICEEG. It is known that neuronal activity generated within the brain is filtered spatially between the neocortex and the scalp. This occurs because of the physical separation of the electrode from the nearest neuronal source and the smearing effect of the skull [41]. Aside from signal attenuation and poor spatial resolution, scalp EEG is well-known to be contaminated by eye blinks and muscle artifacts, which may render delicate and even questionable the detection of changes with current nonlinear measures.
Moreover, ICEEG and scalp EEG probe different dynamic mechanisms. ICEEG

records from relatively small regions of the brain near suspected ictal onset zone, limiting the extent to which it can probe spatially. Scalp EEG cannot be thought of merely as signal degraded ICEEG because of cortical convolutions, anatomic anisotropies, and the orientation, shape, and extension of the underlying generators.
Keeping in mind these uncertainties, Le Van Quyen and colleagues reported on the detection of a pre-ictal state when applying the similarity index, a method previously used on intracranial EEG, to scalp EEG. They demonstrated for the first time that scalp EEG reveals the pre-ictal state. Anticipation of epileptic seizures from non-linear changes in standard EEG recordings has been reported in 25 of 26 recordings of mesial temporal lobe complex partial seizures (mTLCPS) [74].
As was mentioned in [43], these results seem rather surprising given the attenuation and contamination of the scalp recordings. The author stated that a confirmation of these findings by other research groups is needed. Our group tried to replicate these findings and to detect a pre-ictal state preceding mTLCPS using the similarity index of scalp EEG recordings. In the next section, we describe the similarity index and report on our results using this method on a data set of 12 patients with MTLE.

3.3 Prediction of epileptic seizures from scalp EEG recordings: a study on the similarity index

Our group tried to replicate the findings of [74] and to detect a pre-ictal state preceding mTLCPS using the similarity index of scalp EEG recordings. First, the similarity index is described. Next, our results obtained on a data set of 12 patients with MTLE are reported and the robustness of the similarity index to muscle artifacts and eye blinks is tested on synthetic data. Finally, possible reasons for the discrepancies between our findings and those reported in literature are discussed.

3.3.1 Method: similarity index

In this section, the similarity index is described. The method is fully described in [73], and can be summarized briefly as follows: first the EEG is not directly embedded from all of its digital sampled points but only the time points when the trace crosses the zero voltage axis, and the voltage curve is upward, are used to reconstruct a trajectory. The trajectory of the EEG signal is calculated in a 5 min reference window far from seizure onset; it is then compared with the computed trajectories in 30 s test data epochs in the EEG as seizures approach. A pre-ictal state is defined when the similarity index remains 5 standard deviations under the reference state up to the seizure without interruption. Below, each step of the method is discussed in detail. The same parameter settings are used as in [74].

Reconstruction of EEG dynamics by time intervals

The recording was segmented into consecutive non-overlapping windows W_t of 30 s duration. For each window W_t, the signal was transformed to pure-phase information by taking the sequence time intervals between positive going crossings of the signal through the electrical zero (Fig. 3.2 A). Let the times of zero-crossings be denoted by T_n and let $I_n = T_{n+1} - T_n$ be the time intervals between two successive crossings. These timings are not affected by the fluctuation of amplitude (e.g. spikes), and the noise components are to some extent filtered out. Furthermore, the approach achieves a substantial decrease (by ten orders of magnitude) in the volume of data, providing the computational speed for real time procedures. From this sequence of time intervals, the EEG dynamics are reconstructed by the method of delays with m-dimensional embedding (m is the number of dimensions of the reconstructed dynamics; in this study $m = 16$), using m consecutive ($\tau = 1$) time intervals $A_n = (I_n, I_{n+1}, \ldots, I_{n+m-1})$ (Fig. 3.2 B). Finally, $\mathbf{A}(W_t)$ is the trajectory matrix of window W_t (i.e. the matrix whose rows are the embedding vectors A_n), representing the dynamics of W_t .

Measure of similarity between distant EEG windows

The dynamical similarity between any pairs of EEG windows W_i and W_j is quantified by the cross-correlation ratio:

$$S(W_i, W_j) = \frac{C(W_i, W_j)}{\sqrt{C(W_i, W_i)C(W_j, W_j)}}, \tag{3.2}$$

with:

$$C(W_i, W_j) = \frac{1}{N_i N_j} \sum_{n=1,N_i} \sum_{p=1,N_j} \Theta(\|A_n(W_i) - A_p(W_j)\| - r)), \tag{3.3}$$

where Θ is the Heaviside step function, $\|\cdot\|$ the Euclidean norm and N_i (respectively N_j) denotes the number of elements in each set. In the present application, the distance r is defined typically at 30% of the cumulative distribution of pairwise Euclidean distances between the vectors of the reference set. S ranges from 0 to 1 and provides a sensitive measure of closeness between two dynamics (Fig. 3.2 C).

Detection of pre-ictal state by comparison with a reference state

The dynamics corresponding to each successive EEG window W_t were compared with that of a reference window W_{ref}. To give the most general picture of the pre-seizure changes, a long reference period W_{ref} was taken during a stationary sequence. It preceded the seizure by at least 50 min and had a duration of 300 s. This reference window W_{ref} was chosen during a normal state of the patient, i.e. far from the seizure, free of artifacts and containing common features of interictal

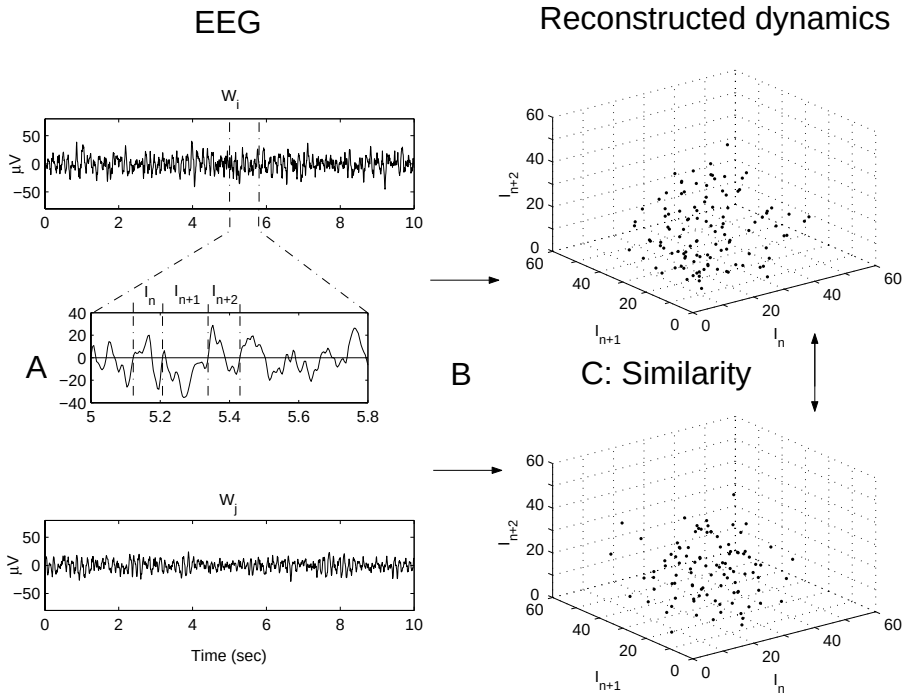

Figure 3.2: *Quantification of the dynamic similarity between different parts of the recording. For pairs of windows W_i and W_j (not necessarily adjacent in time), the first step (A) is to reduce the recording into sequences of time intervals I_n between successive positive going zero-crossings. The second step (B) is to define a multidimensional reconstruction of the dynamics by a time delay embedding of the intervals $(I_n, \ldots, I_{n+1}, \ldots, I_{n+m1})$ where $m = 16$ in our computations, but here $m = 3$ for a schematic representation. The third step (C) is to quantify the statistical measure of closeness between the two reconstructed dynamics by the cross-correlation ratio.*

activity. The reference window started at the same time for all channels. In order to allow comparison of dynamics between this long reference window W_{ref} and shorter test windows W_t (30 s), a subset of points in the reference reconstruction were selected by a random selection. Hereby, the number of points in this subset corresponds to the number of points in the reconstruction of the test window. This subset of embedding vectors form the rows of the trajectory matrix $\mathbf{A}(W_{ref})$. In order to further improve this dynamical reconstruction and reduce the noise level, a Singular Value Decomposition (SVD) of this m-dimensional embedding space was applied, identifying the optimal space that contains the trajectory. A SVD of $\mathbf{A}(W_{ref})$ can be computed with conventional algorithms by the transformation

$$\mathbf{A}(W_{ref}) \rightarrow \mathbf{X}(W_{ref}) = \mathbf{A}(W_{ref}) \cdot \mathbf{V}, \tag{3.4}$$

where $\mathbf{X}(W_{ref})$ is the trajectory matrix projected onto the basis $\mathbf{V}$ defined by the eigenvectors of the covariance matrix $\mathbf{A}(W_{ref})^T \cdot \mathbf{A}(W_{ref})$. The dynamics in the space defined by the largest singular values is identical to the original space [1]. Then the 16-dimensional reconstruction of W_t, $\mathbf{A}(W_t)$, is projected on the principal axes of the reference dynamics

$$\mathbf{X}(W_t) = \mathbf{A}(W_t) \cdot \mathbf{V}, \tag{3.5}$$

where $\mathbf{V}$ is the eigenvector matrix of the reference window. In order to retain the main components of the dynamics and to reduce the noise level, the embedding dimension was reduced to $m = 4$ by truncation of $\mathbf{V}$. We then computed the similarity between this reference dynamics $\mathbf{X}(W_{ref})$ and the dynamics $\mathbf{X}(W_t)$ of the test window, which slides over the whole recording period. The time course of the similarities, the similarity profile, provides information about long-term changes before seizure onset. If the EEG is stationary, the similarity index yields a value close to 1. By contrast, if changes in the dynamical state occur, the similarity index decreases below 1. A pre-ictal state is defined when the similarity index remains 5 standard deviations under the reference state up to the seizure without interruption.

3.3.2 Materials

Scalp EEG recordings from 13 patients who required continuous EEG recording and video monitoring to localize seizure onset were used for this study. Their clinical characteristics are summarized in Table 3.1. Twelve out of thirteen patients had mesial temporal lobe complex partial seizures (mTLCPS) associated with hippocampal sclerosis, and became seizure free for more than two years after surgery. The EEGs of these patients were recorded on 21-channel OSG EEG recorders and Oxford EEG recorders. The electrodes were placed according to the international 10-20 system with additional electrodes $T1$ and $T2$ on the splenoid. The sampling frequency was 250Hz and 256Hz for the OSG and Oxford system setup, respectively, and an average reference was used. To avoid changes induced by variation of arousal states only seizures in which the patients were awake for

the entire recording were studied. The EEG data of 60 minutes preceding and 30 minutes after the clinical seizure onset were used in the analysis. Clinical seizure onset was determined by an experienced neurologist. The thirteenth patient had neocortical partial seizures (NPS) and had simultaneous scalp and intracranial EEG recordings. 29 intracranial electrodes and 3 scalp electrodes ($O1$, $O2$, $TP10$) were used. This recording was performed with a 32 channel Nicolet-BMSI system with a sampling frequency 200 Hz. The EEG data of this patient were kindly provided to us by Le Van Quyen and colleagues [100].

Patient	Age	Gender	Type of seizure	Epileptic Focus (ictal EEG)	No. of seizures analysed
1*	35	F	mTLCPS	Right (antero)temporal	2
2*	38	F	mTLCPS	Right (fronto)temporal	3
3*	51	M	mTLCPS	Right temporal	1
4*	31	F	mTLCPS	Right (antero)temporal	3
5*	36	M	mTLCPS	Right temporal	1
6*	32	F	mTLCPS	Right (fronto)temporal	1
7*	35	F	mTLCPS	Right (antero)temporal	1
8**	31	M	mTLCPS	Left (antero)temporal	1
9**	49	F	mTLCPS	Right (antero)temporal	1
10**	33	M	mTLCPS	(1) Bitemporal/(2) left temporal	2
11**	35	F	mTLCPS	Left temporal	1
12**	38	F	mTLCPS	Left temporal	1
13***	21	M	NPS	-	1

Table 3.1: *Summary of patient data. M= Male; F=Female. *OSG recorder; **Oxford recorder; ***Nicolet recorder.*

3.3.3 Results of study

Fig. 3.3 shows the analysis of the $O1$ scalp-EEG channel before the NPS. Different seizures occurred between window numbers 186-211. The reference state was chosen here from window 1 to 10. A sustained deviation beyond the statistical threshold of 5 standard deviations of the reference state (horizontal line) up to the onset of the seizure was recorded. A pre-ictal state could be defined beginning 21 minutes before seizure onset. The large deviation of the similarity index between window number 60-70 was caused by artifacts present in the analyzed windows. Similar results were obtained on the $O2$ and $TP10$ electrodes.

The similarity index was not able to detect pre-ictal changes in the scalp EEG recordings of all 12 patients with mTLCPS. Fig. 3.4 shows the result of the analysis of the $F4$ EEG channel before the seizure of patient 2. The seizure lasted from window number 146 to 153. The reference state was chosen from window 1

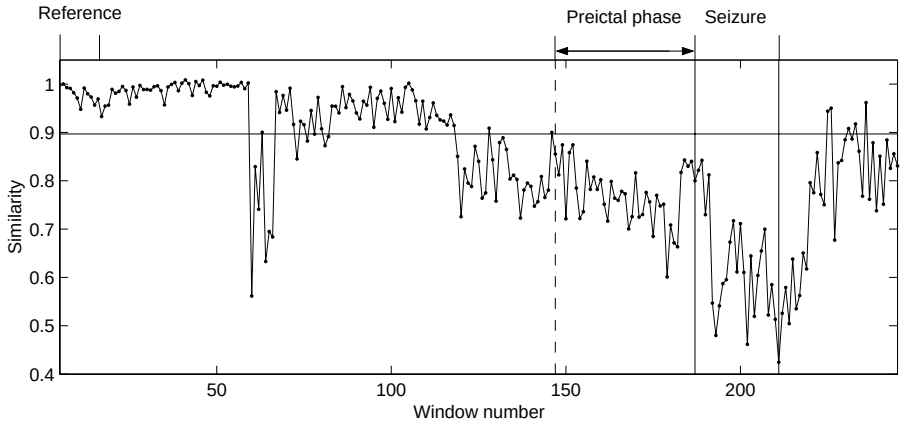

Figure 3.3: *The time course of the similarity index of the $O1$ scalp EEG channel of the patient with NPS (patient 13). The reference state was chosen from window number 1 to 10. Several seizures occurred between window numbers 186-211. The threshold is represented by the horizontal line. A pre-ictal state could be defined beginning 21 minutes before seizure onset. The large deviation of the similarity index between window number 60-70 was caused by artifacts.*

to 10. The similarity measure stayed high until the start of the epileptic seizure. The deviations of the similarity index beyond the statistical threshold are due to artifacts present in the analyzed time window. At the start of the epileptic seizure the similarity measure suddenly dropped. No sustained deviation beyond the statistical threshold of 5 standard deviations of the reference state (horizontal line) up to the onset of the seizure was recorded. A pre-ictal state could not be defined. Similar results were obtained on all other EEG channels and all other EEG recordings of the data set presented in Table 3.1. Furthermore, we tested the sensitivity of the similarity index to different values of the SVD truncation, radius and embedding dimension. The results are discussed in Appendix A.

As we observed that the excessive artifactual contaminated EEG recordings had more similarity drops beyond the statistical threshold, we have investigated the robustness of the similarity index to artifacts in the next subsection.

We also tried to detect pre-ictal changes by using the correlation dimension, previously used to detect pre-ictal changes in intracranial EEG recordings [79, 80]. The correlation dimension was unable to detect a pre-ictal state in the scalp EEG recordings of all patients [19]. However, one must keep in mind that scalp EEG recordings are more noisy than intracranial EEG recordings. Moreover, scalp EEG and intracranial EEG probe different dynamic mechanisms as discussed in section 2.3.3. Therefore, it is not straightforward that the methods used for the analysis

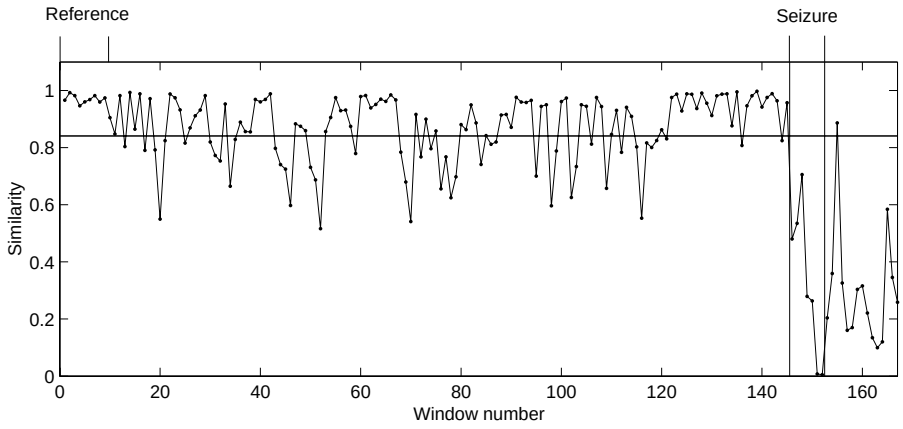

Figure 3.4: *The time course of the similarity index of the F4 scalp EEG channel of the patient 2. The reference state was chosen from window number 1 to 10. The seizure lasted from window number 146 to 153. The threshold is represented by the horizontal line. No pre-ictal state could be identified.*

of intracranial EEG will also reveal pre-ictal changes in scalp EEG recordings.

3.3.4 Robustness to artifacts

As mentioned before in section 3.2.4, one of the problems of scalp EEG is that scalp EEG recordings are well known to be contaminated by eye blinks and muscle artifacts, which may render delicate and even questionable the detection of pre-ictal changes with current nonlinear measures. As a solution to this problem, the authors of [74] suggest to follow the zero-crossing approach. They state that, by following this approach, the similarity index is very robust against noise and artifacts. In this section we test the robustness of the similarity method to muscle artifacts and eye blinks on synthetic data.

Robustness to muscle artifacts

An artifact free reference signal was chosen and a simulated muscle artifact signal was superimposed to this reference signal in order to test the sensitivity of the similarity index to muscle artifacts. Since muscle artifacts appear with different amplitude in the EEG, we performed several simulations with different noise levels.

Reference brain signal Fig. 3.5 (a) shows a 30 s EEG signal W_{Ref} recorded at electrode $C4$. In the selected signal no artifacts were present according to the visual inspection of an experienced neurophysiologist.

Muscle artifact signal The muscle artifact M of 30 s was simulated by filtering white gaussian noise with a band pass filter between 15 and 30 Hz.

Reference signal contaminated with muscle artifact. The simulated muscle artifact was superimposed on the reference EEG. In the simulation study the muscle artifact signal M is superimposed on the brain signal W_{ref}:

$$W_{test}(\lambda) = W_{ref} + \lambda M, \tag{3.6}$$

with $\lambda \in \mathbb{R}$. The Root Mean Squared (RMS) value of the reference brain signal is then equal to

$$RMS(W_{ref}) = \sqrt{\frac{1}{N}\sum_{n=0}^{N-1} W_{ref}^2(n)}, \tag{3.7}$$

and the RMS value of the muscle artifact signal is equal to

$$RMS(\lambda M) = \sqrt{\frac{1}{N}\sum_{n=0}^{N-1} (\lambda M(n))^2}. \tag{3.8}$$

An important measure is the noise level (nl) which is defined as follows,

$$nl = \frac{RMS(\lambda M)}{RMS(W_{ref})}. \tag{3.9}$$

Changing the λ parameter alters the noise level of our simulated signal.

Results Fig. 3.5 (b) shows a simulated signal W_{test} with a noise level equal to 0.89. The 3-dimensional schematic representation of the 16-dimensional reconstruction of the dynamics $\mathbf{X}(W_{ref})$ and $\mathbf{X}(W_{test})$ are shown in Fig. 3.5 (c) and (d), respectively. As the frequency of the muscle artifact is higher than the frequency of the brain signal the time intervals T_n obtained by the zero-crossing approach are shorter than the original time intervals. This results in a non-coinciding dynamics and a similarity index S($\mathbf{X}(W_{ref})$, $\mathbf{X}(W_{test})$) equal to 0.66. Since the underlying brain dynamics are exactly the same, the similarity should be equal to 1, illustrating the sensitivity of the method to muscle artifacts.

For higher noise levels the influence of the superimposed muscle artifact on the similarity index becomes larger. In Fig. 3.6, a 1 second segment of W_{test} is shown for four different noise levels. For high amplitude muscle artifact, more short time intervals T_n are introduced, resulting in a lower similarity index. The similarity index as a function of noise level is shown in Fig. 3.7. For a noise level larger than 3.1 all time intervals T_n are determined by the muscle artifact signal M and the similarity index remains constant.

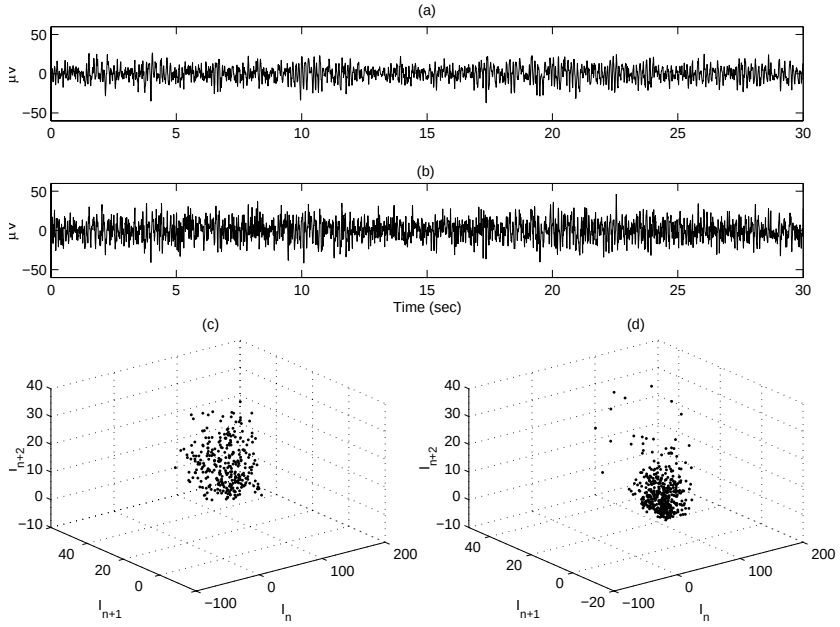

Figure 3.5: *(a) Artifact free reference signal W_{ref}. (b) Simulated signal W_{test} containing the reference signal and superimposed muscle artifact (nl=0.89). (c) The 3-dimensional schematic representation of the 16-dimensional reconstruction of the dynamics $\mathbf{X}(W_{ref})$. (d) The 3-dimensional schematic representation of the 16-dimensional reconstruction of the dynamics $\mathbf{X}(W_{test})$.*

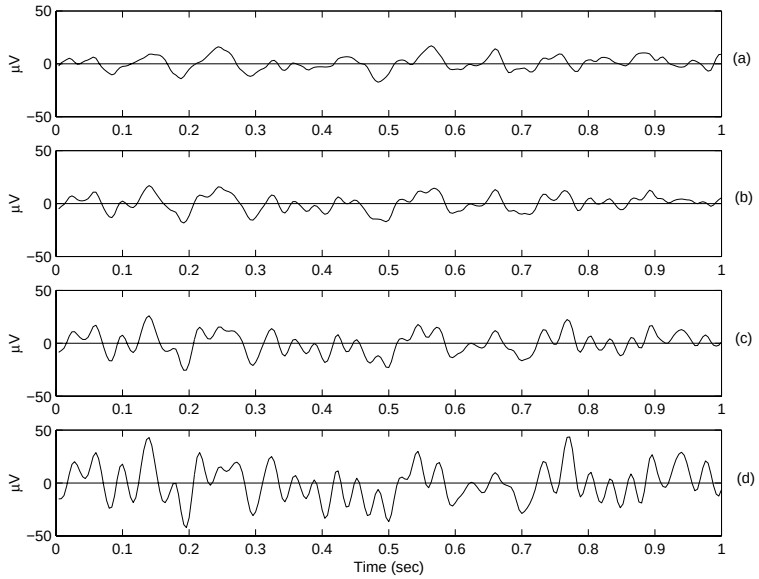

Figure 3.6: *1 second segment of W_{test} is shown for four different noise levels. (a) Original W_{ref} (nl=0), (b) noise level equal to 0.4, (c) noise level equal to 0.89, (d) noise level equal to 1.7.*

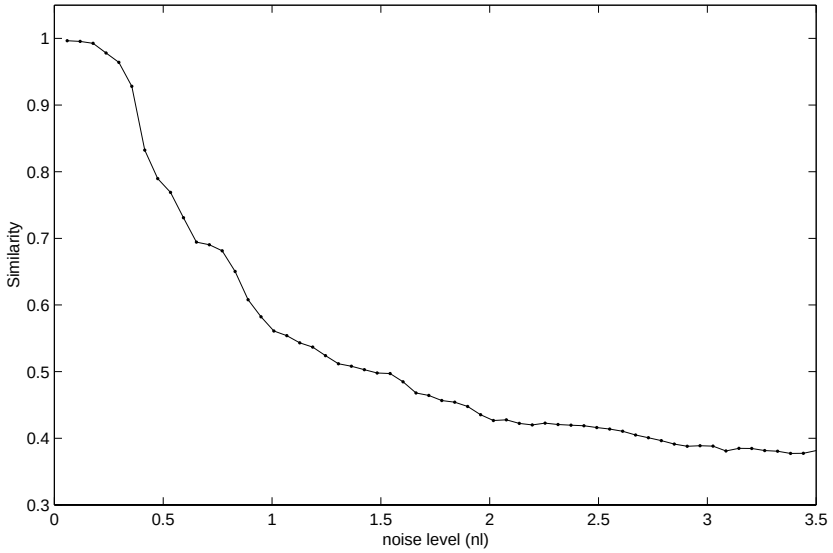

Figure 3.7: *The similarity index as a function of noise level. The contribution of muscle artifact increases with an increase in noise level.*

Robustness to eye blinks

An artifact free reference signal was chosen and an eye blink signal was superimposed to this reference signal in order to test the sensitivity of the similarity index to eye blinks. As the eye blink appears with rather fixed amplitude in the EEG, we performed only one simulation with a realistic contribution of the eye blink single to the reference signal.

Reference signal Fig. 3.8 (a) shows a 30 s EEG signal W_{ref} recorded at electrode $Fp1$. In the selected signal no artifacts were present according to the visual inspection of an experienced neurophysiologist.

Eye blink signal Six short EEG segments containing an eye blink were selected from the $Fp1$ electrode of an EEG recorded at the Video-EEG monitoring unit.

Reference signal contaminated with eye blinks. The selected eye blink signals were superimposed on the reference EEG at different time instances. The amplitude of the eye blinks was chosen in a realistic way. Fig. 3.8 (b) shows the simulated signal W_{test} with superimposed eye blinks.
The 3-dimensional schematic representation of the 16-dimensional reconstruction of the dynamics $\mathbf{X}(W_{ref})$ and $\mathbf{X}(W_{test})$ are shown in Fig. 3.8 (c) and (d), respectively. The eye blinks introduce long time intervals and these result in outliers in the dynamical representation. The similarity index $\mathrm{S}(\mathbf{X}(W_{ref}), \mathbf{X}(W_{test}))$ is equal to 0.87. As the underlying brain dynamics are exactly the same, the similarity should be equal to 1, illustrating the sensitivity of the method to eye blinks. The larger the amount of eye blinks present in a test window, the lower the similarity index will be.

3.3.5 Conclusion

Based on a data set of 12 patients with MTLE, we tried to replicate the findings reported in [74] and to detect a pre-ictal state preceding MTLE seizures using the similarity index of scalp EEG recordings. We were unable to replicate the work of Le Van Quyen et al. The similarity index was unable to detect pre-ictal changes in the scalp EEG recordings of all 12 patients with MTLE. However, in the scalp EEG recording of the patient with NPS the similarity index identified a pre-ictal state. The detection of the pre-ictal state in the patient with NPS ensured that the similarity method was correctly implemented and had the potential to identify a pre-ictal state in scalp EEG recordings.
Furthermore, we illustrated on synthetic data that the similarity index is sensitive to muscle artifacts and eye blinks. The similarity index is especially sensitive to muscle artifacts. As a consequence, the analysis of the scalp EEG recordings would benefit from an additional preprocessing of the signals, in which artifacts like eye blinks and muscle artifacts are removed, and this for two reasons. First,

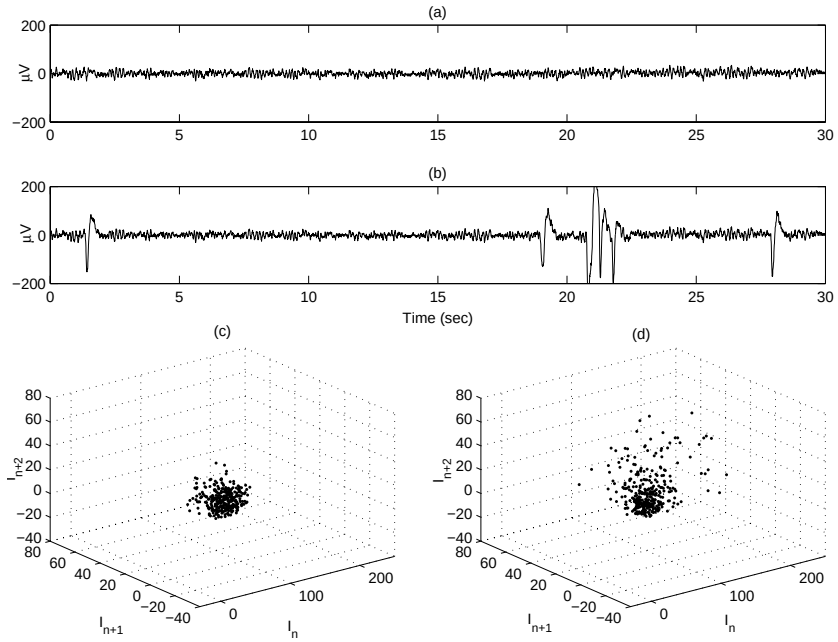

Figure 3.8: *(a) Artifact free reference signal W_{ref}. (b) Simulated signal W_{test} containing the reference signal and superimposed eye blinks. (c) The 3-dimensional schematic representation of the reconstruction of the dynamics $\mathbf{X}(W_{ref})$. (d) The 3-dimensional schematic representation of the reconstruction of the dynamics $\mathbf{X}(W_{test})$.*

the similarity index will drop less below the statistical threshold due to artifacts, making the interpretation of the similarity analysis more straightforward and in this way avoiding false predictions. Second, the presence of artifacts might mask the brain activity related to the pre-ictal state in the scalp EEG recordings. If we want to have any success in predicting seizures from scalp EEG electrodes, we first need to remove the artifacts contaminating it. Other possible reasons for the discrepancies between our findings and those reported by Le Van Quyen and colleagues could be: 1) the evolution towards a seizure does not always contain a pre-ictal transitional phase, 2) technical differences may exist between EEG recorders, 3) the pre-ictal changes are not recorded by scalp EEG recordings. These findings were reported in [21, 19].
With these publications, our group was the first group to report on the inability to reproduce the results of one of the studies reporting on seizure prediction. After our negative results, many other studies reported on the low ability of nonlinear measures to predict seizures, confirming our findings [2, 87, 72, 71, 111]. An overview is given in the next section.

3.4 Critical comments on nonlinear measures and seizure prediction

Lately, other research groups reevaluated the nonlinear methods used for seizure prediction and more critical comments have appeared. Several studies question the relevance of the nonlinear measures for seizure prediction. Other studies were not capable of reproducing the results of the first studies and also questioned the ability of nonlinear measures to predict epileptic seizures.

Are nonlinear methods relevant?

McSharry et al. (2003) questioned the relevance of nonlinear methods when seizure prediction is the aim [90, 91]. The operational use of modern nonlinear methods can be justified only by showing that they systematically outperform well-understood traditional linear methods or provide complementary information. In [90] it is shown that there is no clear evidence of improved performance for nonlinear methods applied to the database of intracranial EEG recordings previously investigated by Martinerie et al. (1998) [89]. The most striking result from their investigation is that variance seems to perform just as well as the nonlinear technique used in [89].

Jerger et al. (2001), compared the results of seven linear and nonlinear methods in detecting the earliest dynamical changes preceding intracranially-recorded seizures [62]. They showed that, for the the data used, the nonlinear methods offered no predictive advantage over linear methods. The authors give the following explanation for their findings. Many behaviors of neurons are known to follow nonlinear dynamics and one expects an underlying nonlinear behavior in EEG that is not fully characterized by linear tools. It is likely that the EEG signals are so complex that nonlinear reconstruction methods may not capture the dynamics accurately. Nonlinear tools are often designed to reveal structure from low-dimensional nonlinear systems. Faced with a truly complex system (with many degrees of freedom), they may be worse than a linear statistic as shown in this study.

Reproducibility of the results

Our group was one of the first groups to report on the inability to reproduce the results of one of the studies reporting on seizure prediction [21, 19]. After our negative results, many other studies reported on the poor ability of nonlinear measures to predict seizures, confirming our findings. A short overview is given below.

One of the major shortcomings for all studies reporting on seizure prediction is the lack of attention to the sensitivity and specificity of the nonlinear method used. Therefore, Maiwald et al. (2004) introduced an assessment criteria called

"seizure prediction characteristic"that incorporates the assessment of seizure prediction and false prediction rate [87]. Within this framework three nonlinear seizure prediction methods were evaluated on a large data pool of intracranial recordings of 21 patients. With a rate of 1 to 3.6 false predictions per day, the dynamical similarity index achieved a sensitivity between 21% and 42%. Sensitivity was between 18% and 31% for the accumulated energy and between 13% and 30% for the effective correlation dimension. With these results, epileptic patients under normal conditions with three seizures per month would have to endure 97% false alarms. These results are far from sufficient for clinical application.

In another study, the same group reported that only one out of 88 seizures was predicted by a significant dimension drop when applied on a data set of long-term ICEEG recordings [2]. They concluded that over all the mean length and amplitude of dimension drops showed no significant differences between interictal and ictal data sets.

Osorio et al. (2001) identified dependencies of the correlation integral and the correlation dimension on frequency and amplitude of the EEG signal, implying that changes in the former are due to trivial changes in the latter [111]. This dependency may result in a reinterpretation of the dynamic importance of the measures and may cast doubts on their predictive abilities for certain classes of seizures.

For more than a decade, it has been claimed that the Lyapunov exponents computed from electroencephalogram (EEG) or electrocorticogram (ECoG) signals can be used for prediction of epileptic seizures minutes or even tens of minutes in advance [57, 58, 59]. Lai et al. (2003,2004), however, showed firmly that the use of Lyapunov exponents, or related quantities from nonlinear dynamics such as the correlation dimension, for seizure prediction is practically impossible as the brain dynamical system generating EEG signals is more complicated than low-dimensional systems, and is noisy [72, 71]. Nonlinear tools are often designed to reveal structure from low-dimensional nonlinear systems. Again, faced with a truly complex system (with many degrees of freedom), it is likely that nonlinear reconstruction methods may not capture the dynamics accurately.

3.5 Conclusion

The prediction of epileptic seizures by quantitative analysis methods applied to EEG has been a focus of much interest in recent years. This resurgence of interest has been motivated by several factors, including the proliferation of powerful new methods for analyzing nonlinear system dynamics, as well as the interest in developing epilepsy control devices. In this chapter a literature overview of the state of the art of nonlinear seizure prediction methods was given. As nowadays the first euphoric state is followed by a critical reevaluation, it turns out that

many of the earlier studies reporting on seizure prediction are incomplete and the predictive ability of the nonlinear measures is very low. In this chapter we reported on the low ability of the similarity index, one of the nonlinear measures used for seizure prediction, to predict seizures. We were the first research group reporting on these negative findings in the Lancet [21]. Later on, many other studies confirmed our results, showing that nonlinear methods have a very low predictive ability not only on scalp EEG signals but also on intracranial EEGs. The obtained results are far from sufficient for clinical application.

Moreover, we have illustrated that the similarity analysis of scalp EEG recordings would benefit from an additional preprocessing of the signals, in which artifacts like eye blinks and muscle artifacts are removed, and this for two reasons: first, the similarity index will drop less below the statistical threshold due to artifacts, making the interpretation of the similarity analysis more straightforward and in this way avoiding false predictions. Second, the presence of artifacts might mask the brain activity related to the pre-ictal state in the scalp EEG recordings. If we want to have any success in predicting seizures from scalp EEG electrodes, we first need to remove the artifacts contaminating it. In the following chapters two newly developed methods for artifact removal are presented.

Chapter 4

Modelling common dynamics in multichannel signals with applications to artifact and background removal in EEG recordings

Removing artifacts and background EEG from multichannel interictal and ictal EEG has become a major research topic in EEG signal processing in recent years. We applied for this purpose a recently developed subspace-based method for modelling the common dynamics in multichannel signals [112]. When the epileptiform activity is common in the majority of channels and the artifacts appear only in a few channels the proposed method can be used to remove the latter. The performance of the method was tested on simulated data for different noise levels. For high noise levels the method was still able to identify the common dynamics. In addition, the method was applied to real life EEG recordings containing interictal and ictal activity contaminated with muscle artifact. The muscle artifacts were removed successfully. For both the synthetic data and the analyzed real life data the results were compared with the results obtained with Principal Component Analysis (PCA). In both cases the proposed method performed better than PCA.

4.1 Introduction

Electroencephalography measures the electric potentials on the skull and provides a continuous measure of cortical function with excellent time resolution. It is a tool to study the brain dynamics non-invasively. Typical waveforms appear in

the EEG of patients with epilepsy. Ictal EEG (activity during a seizure) and interictal events (epileptic activity between seizures) can be distinguished. This activity can be identified on the majority of the EEG electrodes if the underlying electrical sources (the epileptogenic region) are located in deeper cortical structures as in Mesial Temporal Lobe Epilepsy [103]. In reality noise is added to this EEG obscuring the brain function of interest and making the interpretation of the EEG less straightforward. Some typical contributors are the heart, muscle and eye-movement artifacts. In general, these artifacts appear on a limited number of channels in EEG recordings. Apart from these electrical active tissues, many brain areas other than the epileptogenic region are active too. For the purpose of the present study the non-epileptogenic EEG is considered as background.

Many methods exist in the literature which attempt to remove or attenuate artifacts and background EEG from the multichannel interictal and ictal EEG. Among them are broadband filtering methods, regression methods, and component based methods such as principal component analysis (PCA) and independent component analysis (ICA) [136, 69, 64, 68, 99, 60].

In this chapter we introduce a new approach towards removing artifacts and background EEG. A new subspace based method is used to model the common dynamics in a multichannel recording [112]. With common dynamics we mean the same waveform appearing over multiple channels. As the time course of the signals at the different scalp electrodes appears in or out of phase and with different amplitude, we allow the common waveform to have a different phase and amplitude for each channel. The proposed method can be exploited to remove artifacts when epileptiform activity appears in the majority of channels and the artifacts only in few. When the spatial correlation of the background EEG is low, the background EEG will also be removed by applying this method.

The chapter is organized as follows. In section 4.2 the subspace based method for modelling the common dynamics in a multichannel recording is described. A simulation study is presented in section 4.3 where the method is applied to simulated data with known underlying common dynamics in order to test the performance of the method. As proof of concept, section 4.4 shows the results obtained when applying the method to real life multichannel EEG recordings with the aim of modelling the common dynamics along the different electrodes and thereby removing the artifacts and background EEG not related to the epileptiform activity. In both sections, the results are compared with results obtained with PCA decomposition of the EEG. Finally, in sections 4.5 and 4.6 our findings are discussed and suggestions for further work are given.

4.2 Methods

First the Exponentially Damped Sinusoidal (EDS) [114] model will be introduced. This model provides an appropriate framework to describe the common dynamics in a given set of signals. Next, the proposed method for modelling the common dynamics will be explained.

4.2.1 EDS model

A way to analyze EEG signals is to quantify them directly in the time domain by means of model-based (or parametric) methods. We used the parametric EDS model where the signal is modelled as a finite sum of K discrete-time exponentially damped complex sinusoids:

$$\begin{aligned} x(n) &= \sum_{k=1}^{K} a_k \exp(j\phi_k) \exp\left((-d_k + j2\pi f_k)n\Delta t\right) + e(n), \\ n &= 0, 1, \ldots, N-1; \end{aligned} \tag{4.1}$$

where $j = \sqrt{-1}$, $n\Delta t$ is the time lapse between the origin and the sample $x(n)$, Δt is the sampling interval, N is equal to the number of data points and $e(n)$ is white gaussian noise. The parameters of this model are the amplitudes a_k, the phases ϕ_k, the damping factors d_k and the frequencies f_k. The model function (4.1) can be rewritten in terms of complex amplitudes $c_k = a_k \exp(j\phi_k)$ and signal poles $z_k = \exp\left((-d_k + j2\pi f_k)\Delta t\right)$ as follows

$$\begin{aligned} x(n) &= \sum_{k=1}^{K} c_k z_k^n + e(n), \\ n &= 0, 1, \ldots, N-1. \end{aligned} \tag{4.2}$$

Since exponentially damped sinusoids are a set of basis functions, they can be used to model any arbitrary signal sufficiently closely provided the model order is high enough. The EDS model can be extended to real-valued signals since any real-valued sinusoid can be expressed as a superposition of two complex sinusoids. Consequently, the model order K is equal to twice the number of sinusoids that comprise the real-valued signal. The EDS model is proven to be useful for modelling non-stationary signals containing transients such as speech [106, 55, 81], [96, 95]. Adding a damping helps to lower the model order when modelling transients (compared to undamped sinusoidal modelling).

4.2.2 Common dynamics

It is often of great interest to extract the common information present in a given set of signals or multichannel recording. This is possible by going to the subspace representation of the signals and capturing the subspace common to all signals.

In this section we introduce a new method which allows determining this common subspace [112]. The method can be divided into two parts; in the first part each channel is preprocessed separately by selecting the signal subspace of interest. This preprocessing step facilitates capturing the common subspace. The second part determines the common subspace and the parameters of the common signal poles. Before explaining our method the mathematical problem formulation is given.

Problem formulation

Given S channels $x_s(n),\ s = 1, \ldots, S;\ n = 0, \ldots, N-1$ which can be modelled as a sum of exponentially damped sinusoids. Let those S channels have K_c common poles $z_k,\ k = 1, \ldots, K_c$:

$$\begin{aligned} x_1(n) &= \sum_{k=1}^{K_1-K_c} c'_{1,k} z_{1,k}^n + \sum_{k=1}^{K_c} c_{1,k} z_k^n + e_1(n), \\ &\vdots \\ x_s(n) &= \sum_{k=1}^{K_s-K_c} c'_{s,k} z_{s,k}^n + \sum_{k=1}^{K_c} c_{s,k} z_k^n + e_s(n), \\ &\vdots \\ x_S(n) &= \sum_{k=1}^{K_S-K_c} c'_{S,k} z_{S,k}^n + \sum_{k=1}^{K_c} c_{S,k} z_k^n + e_S(n), \end{aligned} \tag{4.3}$$

with $z_{s,k},\ k = 1, \ldots, (K_s - K_c)$ the remaining signal poles at channel s. The common dynamics are described by the common signal poles. The corresponding amplitudes and phases can differ from channel to channel.

Algorithm part 1 (Single-channel preprocessing)

In this section each channel is preprocessed separately. This is done by going to a subspace representation of the channel and selecting the subspace of interest [112, 131]. The selected signal subspace serves as an input of the second part of the algorithm. The preprocessing is summarized as follows:

- **input:** S channels consisting of the data points $x_s(n),\ n = 0, \ldots, N-1;\ s = 1, \ldots, S.$; individual model order K_s for each channel s.
- **output:** a basis $\mathbf{U}_{\mathbf{sK_s}}$ of the signal subspace of each channel $s = 1, \ldots, S$ and the preprocessed data points $x'_s(n)$.

- ***Step 1***. For every channel $s, s = 1, \ldots, S$ arrange the data points $x_s(n), n = 0, \ldots, N-1$ in a Hankel matrix $\mathbf{H_s}$ of dimensions $L \times M$ as follows:

$$\mathbf{H}(x_s) = \mathbf{H_s} = \begin{bmatrix} x_s(0) & x_s(1) & x_s(2) & \cdots & x_s(M-1) \\ x_s(1) & x_s(2) & \iddots & \cdots & \vdots \\ x_s(2) & \iddots & \iddots & \cdots & \vdots \\ \vdots & \vdots & \vdots & \vdots & x_s(N-2) \\ x_s(L-1) & \cdots & \cdots & x_s(N-2) & x_s(N-1) \end{bmatrix}, \quad (4.4)$$

  where $N = L + M - 1$.

- ***Step 2***. Compute the Singular Value Decomposition (SVD) [51, 52] of each Hankel matrix $\mathbf{H_s}$:

$$\mathbf{H_s} = \mathbf{U_s}\mathbf{\Sigma_s}\mathbf{V_s^H}, \quad (4.5)$$

  where the superscript H denotes the hermitian conjugate. According to [131], in the absence of noise the SVD of $\mathbf{H_s}$ reduces to the product

$$\mathbf{H_{s_{K_s}}} = \mathbf{U_{s_{K_s}}}\mathbf{\Sigma_{s_{K_s}}}\mathbf{V^H_{s_{K_s}}}, \quad (4.6)$$

  where $\mathbf{U_{s_{K_s}}}$, $\mathbf{V_{s_{K_s}}}$ are respectively the first K_s columns of $\mathbf{U_s}$, $\mathbf{V_s}$ and $\mathbf{\Sigma_{s_{K_s}}}$ is the leading $(K_s \times K_s)$ submatrix of $\mathbf{\Sigma_s}$. In the presence of noise $\mathbf{H_s}$ is full rank. In this case, the truncated SVD, $\mathbf{H_{s_{K_s}}}$, of $\mathbf{H_s}$ is the best rank-K_s approximation of $\mathbf{H_s}$ and the column vectors of the truncated matrix $\mathbf{U_{s_{K_s}}}$ span the signal subspace [131]. This matrix will serve as an input of the second part of the algorithm. By averaging the anti-diagonals of the truncated matrix $\mathbf{H_{s_{K_s}}}$ we can recover the Hankel structure and extract the filtered time series $x'_s(n)$ [10, 31, 54], i.e.

$$x'_s(n) \quad = \quad \frac{1}{a} \sum_{i+j=n+2} \mathbf{H_{s_{K_s}}}(i,j), \quad (4.7)$$

  with $a = (n+1)$ for $n = 0, \ldots, M-1$ and $a = (N-n)$ for $n = M, \ldots, N-1$.

In practice the number of sinusoids present in a given signal and thus the corresponding model order K_s is not known a priori. Therefore, we introduce the following rule for truncating the $\mathbf{U_s}$ matrices in step 2. The $\mathbf{U_s}$ matrices are truncated when:

$$\sigma_s^2(K_s) \geq \ d \cdot \sigma_s^2(1)\sigma_s^2(K_s+1) < \ d \cdot \sigma_s^2(1) \quad (4.8)$$

with $\sigma_s(k)$ the kth largest singular value corresponding to the kth left singular vector in $\mathbf{U_s}$. The parameter d, which can be defined by the user, determines which left singular vectors belong to the signal subspace. As such, the individual model orders K_s are replaced by d at the input of algorithm part 1.

Algorithm part 2 (Common dynamics extraction)

First it is shown how to estimate the number of common signal poles and select the common subspace of a given set of signals. Once the common subspace is selected the parameters of the common poles are estimated in the second step. Finally, the corresponding estimates for the amplitudes and phase of the common signal poles are determined for each channel separately. The algorithm is summarized as follows:

- **input:** a basis $\mathbf{U_{s_{K_s}}}$ of the signal subspace of each channel $s = 1, \ldots, S$ and the preprocessed data points $x'_s(n)$.
- **output:** the estimate of the parameters $d_k,\ f_k,\ k = 1, \ldots, K_c$ of the common signal poles and the corresponding amplitudes and phases $a_{s,k},\ \phi_{s,k};\ k = 1, \ldots, K_c,\ s = 1, \ldots, S$.
- ***Step 1***. Stack the truncated $\mathbf{U_{s_{K_s}}}$, $s = 1, \ldots, S$ matrices into a $L \times \sum_{s=1}^{S} K_s$ matrix

$$\mathbf{U_{stacked}} = [\mathbf{U_{1_{K_1}}} | \mathbf{U_{2_{K_2}}} | \ldots | \mathbf{U_{S_{K_S}}}]. \tag{4.9}$$

  and compute the SVD of this resulting matrix

$$\mathbf{U_{stacked}} = \mathbf{U_c \Sigma_c V_c^H}. \tag{4.10}$$

  In [112] it is explained why the SVD of $\mathbf{U_{stacked}}$ directly gives information about the number of common poles and the common subspace spanned. Assuming that there are K_c poles common to S signals, the diagonal core matrix $\mathbf{\Sigma_c}$ contains a first set of K_c values equal to $\sqrt{S}$. The K_c first vectors of the left singular vector matrix $\mathbf{U_{c_{K_c}}}$ span the common subspace related to the common signal poles. We select these vectors by truncating $\mathbf{U_c}$ to a matrix of rank K_c, $\mathbf{U_{c_{K_c}}}$.

- ***Step 2***. The parameter estimation of the common signal poles is fully described in [112]. An overview of the different steps of the parameter estimation is given below.
  Form the following overdetermined set of linear equations

$$\mathbf{U^{\uparrow}_{c_{K_c}}} \approx \mathbf{U^{\downarrow}_{c_{K_c}}} \mathbf{Z}, \tag{4.11}$$

  where the arrows $\uparrow$ and $\downarrow$ denote the last and first row-deleting operator respectively. The Total Least Squares (TLS) solution of this set of equations is given by:

$$\tilde{\mathbf{Z}} = -\mathbf{W_{12}} \mathbf{W_{22}^{-1}}, \tag{4.12}$$

  where

$$\mathbf{W} = \begin{bmatrix} \mathbf{W_{11_{K_c \times K_c}}} & \mathbf{W_{12_{K_c \times K_c}}} \\ \mathbf{W_{21_{K_c \times K_c}}} & \mathbf{W_{22_{K_c \times K_c}}} \end{bmatrix}, \tag{4.13}$$

is obtained from the SVD of the matrix $[\mathbf{U}^{\uparrow}_{\mathbf{c_{K_c}}}\mathbf{U}^{\downarrow}_{\mathbf{c_{K_c}}}]$:

$$[\mathbf{U}^{\uparrow}_{\mathbf{c_{K_c}}}\mathbf{U}^{\downarrow}_{\mathbf{c_{K_c}}}] = \mathbf{Y}_{\mathbf{(L-1)\times(L-1)}}\mathbf{\Gamma}\mathbf{W}^{\mathbf{H}}_{\mathbf{2K_c\times 2K_c}}. \tag{4.14}$$

Once $\tilde{\mathbf{Z}}$ is estimated, its K_c eigenvalues λ_k give an estimate of the common signal poles [131]:

$$\lambda_k = \hat{z}_k = \exp\{(-\hat{d}_k + j2\pi\hat{f}_k)\Delta t\}, k = 1, \ldots, K_c. \tag{4.15}$$

From these signal poles, frequencies and dampings are easily calculated.

- ***Step 3***. The corresponding estimates for amplitudes $a_{s,k}$ and phases $\phi_{s,k}$, $s = 1, \ldots, S; k = 1, \ldots, K_c$ of the common signal poles are determined for each channel separately by filling in the obtained signal poles in the model function (4.3) and solving the resulting equations

$$x'_s(n) \approx \sum_{k=1}^{K_c} c_{s,k}\hat{z}_k^n, n = 0, 1, \ldots, N-1. \tag{4.16}$$

The $x_s(n)$ in (4.3) are replaced by the preprocessed $x'_s(n)$ of (4.7) for a better estimation of the amplitudes and phases.

4.3 Simulation study

Simulations are carried out to test the performance of the proposed method for different noise levels.

4.3.1 Simulation

Consider a matrix $\mathbf{X}$ of dimension 250-by-19 representing a 19 channel EEG section of 1.0 s long. Each column vector $\mathbf{x_s}, s = 1, \ldots, 19$ of $\mathbf{X}$ contains the time course of an EEG channel and corresponds to the time series $x_s(n)$ mentioned above:

$$\mathbf{X} = [\mathbf{x_1}, \mathbf{x_2}, \ldots, \mathbf{x_{19}}], \tag{4.17}$$

$$\mathbf{x_s} = [x_s(0), x_s(1), \ldots, x_s(249)]^T, \tag{4.18}$$

with $s = 1, \ldots, 19$. In this simulation study $\mathbf{X}$ includes both seizure activity, and superimposed noise. Both signals are described below.

Seizure activity

The EEG of the ictal activity was generated using a fixed dipole in a three-shell spherical head model with a moment having a 4 Hz sinusoidal waveform (for

example typical in patients with MTLE [103]). The amplification factors at each electrode were computed by solving the forward problem for a dipole in a three-shell spherical head model consisting of a brain, a skull and a scalp compartment [120]. Each compartment had a specific conductivity with a ratio equal to 1:1/16:1 for the brain, skull and scalp compartment respectively [108]. The brain and scalp conductivity was $3.3 \times 10^{-4}/\Omega mm$ [18]. Radii of the outer boundary of the brain, skull and scalp region equal to respectivly 8 cm, 8.5 cm and 9.2 cm were used. The dipole coordinates x (left ear to right ear), y (posterior to anterior) and z (up, through the Cz electrode) were (0.5, 0, 0.1) relative to the outer radius and the dipole orientations d_x, d_y and d_z were equal to (1, 0, 0). The amplification factors at each electrode were then multiplied with a 4Hz sine wave. 19 electrodes were used: *Fp2, F8, T4, T6, O2, F4, C4, P4, Fz, Cz, Pz, Fp1, F7, T3, T5, O1, F3, C3* and *P3* placed according to the 10-20 system for electrode placement [107]. The time course of the scalp potentials was stored in a 250-by-19 dimensional matrix $\mathbf{A}$ and is shown in Fig. 4.1 (a).

Noise

Let $\mathbf{B}$ denote a 250-by-19 noise matrix representing awake background EEG activity from a normal subject, 50 Hz line noise, and muscle artifact. The 50 Hz line noise was superimposed on the background EEG on electrodes *O1* and *P3* and was simulated by a 50 Hz sinusoid waveform sampled at 250 Hz. The muscle artifact was simulated by filtering white gaussian noise with a band pass filter between 15 and 30 Hz. The simulated muscle artifact was superimposed on the background EEG on channels *F8* and *Cz*. The amplitudes of the muscle artifact and 50Hz noise signal were chosen in a realistic way. The noise matrix is shown in Fig. 4.1 (b). Since the spatial correlation of the selected background EEG is low, no common waveform appears on all channels of $\mathbf{B}$.

The simulated signal

In the simulation study the noise matrix $\mathbf{B}$ is superimposed on the signal matrix $\mathbf{A}$ containing the common dynamics:

$$\mathbf{X}(\lambda) = \mathbf{A} + \lambda \cdot \mathbf{B}, \tag{4.19}$$

with $\lambda \in \mathbb{R}$. The Root Mean Squared (RMS) value of the signal is then equal to

$$RMS(\mathbf{A}) = \sqrt{\frac{1}{S \cdot N} \sum_{s=1}^{S} \sum_{n=0}^{N-1} \mathbf{A}^2(n,s)}, \tag{4.20}$$

and the RMS value of the noise is equal to

$$RMS(\lambda \cdot \mathbf{B}) = \sqrt{\frac{1}{S \cdot N} \sum_{s=1}^{S} \sum_{n=0}^{N-1} (\lambda \cdot \mathbf{B}(n,s))^2}. \tag{4.21}$$

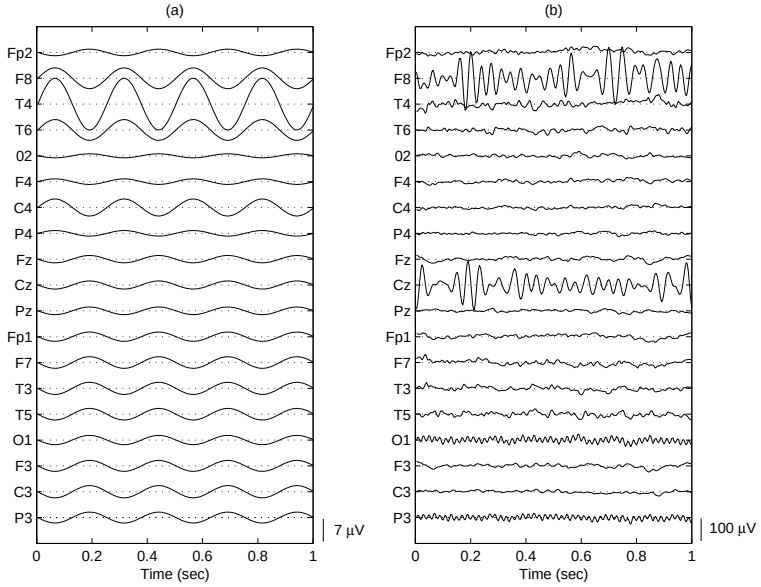

Figure 4.1: *Simulated data. (a) The time course of the scalp potentials reflecting the 4 Hz epileptiform activity on each electrode. (b) The noise matrix containing awake background EEG, 50 Hz line noise (electrodes O1, P3) and muscle artefact (electrodes F8, Cz).*

An important measure is the noise level (nl) which is defined as follows,

$$nl = \frac{RMS(\lambda \cdot \mathbf{B})}{RMS(\mathbf{A})}. \tag{4.22}$$

Changing the λ parameter alters the noise level of our simulated signal.

4.3.2 Results of simulation study

Aim of the simulation study

The aim of this simulation study was to evaluate the performance of the proposed method in modelling the common dynamics, the 4Hz epileptiform activity, for different noise levels. We performed several simulations with different noise levels. The performance is expressed in terms of the Relative Root Mean Squared Error (RRMSE):

$$RRMSE = \frac{RMS(\mathbf{A} - \hat{\mathbf{A}})}{RMS(\mathbf{A})} \cdot 100[\%], \tag{4.23}$$

where $\hat{A}$ is an estimate of the common dynamics.

Results

Fig. 4.2 (a) shows a simulation data matrix $\mathbf{X}$ under study with a noise level equal to 0.95. The signal matrix $\mathbf{A}$ containing the common dynamics is shown in Fig. 4.2 (b). The set of signals $\mathbf{X}$ was processed with the following parameters: $N = 250$, $L = 126$, $M = 125$. The $\mathbf{U_s}$ matrices are truncated according to (4.8) with d equal to 0.1. Fig. 4.2 (c) shows the EEG signals after preprocessing the channels separately based on this truncation. The background activity is reduced for each channel. For channels *F8* and *Cz* the muscle activity is still present as it is the dominant activity for those channels. Also the 50 Hz line noise is still present in channels *O1* and *P3* after preprocessing.

Fig. 4.3 shows the resulting squared singular values σ_c^2 of the stacked matrix $\mathbf{U_{stacked}}$ (4.10). There are two squared singular values close to 19, indicating that there are two common signal poles in all 19 channels. The reconstructed EEG based on these two signal poles had an RRMSE of 13% and is shown in Fig. 4.2 (d). By modelling the common dynamics in the 19 channels the remaining noise after preprocessing was successfully removed.

For comparison, we applied SVD directly to the data matrix $\mathbf{X}$ to derive the principal components of the simulated EEG signal (= PCA) [64]. The $(N \times S)$ matrix X is then decomposed as a product of three matrices:

$$\mathbf{X} = \mathbf{U\Sigma V^T}, \tag{4.24}$$

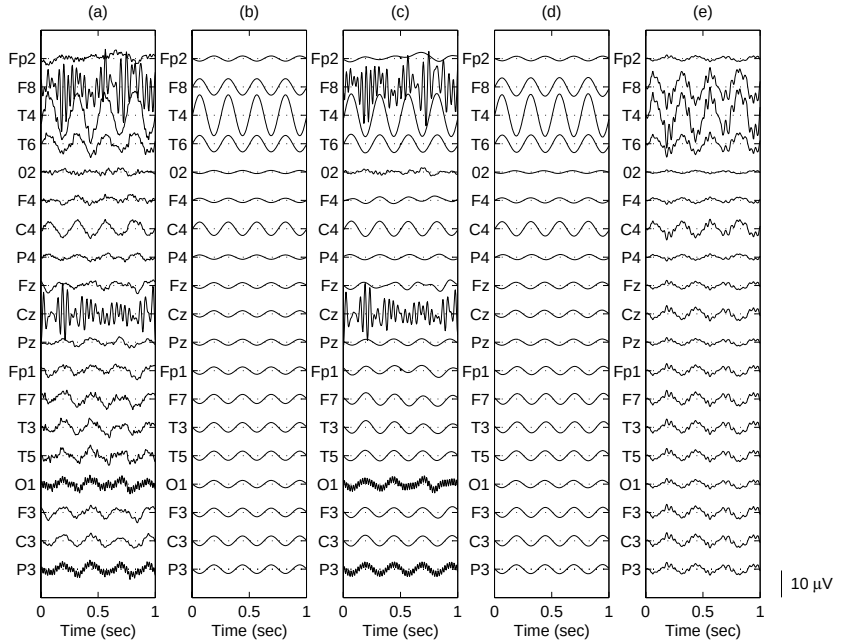

Figure 4.2: *(a) The simulation data matrix* $\mathbf{X}(\lambda)$ *for a noise level equal to* $nl = 0.95$*. (b) The signal matrix A containing the common dynamics. (c) The EEG signals after preprocessing each channel separately. (d) The reconstructed EEG based on the common signal poles. (e) The reconstructed EEG based on the first principal component.*

where $\mathbf{U}$ is an $(N \times S)$ matrix containing the S normalized component waveforms that are decorrelated linearly and can be remixed to reconstruct the original EEG. The first principal component contained the 4 Hz epileptiform waveform and was selected. The reconstructed EEG based on this truncation had an RRMSE of 34% and is shown in Fig. 4.2 (e).

The RRMSE as a function of the noise level is shown in Fig. 4.4. In this figure a comparison is made between the proposed method and PCA. For a noise level higher than 1.82 the background activity is too dominant on channel O2 compared to the epileptiform activity and the EDS model does not estimate the signal pole related to the epileptic activity in this channel. As a result the first squared singular values σ_c^2 of $\mathbf{U}_{\mathbf{stacked}}$ drop to 18. We stopped our simulation at this noise level. However, one could still continue by selecting the signal poles close to 18. The estimate of the common dynamics in channel *O2* will then be equal to zero.

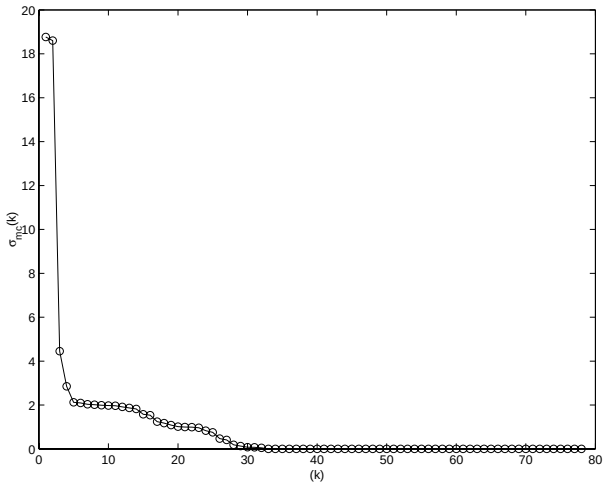

Figure 4.3: *The singular values of the stacked matrix* $\mathbf{U}_{\mathbf{stacked}}$ *generated in the simulation study.*

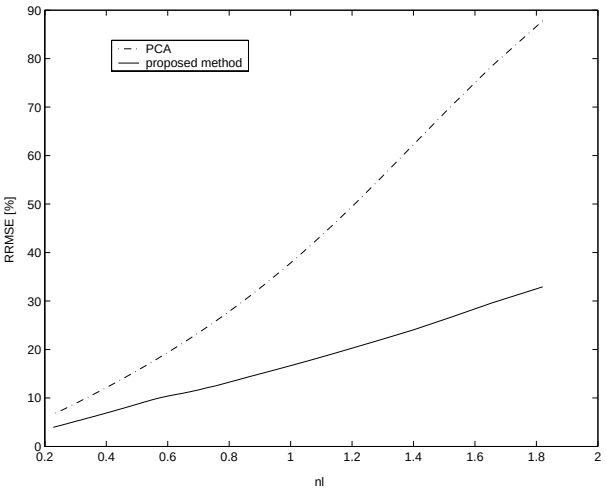

Figure 4.4: *The RRMSE as a function of the noise level is shown for the proposed method and PCA.*

4.4 Method applied to real life data

4.4.1 Method applied to interictal activity

Fig. 4.5 shows a 10 s epoch of 19 channel scalp EEG recorded from a long-term Epilepsy Monitoring Unit. The electrodes are placed according to the 10-20 electrode placement system [107]. The sampling frequency is 250 Hz and an average reference is used. This EEG epoch contains several epileptic spikes. Channels *O1* and *F3* are contaminated with muscle artifact which obscures the epileptic spike activity on those channels. The EEG between the two vertical lines containing the epileptic spike is used for further analysis and is enlarged in Fig. 4.6 (a). By determining the common dynamics present in all channels we wanted to enhance the spike activity and remove the artifact from channels *O1* and *F3*. The following parameters were applied: $N = 70$, $L = 36$, $M = 35$. The U_s matrices are truncated according to (4.8) with d equal to 0.01. Fig. 4.6 (b) shows the EEG signals after preprocessing the channels based on this truncation. For channels *O1* and *F3* the muscle artifacts can still be observed. For these channels the artifact is the dominant activity which can not be removed by the preprocessing part only.

Fig. 4.7 shows the resulting squared singular values σ_c^2 of the stacked matrix $\mathbf{U_{stacked}}$ (4.10). There are four squared singular values close to 19, indicating that there are four common signal poles in all 19 channels. The reconstructed EEG based on these common signal poles is shown in Fig. 4.6 (c). The muscle artifact is removed successfully on channels *O1* and *F3*.

For comparison, Fig. 4.6 (d) shows the result of the noise removal based on the truncated SVD of the data matrix. Hereby, the first principal component is selected for reconstruction.

Similar results were obtained on the epileptic spikes at $t = 3.9$ and $t = 5.6$ in the EEG recording shown in Fig. 4.5. The horizontal EOG activity present in channels *Fp1* and *Fp2* at $t = 3.9$ was removed, as it was not present in all channels.

4.4.2 Method applied to ictal activity

Fig. 4.8 (a) shows a 4 s epoch of a scalp EEG recording collected from 21 scalp electrodes placed according to the International 10-20 System with additional electrodes *T1* and *T2* on the temporal region. The sampling frequency was 250 Hz and an average reference was used. This EEG contains ictal activity from a patient with MTLE. The epileptic activity is mainly present on the *T2* and *F8* electrodes. The seizure EEG recording is contaminated with muscle artifact. This set of signals was processed with the following parameters: $N = 1000$, $L = 501$, $M = 500$, $d = 0.01$. As the influence of noise tends to decrease the squared singular values σ_c^2 that are theoretically equal to 21, [112], we selected all signal

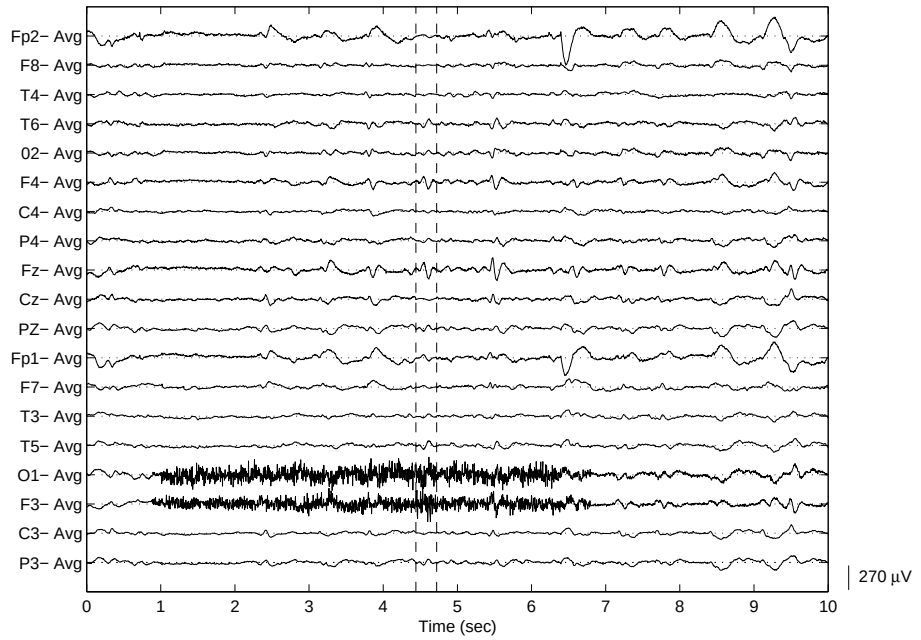

Figure 4.5: *10 s epoch of an EEG recorded from a long-term Epilepsy Monitoring unit. The EEG between the dashed lines is selected for further analysis and is shown in fig. 4.6(a).*

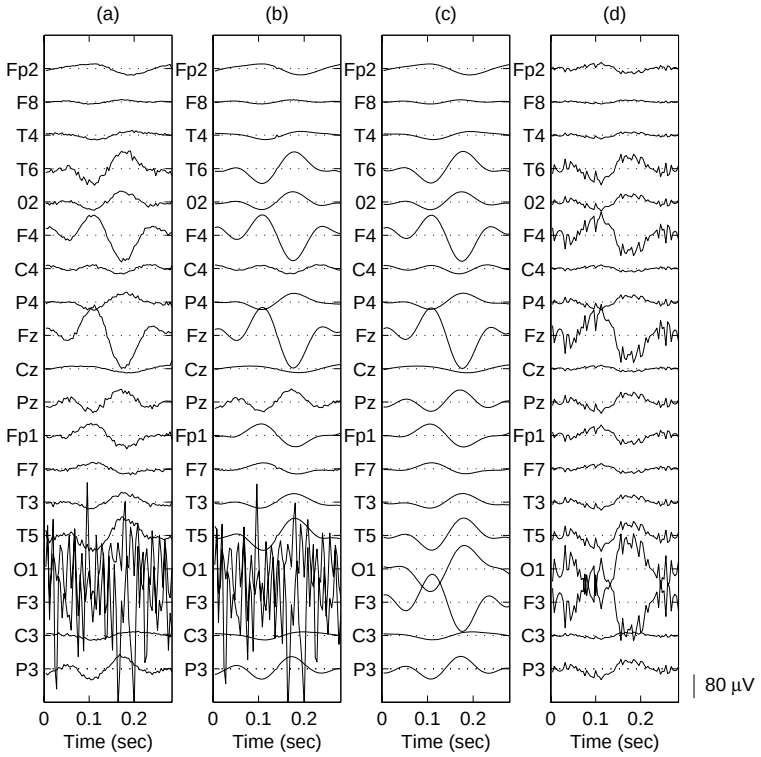

Figure 4.6: *(a) Shows the original spike. The EEG after preprocessing each channel separately is shown in (b). The fit based on the common signal poles is shown in (c). The reconstructed EEG based on the first principal component is shown in (d).*

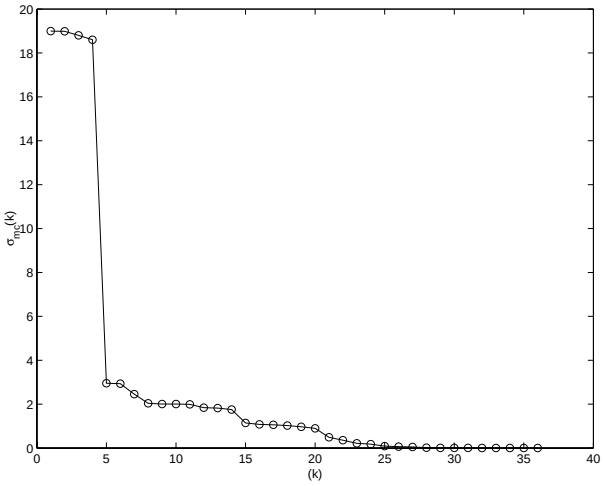

Figure 4.7: *The singular values of the stacked matrix* $U_{\mathbf{stacked}}$ *generated in the real-life interictal EEG example.*

poles belonging to the squared singular values above 20. Fig. 4.8 (b) shows the reconstructed EEG based on the common poles. The muscle artifact is removed successfully while the epileptic activity is enhanced. Next to the epileptic activity there is a slower activity present in all channels, mainly visible on electrodes *F3, F7* and *Fz*, which is preserved by the method. For comparison, the result of the noise removal based on the truncated SVD of the data matrix was determined for different truncation values. Fig. 4.8(c) shows the result based on the 3 most energetic principal components. In Fig. 4.8 (d) only the first principal component is selected for reconstruction.

4.5 Discussion

In this chapter, we introduced a new method for modelling the common dynamics in a multichannel recording. We showed that this method can be used to remove artifacts and background EEG from epileptiform EEG when they contain activity with a low spatial correlation.

The algorithm is divided into two parts. First each channel is preprocessed separately to select the subspace of interest. Here the parameter d determines the threshold between the signal and noise subspace. Truncating at a low value of d will not remove all the noise from each channel. Truncating at a high value of d has the danger of removing the signal poles modelling the common dynamics. In the second part of the algorithm the common signal poles are determined. Here all the signal poles not belonging to all channels are removed. It has the

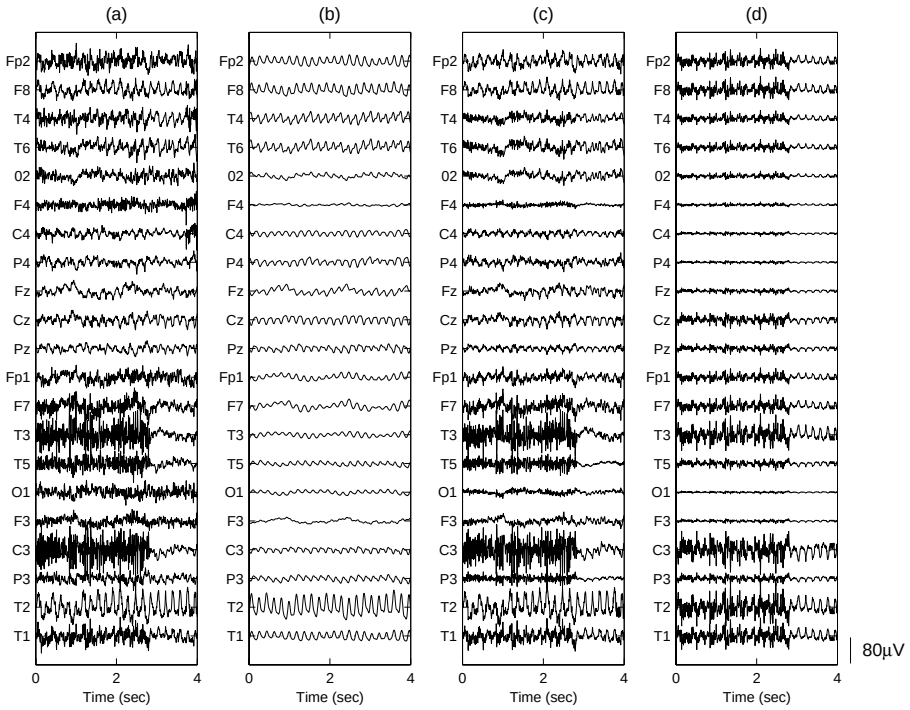

Figure 4.8: *(a) 4 s EEG epoch containing ictal activity. (b) The reconstructed EEG based on the common signal poles. (c) The reconstructed EEG based on the three most energetic principal components. (d) The reconstructed EEG based on the first principal component.*

advantage that it also removes the signal poles that are more energetic than the signal poles representing the common dynamics (for example the muscle artifact is more energetic than the epileptiform activity on channels *O1* and *F3* in Fig. 4.6). These poles could never be removed by the preprocessing step only. Moreover, the truncation parameter d in the preprocessing step becomes less critical when applying the second part of the algorithm. The signal poles representing the noise that are not removed by the preprocessing step will be removed in the second part of the algorithm. However, putting d too low in the preprocessing part will lead to a less accurate estimate of the amplitudes and the phases of the common signal poles in the second part (cf. Eq. 4.16).

It is important to notice that the proposed method can be used on any multichannel EEG recording starting from 2 to N channels. One is not obliged to use the method on all recorded EEG channels. The method can be used on a selection of EEG channels of interest to look for the common dynamics within the selected channels (for example, if a lateralization of the epileptic focus is a priori known).

When no prior knowledge is available of the location of the epileptic source then an average reference or a common reference (such as linked ears) should be used. The epileptic EEG will then appear in most of the channels and the proposed method will keep this activity and reduce the background activity. However, the method will not work so well when applying a bipolar montage, where two electrodes representing a channel, are located close to each other. Here the epileptic activity will only be present on a small number of channels and the interesting activity would rather be suppressed than amplified.

There are different gradations of contamination of artifacts possible. We have applied our method on ictal EEG contaminated with sever artifacts on *C3* and *T3* and have presented the cleaned results in Fig. 4.8. However, there exist worse examples of ictal EEG (with a majority of the channels contaminated) in which the performance of our method, but also other methods, will deteriorate.

As explained in section 4.2.2, the first part of the algorithm preprocesses each channel separately by selecting the signal subspace of interest. The data points are arranged in a Hankel matrix and the SVD of this matrix is computed. The selection of the signal subspace is automated based on the energy of the components (Eq. 4.8). This proposed method for the selection of the channel subspace is not unique. In [61] the selection of the channel subspace is done by applying ICA on a Hankel matrix. The advantage of the ICA-based method is that a better selection of the channel subspace is possible compared to SVD. However, we have shown that the preprocessing part of the algorithm must not be optimal since the remaining noisy components are removed by the second part of the algorithm as discussed above. Moreover, the obtained components after applying ICA are not ordered as in SVD and a manual selection of the subspace of interest is needed

for each channel.

In this chapter the proposed method was also compared to PCA for both the simulation study and the analyzed real life data (Fig. 4.2, 4.4, 4.6 and 4.8). In both cases the proposed method performed better than PCA because the latter was not able to segregate the source of interest and the muscle artifact into a separate component. A thorough comparison with other artifact and noise removal techniques described in literature like frequency filtering, adaptive filtering, regression methods and the various ICA algorithms will be the subject of further research. Frequency filtering methods will perform worse in cases where the common activity consists of frequency components that are located in a priori unknown frequency bands. Regression methods and adaptive filter techniques become problematic when a good regressing or noise reference channel is not available as is the case for muscle artifacts. ICA performs well in removing a wide variety of artifacts from EEG records. However, a manual selection of the obtained independent components is required. Moreover, often the muscle artifact appears in nearly all the independent components and even accompanies the ictal component [99].

If one wants to automate the proposed method one must keep in mind that the EDS model becomes ineffective when the signals of interest are not yet started at the onset (n=0) of the selected time window. Consequently, the window length and onset must be chosen adaptively as suggested in [106]. Furthermore, the EDS model can also be used for the detection of epileptic seizures [22]. In Appendix C, several measures were derived based on the EDS model which allowed to make the distinction between three types of EEG recordings containing awake, sleep and epileptic seizure activity in all patients studied.

Finally, the method can be applied to other biomedical and nonbiomedical signals where there is a need to find the common information within a set of signals (e.g.[82, 96, 132]).

4.6 Conclusion

Modelling the common dynamics in multichannel EEG recordings opens new perspectives to removing artifacts and background EEG from interictal and ictal EEG. This chapter proposed a subspace based method for modelling the common dynamics which was applied to synthetic data and interictal and ictal EEG. In all cases the proposed method removed successfully the artifact and background activity and performed better than PCA. Further research will be required to compare the method with other existing artifact removal methods in order to fully assess the potential and limitations of this new method.

Chapter 5

Canonical Correlation Analysis applied to remove muscle artifacts from the scalp EEG

As described in section 2.3.4, the electroencephalogram is often contaminated by muscle artifacts. In this chapter a new method for muscle artifact removal in EEG is presented, based on Canonical Correlation Analysis (CCA) as a Blind Source Separation technique (BSS). This method is demonstrated on a synthetic data set and on a real ictal EEG recording contaminated with muscle artifacts. The proposed method removed successfully the muscle artifact without altering the recorded underlying brain activity. The method outperformed a low pass filter with different cutoff frequencies and an Independent Component Analysis (ICA) based technique for muscle artifact removal. Moreover, the fast computational time and the ordering of the CCA components make the proposed method applicable in clinical practice. The first preliminary results of a clinical study on 26 ictal EEGs of patients with refractory epilepsy illustrated that the removal of muscle artifact results in a better interpretation of the ictal EEG, leading to an earlier detection of the seizure onset and a better localization of the seizures onset zone. These findings make the current method indispensable for every Epilepsy Monitoring Unit.

5.1 Introduction

The EEG is frequently contaminated by electrophysiological potentials associated with muscle contraction due to biting, chewing and frowning. These muscle ar-

tifacts, also known as ElectroMyoGram (EMG) artifacts, obscure the EEG and complicate the interpretation of the EEG or even make the interpretation unfeasible [125]. In the domain of Event Related Potentials (ERP), epochs heavily contaminated with muscle artifacts are typically rejected. When a small number of epochs is available, for instance in complex memory tasks, each rejected epoch will reduce the interpretability of the ERP [126]. In automated epileptic seizure detection, muscle artifacts considerably reduce the selectivity of the method [119]. In the field of seizure prediction, muscle artifacts obscure the interpretation of the nonlinear measures when looking for a pre-ictal state in scalp EEG recordings (Chapter 3 and [21]). Hence, there is a clear need to remove these artifacts from the EEG.

Low-pass filters are commonly used to remove muscle artifact. However, as the frequency spectrum of the muscle artifacts overlaps with that of interesting brain signals [53], frequency filters not only suppress muscle artifacts but also valuable information, such as ictal beta activity [137]. Most EEG artifact removal techniques only consider ocular artifacts, while, to our knowledge, little effort has been made on the removal of muscle artifacts. Regression methods, investigated for eye blink and eye movement artifact correction [17, 136], are impractical when muscle artifacts are considered, because no reference channel is available. A more recently explored approach is Independent Component Analysis (ICA) which separates the EEG into statistical independent components. This method was already successfully applied to ocular artifact removal [63, 99]. However, cross-talk can be observed when the separation of brain and muscle activity is considered [99, 130, 97]. Moreover, when applying ICA, the identification of the components containing artifacts in general, and muscle activity in particular, is not obvious, and requires additional user attention. ICA based techniques that try to overcome this problem, like constrained ICA (cICA) [60], cannot be applied for muscle artifact removal. This method extracts only that independent component that is most similar to a specific reference signal [86]. However, for muscle artifacts the construction of a good reference signal is impractical.

In this chapter a new method for muscle artifact correction in EEG is presented, based on the statistical Canonical Correlation Analysis (CCA)[56] applied as a Blind Source Separation (BSS) technique [47], further referred to as BSS-CCA. The BSS-CCA method, as ICA and PCA, thus belongs to the group of data-driven techniques solving the BSS problem. The blind source separation can be defined as the determination of the original or underlying sources which generate multisensor signals, while knowing very little, if anything, of how these sources project on the sensors and making little assumptions on these source signals. The BSS-CCA method requires the sources to be uncorrelated and to be maximally correlated with a given function, which is in our case a time shifted version of the original signal. By consequence, in our case, the last requirement imposes the sources to be maximally autocorrelated, inducing an order on the sources based

on the autocorrelation index. Moreover, the BSS-CCA method is computationally much faster than ICA [47].

BSS-CCA is already used for exploratory data analysis in functional Magnetic Resonance Imaging (fMRI) [47], to extract temporal structures or spatial patterns, which are difficult to specify a priori, such as unexpected activations, drifts and motion related artifacts. The method is also applied to EEG data [67]. This pilot study demonstrated that BSS-CCA can be used for separating ocular artifacts, introduced in background EEG by an artificial mixing process. However, according to our knowledge, BSS-CCA is not yet applied on EEG for muscle artifact correction.

The remainder of the chapter is organized as follows. In section 5.2, BSS by CCA is outlined, and its application as artifact corrector of EEG data is described. The synthetic data and the real life EEG recording used to test the performance of the method are described in section 5.3. For both the synthetic data and the EEG recording, the performance was compared with the performance of a low-pass-filter and an ICA based technique. The obtained results are shown in section 5.4. Furthermore, in section 5.5 our findings are discussed and a semi-automatic method to remove muscle artifacts is illustrated in section 5.6. The preliminary results of a clinical study evaluating the potential clinical relevance of the method are presented in section 5.7. Finally, conclusions are drawn in section 5.8

5.2 Blind source separation by canonical correlation analysis for artifact removal

5.2.1 Blind source separation by canonical correlation analysis

In the blind source separation problem, the observed time course $\mathbf{x}(t) = [x_1(t), x_2(t), ..., x_K(t)]^T$, with $t = 1, ..., N$, with N the number of samples and K the number of sensors, is the result of an unknown linear mixture of a set of unknown source signals $\mathbf{s}(t) = [s_1(t), s_2(t), ..., s_K(t)]^T$:

$$\mathbf{x}(t) = \mathbf{A}\mathbf{s}(t), \tag{5.1}$$

where $\mathbf{A}$ is the unknown mixing matrix. The goal is to estimate the mixing matrix and recover the original source signals $\mathbf{s}(t)$. This is carried out by introducing the de-mixing matrix $\mathbf{W}$ such that

$$\mathbf{z}(t) = \mathbf{W}\mathbf{x}(t), \tag{5.2}$$

approximates the unknown source signals in $\mathbf{s}(t)$, by a scaling factor.
Unless there are extra constraints imposed, it is in general impossible to solve this problem. Canonical correlation analysis solves the problem by forcing the sources

to be mutually uncorrelated and maximally correlated with a predefined function [7, 46].
Let $\mathbf{x}(t)$ be the observed data matrix with K mixtures and N samples, then we define the predefined function $\mathbf{y}(t)$ as a temporally delayed version of the original data matrix, to enforce the sources to be maximally autocorrelated [7, 46]:

$$\mathbf{y}(t) = \mathbf{x}(t-1). \tag{5.3}$$

For the remainder of the chapter, BSS-CCA refers to this autocorrelation version. When the mean of each row from the data matrices $\mathbf{x}(t)$ and $\mathbf{y}(t)$ is removed, canonical correlation analysis obtains two sets of basis vectors, one for $\mathbf{x}$ and the other for $\mathbf{y}$, such that the correlations between the projections of the variables onto these basis vectors are mutually maximized. Consider the linear combinations of the components in $\mathbf{x}$ and $\mathbf{y}$:

$$\begin{array}{l} x = w_{x_1}x_1 + ... + w_{x_K}x_K = {\mathbf{w_x}}^T\mathbf{x}, \\ y = w_{y_1}y_1 + ... + w_{y_K}y_K = {\mathbf{w_y}}^T\mathbf{y}, \end{array} \tag{5.4}$$

CCA finds the vectors $\mathbf{w_x} = [w_{x_1}, ..., w_{x_K}]^T$ and $\mathbf{w_y} = [w_{y_1}, ..., w_{y_K}]^T$ that maximize the correlation ρ between x and y by solving the following maximization problem:

$$\begin{aligned} \max_{\mathbf{w_x},\mathbf{w_y}} \rho(x,y) &= \frac{E[xy]}{\sqrt{E[x^2]E[y^2]}} \\ &= \frac{E[({\mathbf{w_x}}^T\mathbf{x})({\mathbf{w_y}}^T\mathbf{y})]}{\sqrt{E[({\mathbf{w_x}}^T\mathbf{x})({\mathbf{w_x}}^T\mathbf{x})]E[({\mathbf{w_y}}^T\mathbf{y})({\mathbf{w_y}}^T\mathbf{y})]}} \\ &= \frac{{\mathbf{w_x}}^T\mathbf{C_{xy}}\mathbf{w_y}}{\sqrt{({\mathbf{w_x}}^T\mathbf{C_{xx}}\mathbf{w_x})({\mathbf{w_y}}^T\mathbf{C_{yy}}\mathbf{w_y})}}, \end{aligned} \tag{5.5}$$

with $\mathbf{C_{xx}}$ and $\mathbf{C_{yy}}$ the within-set covariance matrices of $\mathbf{x}$ and $\mathbf{y}$, respectively, and $\mathbf{C_{xy}}$ the between-sets covariance matrix. The maximization problem can be solved by setting the derivatives of Eq. (5.5) with respect to $\mathbf{w_x}$ and $\mathbf{w_y}$ to zero, which after manipulation results in the following two eigenvalue problems [48, 46]:

$$\left\{ \begin{array}{lcl} \mathbf{C}_{xx}^{-1}\mathbf{C}_{xy}\mathbf{C}_{yy}^{-1}\mathbf{C}_{yx}\hat{\mathbf{w}}_\mathbf{x} &=& \rho^2\hat{\mathbf{w}}_\mathbf{x}, \\ \mathbf{C}_{yy}^{-1}\mathbf{C}_{yx}\mathbf{C}_{xx}^{-1}\mathbf{C}_{xy}\hat{\mathbf{w}}_\mathbf{y} &=& \rho^2\hat{\mathbf{w}}_\mathbf{y}. \end{array} \right. \tag{5.6}$$

In the BSS-CCA version it is sufficient to solve Eq. (5.6) for $\hat{\mathbf{w}}_\mathbf{x}$ resulting in K solutions $\{\rho_i, \hat{\mathbf{w}}_{\mathbf{x_i}}\}$, $i = 1...K$, sorted by autocorrelation ρ_i. The K estimates of the sources $\mathbf{s}_i(t)$ are then given by $\mathbf{z}_i(t) = \hat{\mathbf{w}}_{\mathbf{x_i}}^T\mathbf{x}(t)$.

The canonical correlations ρ, which are in the BSS-CCA case equal to the autocorrelations of the sources, are also given by the cosines of the principal angles between the row spaces of $\mathbf{x}^T$ and $\mathbf{y}^T$ [52]. The canonical variates x^T and y^T correspond to the principal directions in the corresponding row space of $\mathbf{x}^T$ and

$\mathbf{y}^T$. Let $\mathbf{x}^T = \mathbf{Q_x R_x}$ and $\mathbf{y}^T = \mathbf{Q_y R_y}$ be the QR decompositions of $\mathbf{x}^T$ and $\mathbf{y}^T$, respectively. The canonical correlations and canonical variates can then be obtained from the SVD of ${\mathbf{Q_x}}^T \mathbf{Q_y}$ as follows [52]:

$$ {\mathbf{Q_x}}^T \mathbf{Q_y} = \mathbf{ECF}^T. \tag{5.7} $$

The canonical correlations ρ are given by the diagonal elements of $\mathbf{C}$. The columns of $\mathbf{z}^T = \mathbf{Q_x E}$ give the canonical variates of $\mathbf{x}^T$, corresponding to the estimates of the sources $\mathbf{s}_i(t)$. The columns of $\mathbf{z}^T$ are ordered by decreasing autocorrelation.

5.2.2 Applying BSS-CCA to EEG for artifact correction

BSS-CCA is effective in performing source separation if the following assumptions are valid: (1) the mixing medium is linear and propagation delays are negligible, (2) the courses of time of the sources are uncorrelated, (3) the courses of time of the sources have different autocorrelation structures, and (4) the number of sources is equal to or less than the number of sensors. In the case of EEG signals, assumption (1) is satisfied, because volume conduction is thought to be linear and instantaneous [113]. The sources in case of EEG, are related to brain activity and artifacts, which are anatomically and physiologically separate processes, meaning that those processes are uncorrelated, hence assumption (2) is fulfilled. It will be demonstrated in this study that brain activity produces structured signals having a high autocorrelation, whereas muscle activity is less structured and encompass more properties related to temporally white noise. Therefore different sources seem to have different autocorrelation structures and hence assumption (3) seems to be satisfied. It is questionable whether assumption (4) is fulfilled because the effective number of uncorrelated sources contributing to the scalp EEG is not known.
Nevertheless, simulation studies have demonstrated that BSS-CCA can be used for separating ocular artifacts that are introduced in background EEG by an artificial mixing process [67], as already mentioned in the introduction.
Once BSS-CCA is applied to the EEG and the sources, or components, contributing to the EEG are derived, then the manual or automatical identification of the components containing the artifacts is required. Next, the EEG is reconstructed without these components, by projecting the selected non-artifactual components back onto the scalp. The enhanced EEG $\mathbf{x}_{clean}(t)$ is then:

$$ \mathbf{x}_{clean}(t) = \mathbf{A}_{clean}\mathbf{z}(t), \tag{5.8} $$

with $\mathbf{z}(t)$ the sources obtained by BSS-CCA, and $\mathbf{A}_{clean}$ the mixing matrix with the columns representing activations of the artifactual sources, set to zero.

5.3 Materials and Methods

5.3.1 Construction of the synthetic data

The aim of the simulation study was to evaluate the performance of the proposed method in removing muscle artifacts. Several simulations with different signal-to-noise ratios were performed.

Brain activity

Three EEG epochs of 10 s containing respectively mainly delta ($0.5-4$Hz), alpha ($8-13$Hz) and beta ($13-30$Hz) activity, were selected as underlying brain signals. In the selected EEGs no muscle artifact was present according to the visual inspection of an experienced neurophysiologist. The data was collected from 21 scalp electrodes placed according to the International 10-20 System [107] with additional electrodes $T1$ and $T2$ on the temporal region. The sampling frequency was 250 Hz and an average reference was used. The three EEG epochs containing delta, alpha and beta activity were stored in three 21-by-2500 dimensional matrices $\mathbf{B_1}$, $\mathbf{B_2}$ and $\mathbf{B_3}$, respectively.

Muscle activity

To obtain only muscle activity, necessary for the simulation study, it is not sufficient to select muscle artifacts in the EEG as these events will not only contain muscle activity but also activity from the brain. To remove the EEG activity we used ICA (SOBI)[4] to decompose these events. Note that for a large number of events, which we visually inspected, no clear separation was established. For those events where a clear separation between EMG and brain activity was obtained, we selected a component that accounted for muscle artifact together with the corresponding field distribution. This procedure was repeated for three different 10 s EEG epochs recordings from three different subjects. The selected components and their corresponding field distributions (topographical maps) are shown in Fig. 5.1 (a-c). The individual components were reconstructed into a conventional EEG format. The resulting average referenced signal $\mathbf{M}$ containing all three independent muscle activities is shown in Fig. 5.1 (d).

Data and measures to test the performance

In the simulation study the average referenced muscle artifact signal $\mathbf{M}$ was superimposed on the average referenced signal $\mathbf{B}$ containing only brain activity:

$$\mathbf{X}(\lambda) = \mathbf{B} + \lambda \cdot \mathbf{M}, \tag{5.9}$$

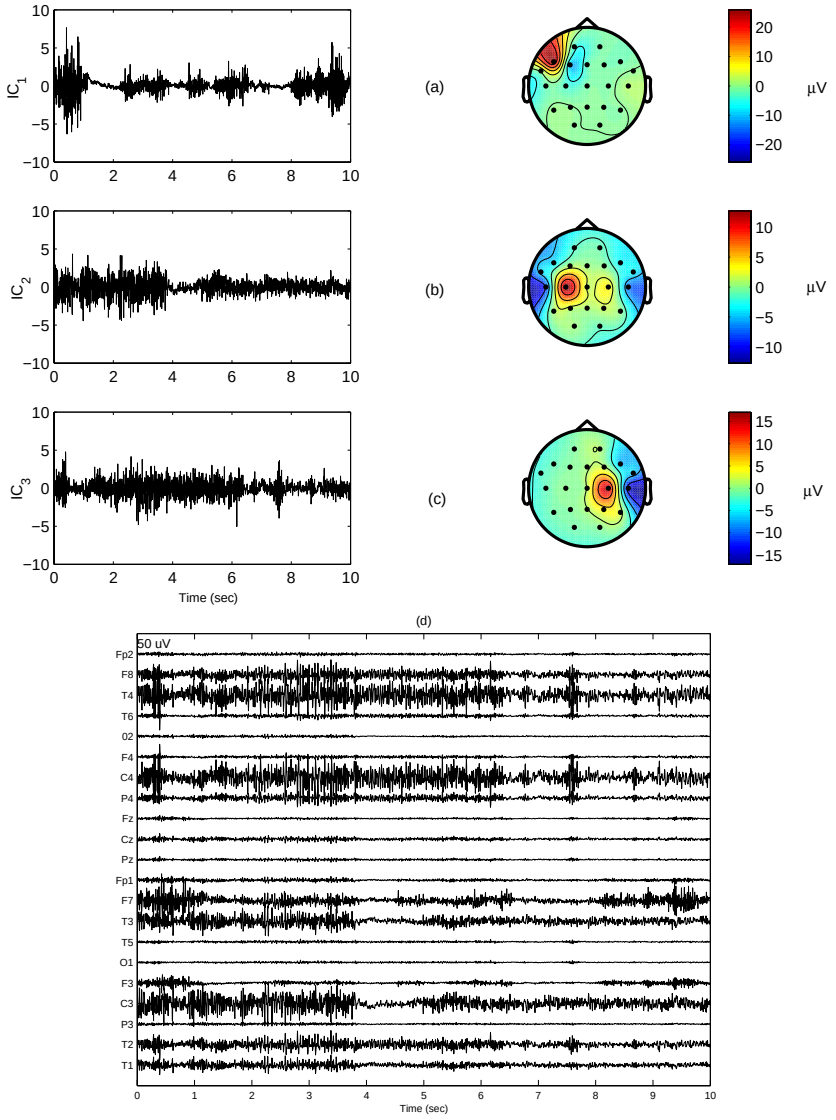

Figure 5.1: *(a), (b) and (c) The three selected (normalized) independent components (IC) representing muscle activity and their corresponding field distributions. (d) The resulting EEG epoch containing all three independent muscle activities.*

with $\lambda \in \mathbb{R}$, representing the contribution of muscle activity. The Root Mean Squared (RMS) value of the brain signal is then equal to

$$RMS(\mathbf{B}) = \sqrt{\frac{1}{K \cdot N} \sum_{k=1}^{K} \sum_{n=1}^{N} \mathbf{B}^2(k,n)}, \tag{5.10}$$

with N equal to the number of time samples and K equal to the number of EEG channels. The RMS value of the muscle artifact signal is equal to

$$RMS(\lambda \cdot \mathbf{M}) = \sqrt{\frac{1}{K \cdot N} \sum_{k=1}^{K} \sum_{n=1}^{N} (\lambda \cdot \mathbf{M}(k,n))^2}. \tag{5.11}$$

An important measure is the Signal-to-Noise Ratio (SNR) which is defined as follows,

$$SNR = \frac{RMS(\mathbf{B})}{RMS(\lambda \cdot \mathbf{M})}. \tag{5.12}$$

Changing the λ parameter alters the signal-to-noise ratio of our simulated signal. Several simulations with different signal-to-noise ratios were performed. The performance is expressed in terms of the Relative Root Mean Squared Error (RRMSE):

$$RRMSE = \frac{RMS(\mathbf{B} - \hat{\mathbf{B}})}{RMS(\mathbf{B})}, \tag{5.13}$$

where $\hat{\mathbf{B}}$ is the signal after muscle artifact removal.
The simulations were carried out for the three different brain signals $\mathbf{B_1}$, $\mathbf{B_2}$ and $\mathbf{B_3}$, described in section 5.3.1

5.3.2 Methods for comparison

For comparison, the proposed technique for muscle artifact removal is compared with other commonly used techniques for this purpose:

- Low pass filter: a low pass butterworth filter of order 8 was used with four different cutoff frequencies equal to 10Hz, 15Hz, 20Hz and 30Hz.
- ICA: as it is not in the scope of this chapter to compare all different ICA algorithms, we limit ourself to the Joint Approximate Diagonalization of Eigen-matrices (JADE) algorithm [11]. This ICA algorithm was previously used in a study for eye and muscle artifact removal in ictal scalp EEG recordings [130]. The muscle artifact was removed as follows. The ICA components were calculated by using the JADE algorithm. The selection of the components accounting for the muscle artifact was based on visual

inspection and the signal was reconstructed, excluding the components related to the artifact. It is worth mentioning that, for the muscle artifact removal based on ICA (JADE) to be unbiased, a different ICA algorithm (namely SOBI) as the JADE algorithm was used in the construction of the simulation study in section 5.3.1.

5.3.3 Ictal EEG recording

Because ictal EEG is often severely contaminated with muscle artifact, complicating the determination and localization of the ictal onset, the study is focussed on the artifact correction of ictal EEG. Fig. 5.6 (a) shows a 10 s epoch of a scalp EEG recording from a long-term Epilepsy Monitoring Unit. The acquisition settings were the same as for the brain activity in section 5.3.1. This EEG contains ictal activity from a patient with Mesial Temporal Lobe Epilepsy. The epileptic activity is mainly present on the $T2$, $F8$ and $T4$ electrodes. The seizure EEG is contaminated with muscle artifact and eye blinks. Again we applied CCA, ICA and frequency filtering to this epoch. The results were then visually inspected. Error measures could not be used as we did not have a-priori information available of the brain (epileptic) sources.

5.4 Results

5.4.1 Results on the synthetic data

Fig. 5.2 (a) shows a simulated signal $\mathbf{X}$ with a signal-to-noise ratio equal to 0.65 (λ=3.25). For this simulated signal, the brain activity signal $\mathbf{B_2}$, which is shown in Fig. 5.2 (b), is used. The (normalized) components obtained by applying the BSS-CCA algorithm on $\mathbf{X}$ are shown in Fig. 5.3 (a). The autocorrelation of the components is shown in Fig. 5.3 (b). The components accounting for the muscle artifact are present in the three lowest autocorrelated components. The corresponding field distributions are shown in Fig. 5.3 (c-e). Both the derived time courses and field distributions are very similar to the ones of the original muscle sources shown in Fig. 5.1 (a-c). Fig. 5.4 shows the RRMSE as a function of the number of lowest autocorrelated CCA components that are excluded in the EEG reconstruction. A minimum is reached when the last three components are removed. Excluding those components in the reconstruction of the EEG results in the cleaned EEG shown in Fig. 5.2 (c). The RRMSE of the BSS-CCA processed data was equal to 0.11.

Fig. 5.2 (d-g) shows the results of applying the low pass filter on the simulated signal $\mathbf{X}$ with cutoff frequencies of 10Hz, 15Hz, 20Hz and 30Hz respectively. Because the frequency spectrum of the muscle artifacts overlaps with that of the brain signal, the low pass filters were not capable of removing the whole artifact without altering the underlying brain activity. The 10 Hz low pass filter removed

most of the artifact activity, but also altered the fast activity present in the $\mathbf{B_2}$ EEG recording. Moreover, the slow activity related to the muscle artifact between t= $0-2$ s was not removed. The higher the cutoff frequency, the less complete the filter removed the muscle artifact. In Fig. 5.2 (h) the result of removing the artifactual JADE components is shown. As some of the muscle activity was present in ICA components containing brain activity, the removal of the muscle artifact based on the three muscle artifact components, which were selected by visual inspection, was not complete. The RRMSE of the 10Hz , 15Hz, 20Hz and 30Hz low pass filtered data was equal to 0.35, 0.33, 0.36 and 0.51 respectively. The RRMSE of the JADE processed data was equal to 0.25.

The RRMSE as a function of signal-to-noise ratio on the $\mathbf{B_2}$ brain signal for the different artifact removal techniques (BSS-CCA, ICA(JADE) and the low pass filter with cutoff frequency at 10Hz, 15Hz, 20Hz and 30Hz) is shown in Fig. 5.5 (a). For high signal-to-noise ratios the 10 Hz filter performed worst because the brain signal $\mathbf{B_2}$ has mainly alpha (8-13Hz) activity, and consequently, the 10 Hz filter altered the brain signal the most. For lower SNR the performance of the 10 Hz filter compared to the other low pass filters improved as it removed most of the muscle artifact. Compared to the low pass filters, the performance of ICA was better for all signal-to-noise ratios. The BSS-CCA method outperformed all methods for all SNRs.

The results of the simulation study on the $\mathbf{B_1}$ (Fig. 5.5 (b)) and $\mathbf{B_3}$ brain signals containing delta and beta activity are similar to that of $\mathbf{B_2}$. The results on the $\mathbf{B_3}$ brain signals containing beta activity are published in [135].

5.4.2 Results on the ictal EEG recording

This section shows the results obtained by applying the method to the epoch of multichannel EEG containing ictal EEG and muscle artifacts shown in Fig. 5.6 (a). The (normalized) components as obtained by BSS-CCA are depicted in Fig. 5.7 (a); their corresponding autocorrelation is shown in Fig. 5.7 (b). We observed that the muscle activity is well separated from the ictal component (component 3), and is present in the lowest autocorrelated CCA components. Fig. 5.6 (b) shows the reconstructed EEG after excluding components (9-21).

For comparison, the low pass filter with cutoff frequency equal to 10 Hz and the JADE algorithm were also applied. Fig. 5.7 (c) shows the ICA components as obtained by JADE. The selection of the artifactual components by visual inspection becomes difficult because the muscle artifact is present in almost all components and even accompanies the ictal component (component 3). Fig. 5.6 (c) shows the reconstructed EEG based on excluding suspected muscle artifactual components 4, 7, 8, 13, 14, 16-19, 20 and 21. The muscle artifact removal based on ICA is less complete as the CCA result. Fig. 5.6 (d) shows the result of the

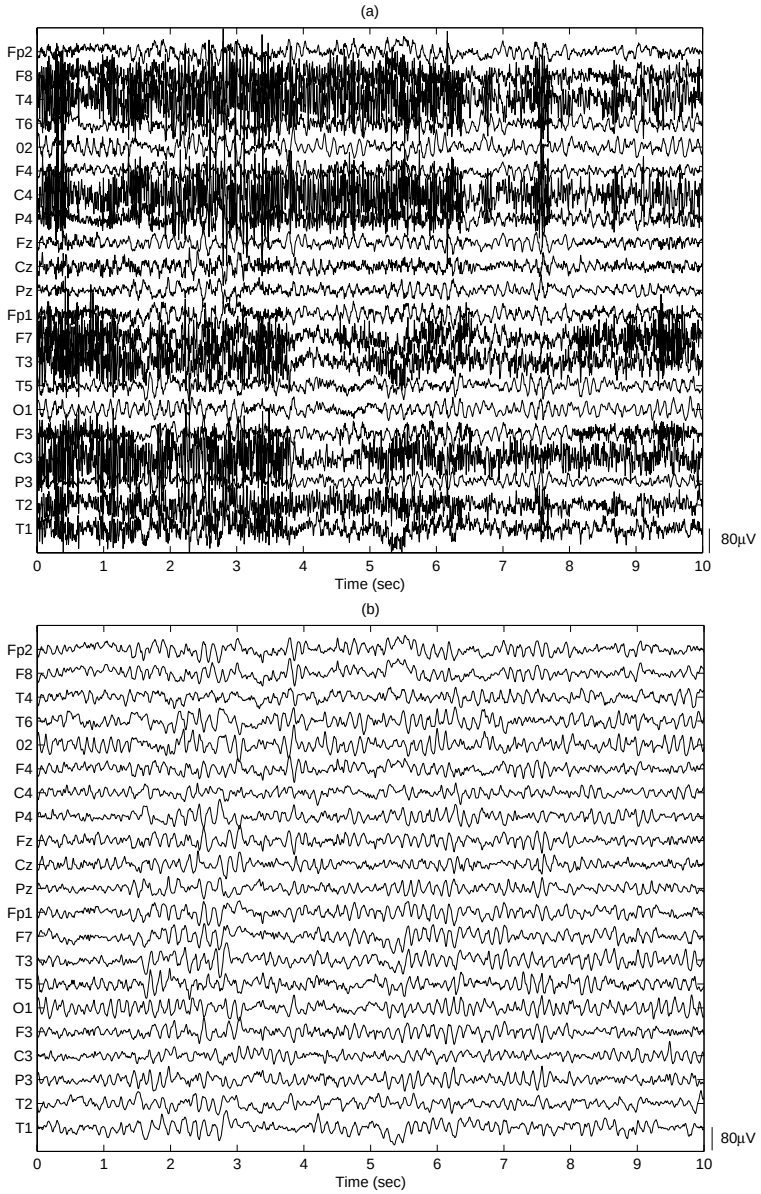

Figure 5.2: *(a) Simulation matrix* $\mathbf{X}$ *containing: alpha activity* $\mathbf{B_2}$ *and superimposed muscle activity* $\mathbf{M}$ *with SNR = 0.65 (λ=3.25); (b) Original EEG epoch* $\mathbf{B_2}$*;*

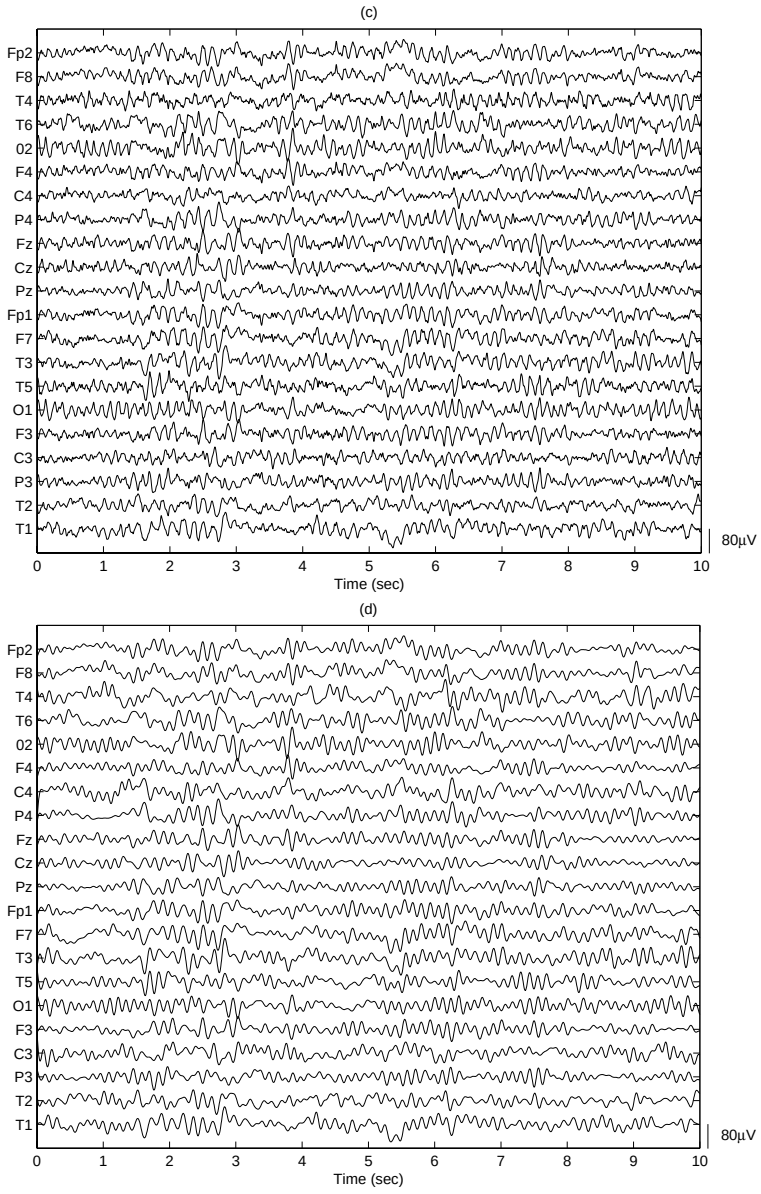

Figure 5.2: *(c) BSS-CCA processed data; (d) low pass filtered data with cutoff frequency equal to 10Hz;*

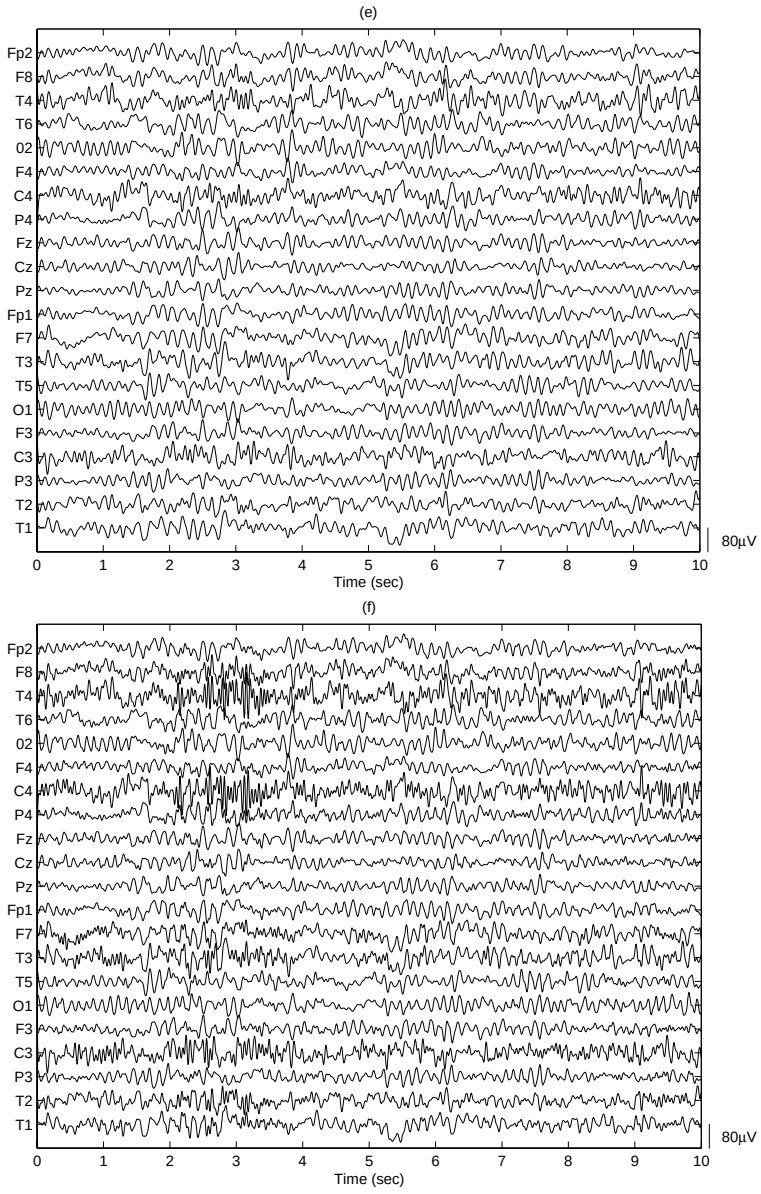

Figure 5.2: *(e) and (f) low pass filtered data with cutoff frequency equal to 15Hz and 20Hz respectively;*

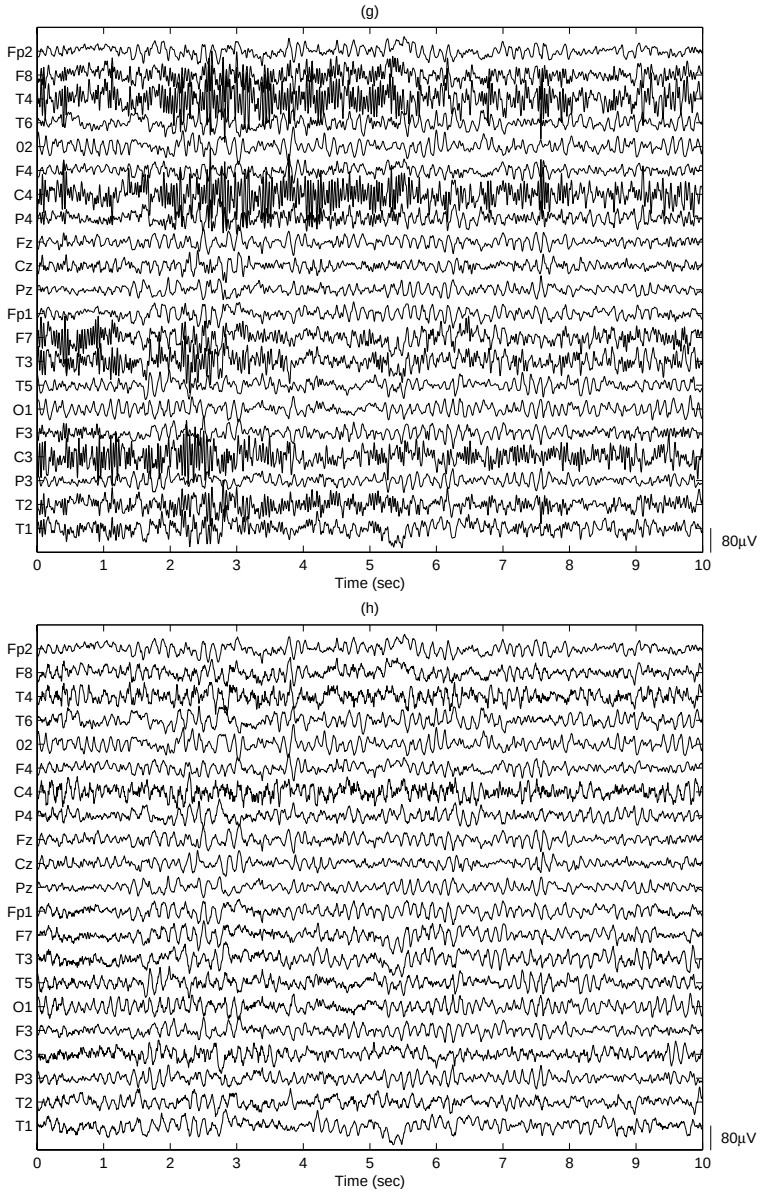

Figure 5.2: *(g) low pass filtered data with cutoff frequency equal to 30Hz; (h) JADE processed data.*

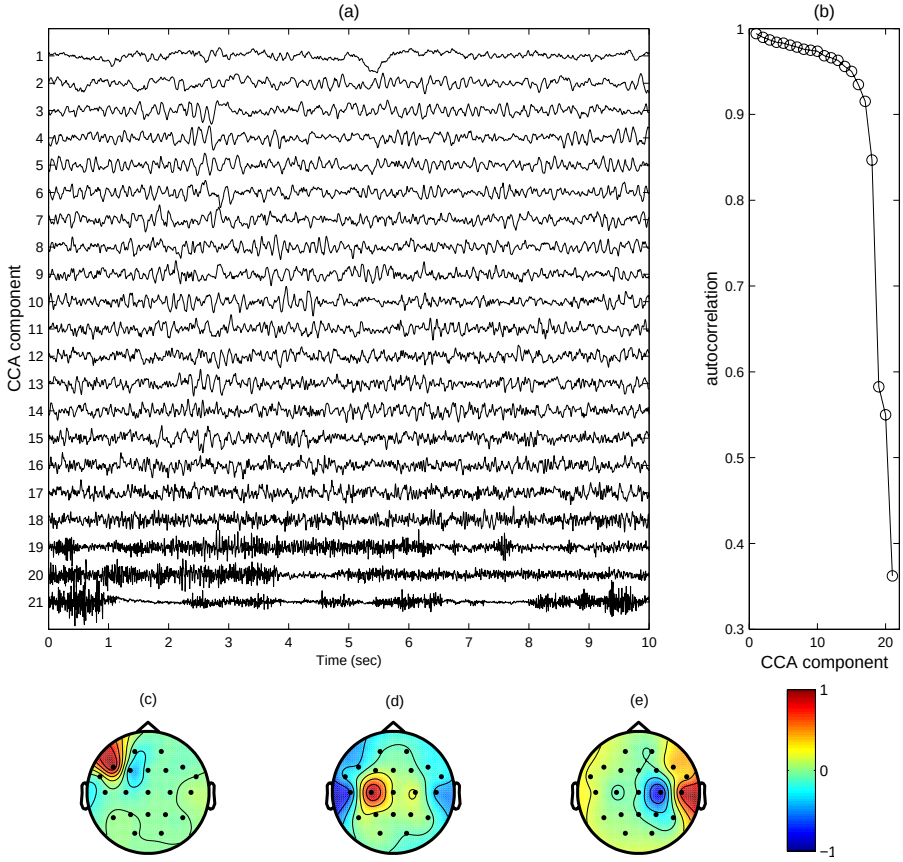

Figure 5.3: *(a) CCA components (normalized) obtained by applying BSS-CCA on the 10 sec EEG epoch shown in Fig 5.2 (a); (b) The autocorrelation of the CCA components; (c-e) Normalized scalp distributions of the three lowest autocorrelated CCA components ((c) component 21, (d) component 20, (e) component 19). The distributions must be multiplied by (c) 78 μV, (d) 40 μV and (e) 51 μV to obtain the unnormalized distributions.*

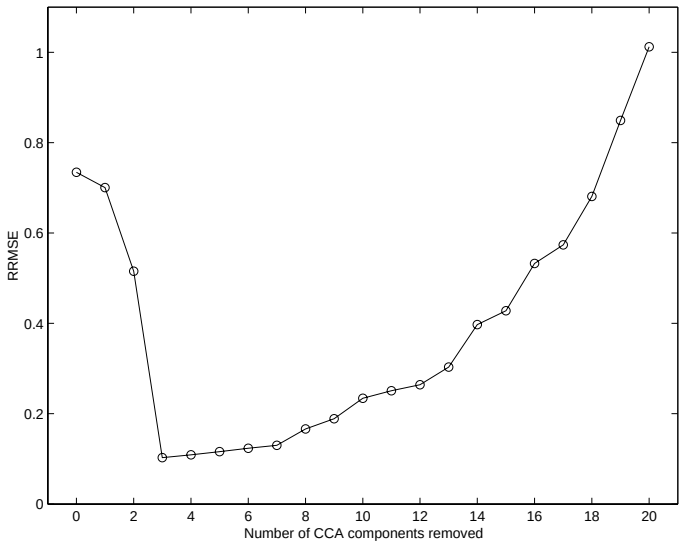

Figure 5.4: *The RRMSE as a function of the number of lowest autocorrelated CCA components excluded in the reconstruction of the EEG.*

low pass filter (10 Hz). As the frequency of the epileptic activity is lower than 10 Hz, the low pass filter was able to remove most of the muscle artifact without altering the epileptic activity, although a flattening of the signal is observed.

5.5 Discussion

In this chapter a new method for muscle artifact correction in EEG based on CCA was presented. The method belongs to the group of blind source separation techniques. The performance of the method was tested on simulated data with the aim to remove muscle artifacts without altering the known underlying brain signal. In the simulation study, the performance of the proposed method was compared to the performance of other commonly used methods. A low pass filter with different cut-off frequencies and ICA (JADE) were used as contenders. The BSS-CCA method succeeded in removing the superimposed muscle artifact from the brain signal and performed this task better than its competitors. The frequency spectrum of the muscle artifacts overlaps with that of the brain activity signal, leading to the fact that the low pass filters were not capable of removing the whole artifact without altering the underlying brain signal; as shown in Fig. 5.2 (d-g). Due to mixing of the muscle artifact in ICA components accounting for brain activity, BSS-CCA outperformed ICA for all considered signal-to-noise ratios. Especially for low SNRs it significantly outperformed the other methods (Fig. 5.5).

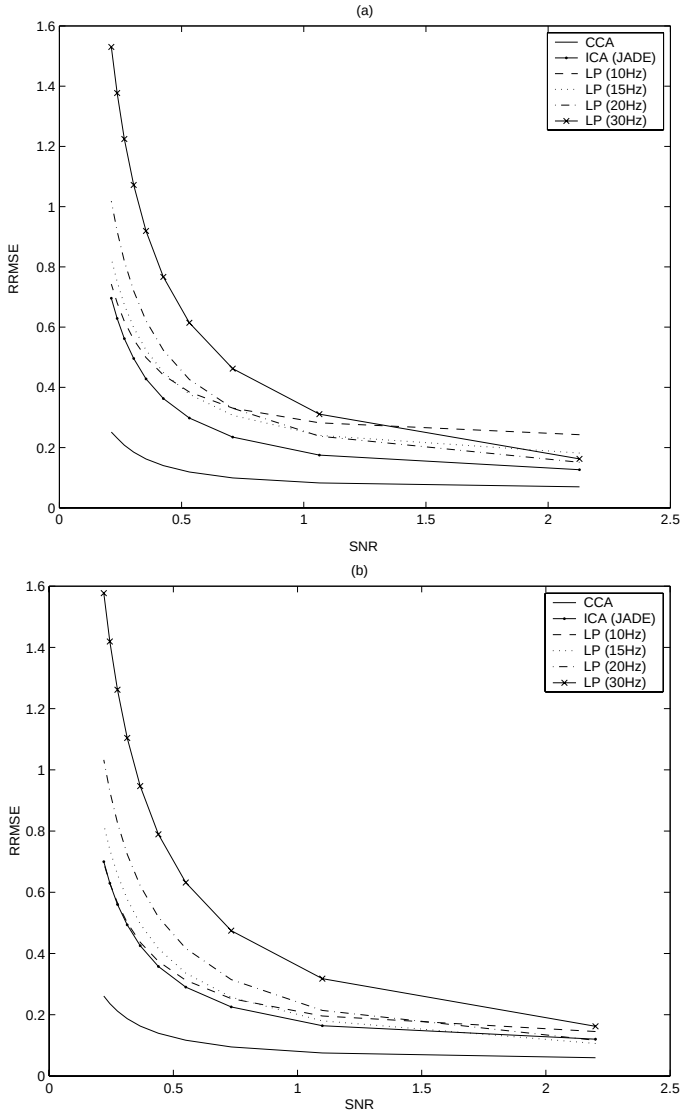

Figure 5.5: *The RRMSE as a function of SNR on the EEG epoch* $\mathbf{B_2}$ *containing alpha (8-13Hz) activity.; (b) The RRMSE as a function of SNR on the EEG epoch* $\mathbf{B_1}$ *containing delta (<4Hz) activity.*

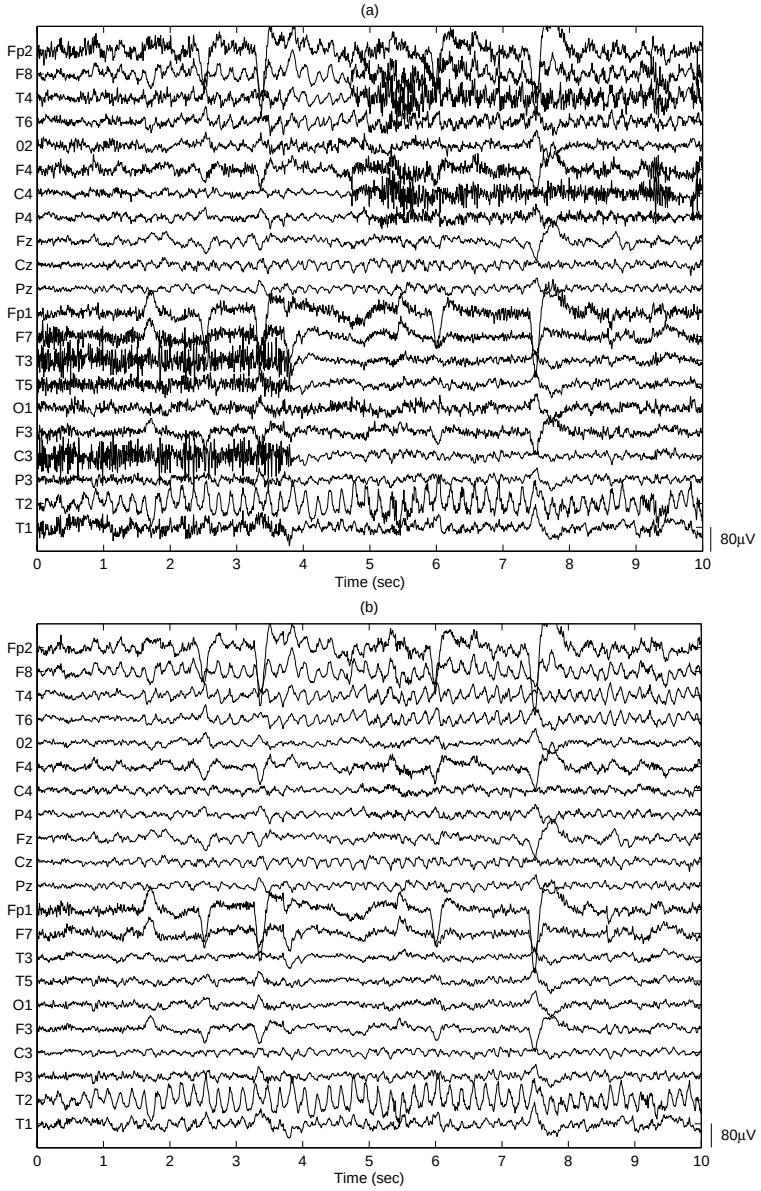

Figure 5.6: *(a) Original 10 s EEG epoch; (b) EEG reconstruction after excluding artifactual CCA components. Notice that the muscle artifact was removed completely, while preserving the sharp quality ictal theta activity in the right temporal lobe (T2 (=right spenoidal electrode), F8, and lesser degree T4 and T6).*

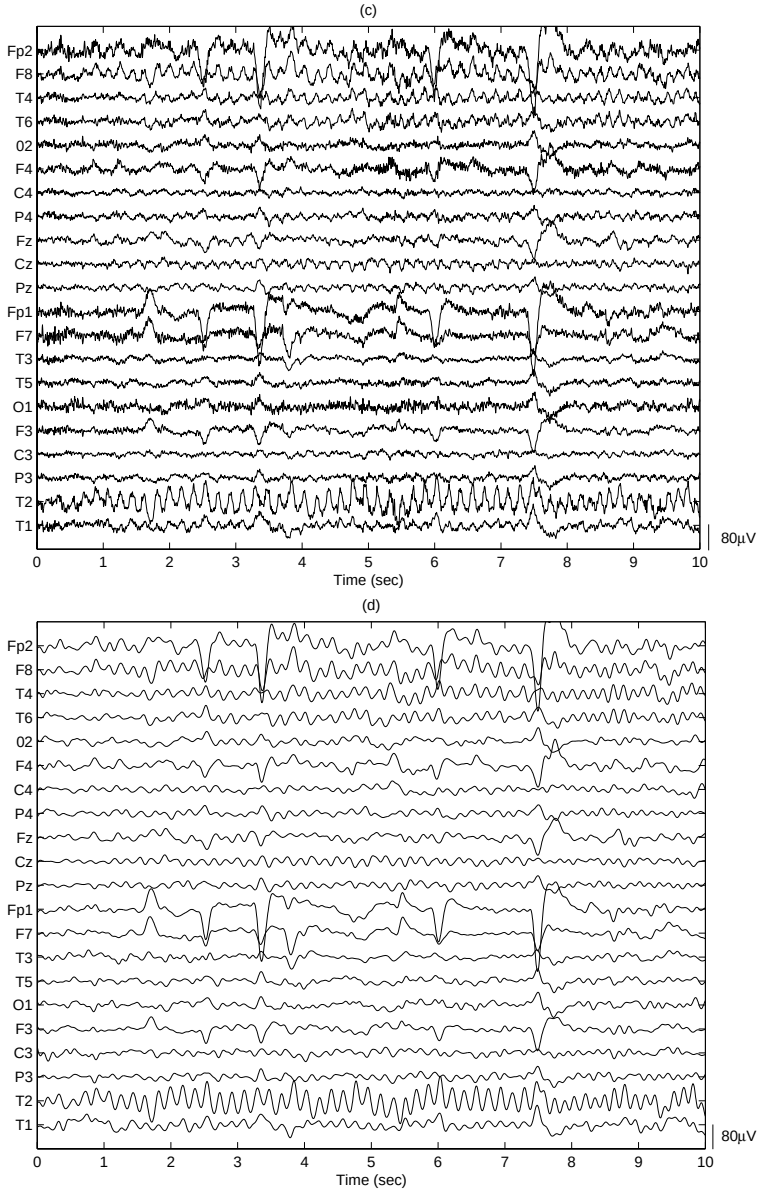

Figure 5.6: *(c) EEG reconstruction based on JADE components. (d) EEG filtered by the low pass filter with cutoff frequency equal to 10 Hz. Notice that the 10 Hz filter has removed not only the muscle artifact, but also the sharp, ictal quality of the recruiting right temporal lobe theta activity.*

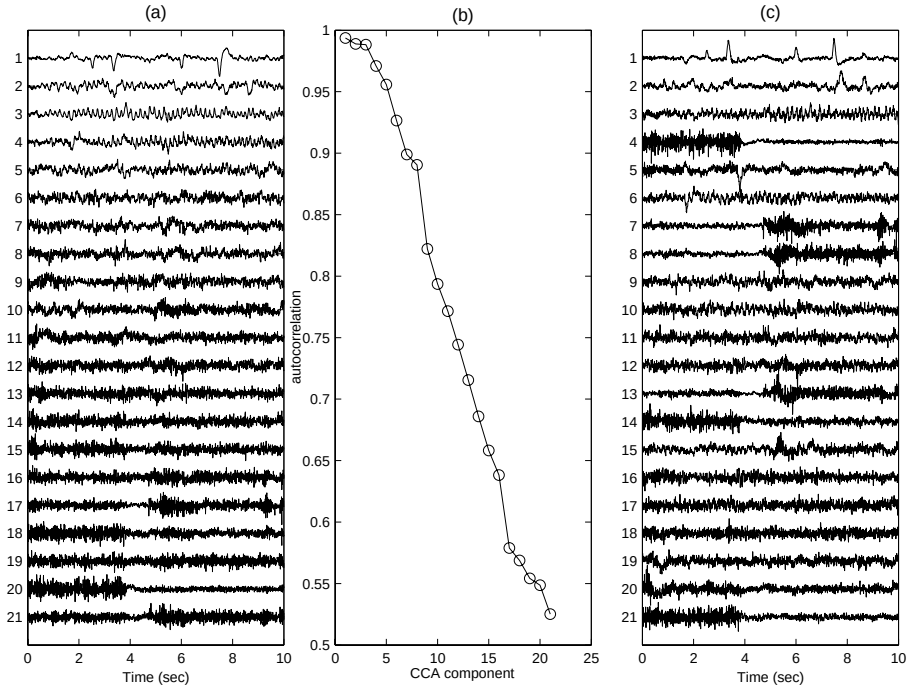

Figure 5.7: *(a) Components (normalized) obtained by applying BSS-CCA on the ictal EEG recording shown in Fig. 5.6 (a). (b) The autocorrelation of the CCA components. (c) ICA components obtained by applying JADE on the same recording.*

The method was applied to a real ictal EEG recording. The muscle artifact was removed with success without altering the ictal EEG. Since the BSS-CCA method is designed for finding maximally autocorrelated signals, the method succeeded in extracting the brain activity without cross-talk of the muscle artifacts, which have very different autocorrelation structures. The muscle artifact removal based on ICA (JADE) was more difficult and again less complete than the BSS-CCA results. The muscle artifact appeared on nearly all ICA components and even accompanied the ictal component, as shown in Fig. 5.6 (c) and Fig. 5.7 (c). As a consequence, the selection of the ICA components accounting for the muscle artifact that should be excluded in the reconstruction became difficult or even problematic. These results correspond to the findings of [99] and [130]. Both studies reported that the removal of muscle artifacts with ICA was more difficult and less complete than that of eye artifacts because of mixture of the muscle artifact with EEG components.

Compared to ICA, the BSS-CCA method as a blind source separation technique, has three major advantages. First, the CCA components are ordered according to their autocorrelation, whereas the ICA components have no order. Second, the BSS-CCA algorithm has a much smaller computational time, which makes the algorithm applicable for real-time/on-line performance [47, 7]. In addition, the outcome of the BSS-CCA method is unique, while the ICA output can be different for the same input, depending on the algorithm [47].
The muscle activity is present in the lowest components in the CCA decomposition, which indicates that they are a more noise like signal (small autocorrelation) than the brain activity.
A possible explanation for these observations could be found in the origin of the muscle artifact signal. A muscle is composed out of different motor units, each compromising a motor neuron and a group of innervated muscle fibres. The recruitment of several motor units when contracting a muscle, leads therefore to a complex electrical activity. This complex signal is a summation of asynchronized potentials, caused by the muscle fibres of the different activated motor units, and results in a low autocorrelated signal. This property is not apparent in other EEG activity and consequently, their time course has a higher autocorrelation compared to that of muscle activity, resulting in a good separation between both signals.
These observations can be exploited to automatically remove the muscle artifact from the EEG. Further research will indicate whether thresholding on the autocorrelation index will be sufficient to remove muscle artifact automatically in a large subject group.
For now, we have established a semi-automatic removal of muscle artifacts based on a scrolling system as discussed in the next section. In this way, the BSS-CCA method becomes practical for people without experience in the field of BSS and avoids manual selection of a fairly large set of components as in ICA. ICA based techniques that try to avoid this need for a selection of artifactual components,

like constrained ICA [60], can not be applied for muscle artifact removal. The cICA needs a good reference signal which is lacking for the muscle artifact. An important factor in the clinical applicability of the method is that the user can easily determine the optimal number of components to be removed by observing the EEG of interest while scrolling, hereby avoiding the removal of important information. The proposed semi-automatic removal of muscle artifact is (already) of great importance in the visual evaluation of ictal EEGs.

The method is now being validated on a large data set of ictal EEGs of patients with different types of epileptic seizures. A study is set up in which the performance of the proposed method and low pass filters are evaluated and compared. The preliminary results of this clinical study are presented in section 5.7.

The modelling of the common dynamics to remove muscle artifacts (Chapter 4 and [24]), is dependent on the selection of the time interval and EEG montage used, and is therefore less general applicable than the proposed method. Moreover, this method removes everything that is not common in the different EEG channels, which is more than only muscle artifact.

As described above, the proposed EMG removal technique can be used to clean the EEG resulting in a better visual interpretation. Next to this visual interpretation tool, the removal of muscle artifact can be used as a preprocessing step to facilitate the signal processing of scalp EEG signals. As the muscle artifacts give rise to false positives in current seizure detection methods [119], preprocessing the EEG with CCA could improve the sensitivity and specificity of the detectors. In the field of seizure prediction, muscle artifacts obscure the interpretation of nonlinear measures when looking for a pre-ictal state in scalp EEG recordings [21]. Removing the artifacts could again improve the performance of the nonlinear measures. Furthermore, ictal dipole source localization would benefit considerably when muscle artifacts were removed. In the domain of the event related potentials, heavily EMG contaminated epochs will no longer need to be rejected. This could lead to a better interpretability of the ERP, especially in cases where a small number of epochs is available, as for example in complex memory tasks.

The method could also be applied to MagnetoEncephaloGraphic (MEG) recordings. In MEG recordings the number of channels is usually much larger than in EEG. As a consequence, the number of components derived by ICA is also much larger and the selection of the artifactual ICA components on visual inspection becomes even more demanding than in EEG. For this reason, the ordered CCA components, could be of major use to MEG signals too.

A previous pilot study has demonstrated that BSS-CCA can be used for separating ocular artifacts that are introduced in background EEG by an artificial mixing process [67]. It is for now, not clear yet whether BSS-CCA will outper-

form ICA on eye-blink removal from the EEG. Therefore, a study needs to be undertaken in which the performance of the eye blink removal based on BSS-CCA is compared with the performance of ICA on a large data set containing EEG recordings with eye blinks.
Furthermore, it is not clear whether BSS-CCA will be the method of choice in separation of EEG brain signals in their underlying sources.

5.6 Semi-automatic removal of muscle artifacts

For now, we established a semi-automatic removal of muscle artifacts. CCA components are gradually removed from bottom upwards based on the ordering of the components. An example of use is given below. Fig. 5.8 (a) shows a 10 s EEG epoch containing, in the opinion of an experienced neurologist, sharp epileptic activity at channel $O2$. This EEG epoch is severely contaminated by repeated eye blinking and muscle artifacts. The activity on channel $O2$ is used to inspect the performance of the semi-automatic artifact removal of muscle artifacts. Fig. 5.8 (b-e) shows, respectively, the reconstructed EEG with exclusion of the 5, 7, 10, 14 lowest autocorrelated CCA components, respectively. By gradually excluding CCA components the muscle artifact is progressively removed, while the background EEG and the sharp epileptic activity on channel $O2$ remain unaltered. Fig. 5.8 (f) shows the EEG reconstruction with exclusion of the 15 lowest autocorrelated CCA components. Here, too many components were removed as the clinical relevant activity was removed on channel $O2$. This means that the maximal number of CCA components which can be removed is equal to 14.
This proposed semi-automatic method for muscle artifact removal can be implemented in a Graphical User Interface (GUI) with a scrolling system where moving the scroll bar corresponds to removing/adding CCA components. In this way, the BSS-CCA method becomes practical for people without experience in the field of BSS and avoids manual selection of a fairly large set of components as in ICA. An important factor in the clinical applicability of the method is that the user can easily determine the optimal number of components to be removed by observing the EEG of interest while scrolling, hereby avoiding the removal of important information. Furthermore, the method does not have the adverse effects of the existing filtering methods and removes the muscle artifact without altering the underlying brain activity (and thus without removing the interesting information). Heavily EMG contaminated recordings, that could not be interpreted with the existing filtering methods, can be correctly interpreted with the current method. Since the muscle artifact is one of the most common artifacts in scalp EEG recordings, every digital EEG acquisition station could benefit from incorporating this method.

The method is particularly suitable in an Epilepsy Monitoring Unit as at the onset of epileptic seizures the patients tend to bite, generating muscle artifacts which previously hampered the interpretation of the ictal EEG. In section 5.4

we have demonstrated that the method successfully removes the muscle artifact without altering the underlying clinical relevant ictal EEG. The method is now being evaluated on a group of 44 patients with different types of epilepsy. The first preliminary results on a subgroup of 26 patients are presented in the next section.

5.7 Clinical validation: improving the interpretation of the ictal scalp EEG

The method is now being evaluated on a group of 44 patients with different types of epilepsy. The aims of this study were:

- to study the impact of muscle artifact on the readability of ictal EEG,
- to study the impact of our new muscle artifact removal algorithm on the readability of ictal EEG,
- to study the improvement of the new method compared to the existing algorithms available for muscle artifact removal.

In this section we report on the first preliminary results on a subgroup of 26 patients.

5.7.1 Methods

One ictal EEG of 26 patients with refractory partial epilepsy and an ictal onset zone that was well-defined during a presurgical evaluation, were processed with the muscle artifact removal technique. The artifact-free recordings were compared with the band pass (0.3-35 Hz) filtered original EEGs by an unblinded neurologist.

5.7.2 Results

In 24 of 26 cases (92%) muscle artifact contaminated the ictal EEGs significantly. In all 24 cases the ictal EEG was easier to interpret after the muscle artifact was removed. In 11 out of 24 cases (42%) the interpretation of the ictal EEG improved in a clinically significant way; a more precise overview of the improvements is given below. The time of ictal onset on EEG was detected earlier in 9 out of 26 cases (35%), the onset of the seizure was better localized in 7 out of 26 (27%) and the ictal-pattern of the onset was located in a higher frequency range for 8 out of 26 cases (31%). Furthermore, we observed localized ictal-onset beta activity only after removal of muscle artifact in 5 patients (19%). Worell et al. (2002) have shown that focal ictal beta discharges localize the ictal onset zone accurately and are highly predictive of excellent postsurgical outcome [137]. The muscle artifact removal technique did not degrade the EEG signal in any of the patients. The

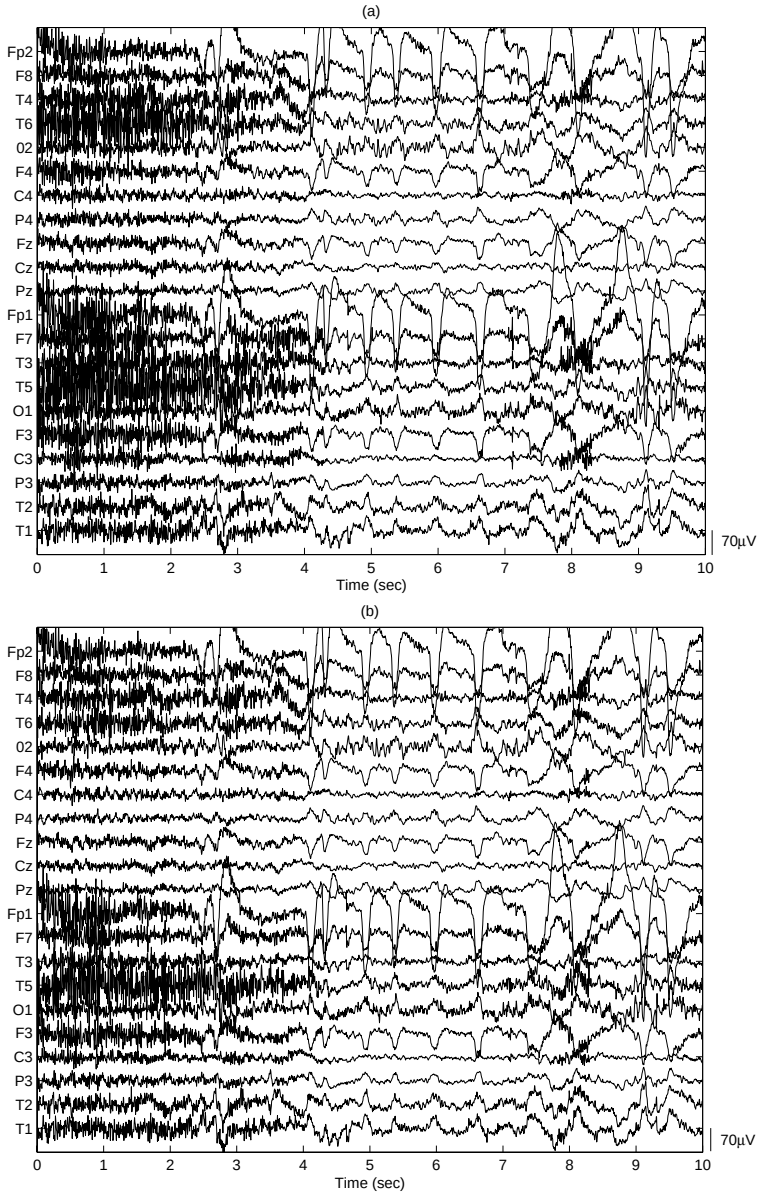

Figure 5.8: *(a) Original EEG with sharp epileptic activity on channel O2; (b) EEG after exclusion of components (17-21);*

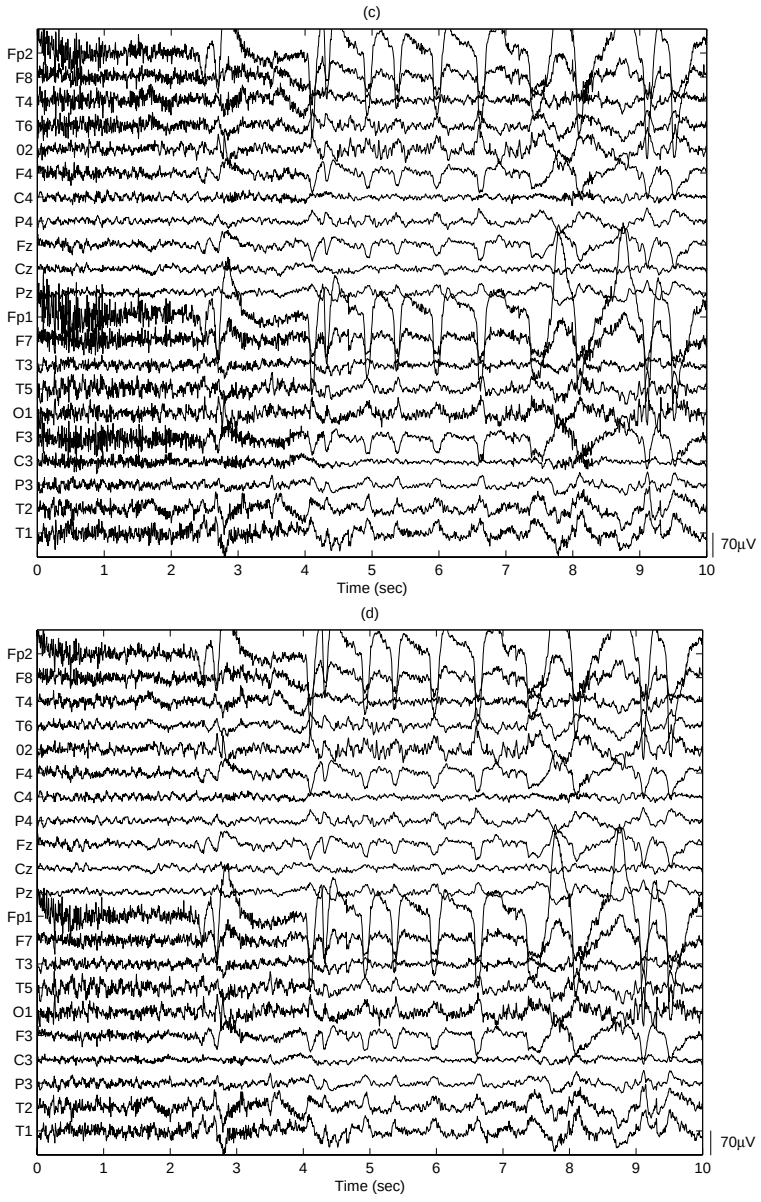

Figure 5.8: *(c) EEG after exclusion of components (15-21); (d) EEG after exclusion of components (12-21).*

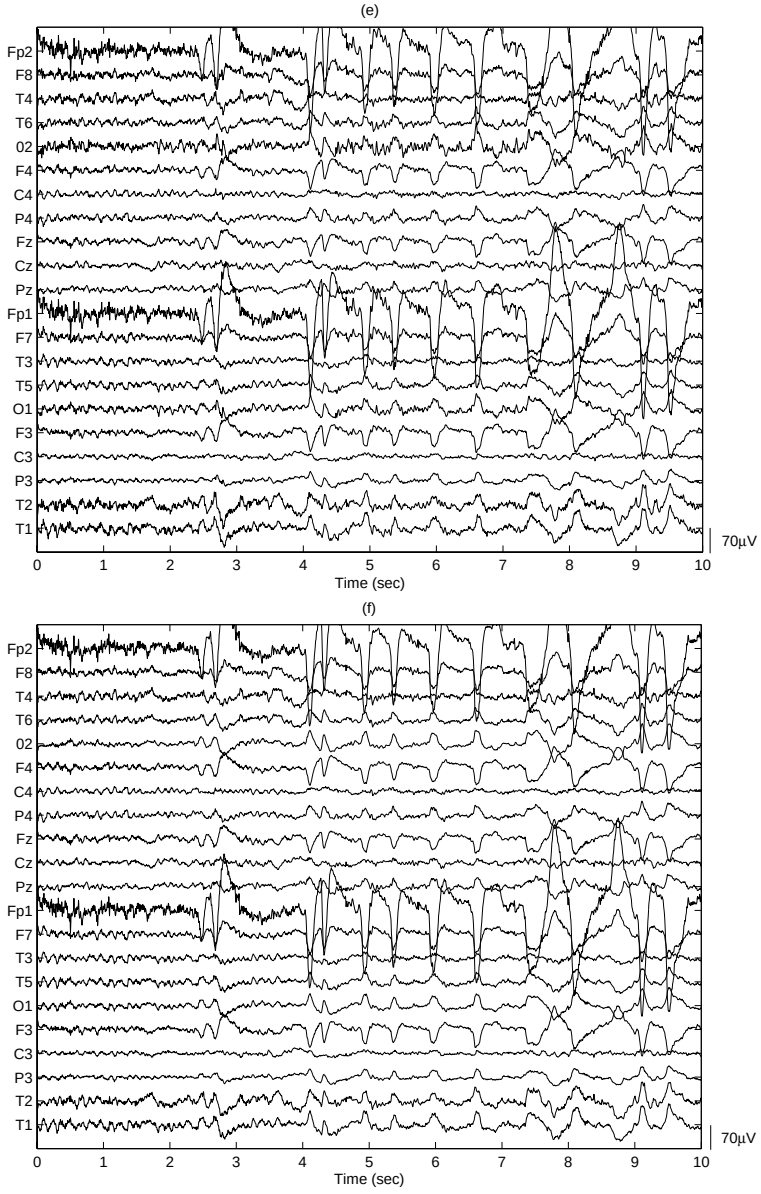

Figure 5.8: *(e) after exclusion of components (8-21); (f) EEG after exclusion of components (7-21).*

Muscle artifact contamination	24/26 (92%)
Easier interpretation	24/24 (100%)
Improved interpretation	11/24 (42%)
Earlier detection of ictal-onset in EEG	9/26 (35%)
Better localization of onset	7/26 (27%)
Onset pattern of higher frequency	8/26 (31%)
Localized onset beta activity only after removal of muscle artifact	5/26 (19%)
Degradation of EEG by the method	0/26 (0%)

Table 5.1: *Preliminary results of the clinical study.*

results are summarized in Table 5.1.

Fig. 5.9 shows an ictal EEG epoch of one of the 11 cases for which the muscle artifact removal method improved the interpretation. In Fig. 5.9 (a) the band pass (0.3-35 Hz) filtered EEG epoch is shown. Fig. 5.9 (b) shows the resulting ictal EEG epoch after muscle artifact removal by BSS-CCA. Notice that the muscle artifact was removed completely, while preserving the sharp quality ictal activity on the $T6$ and $O2$ electrodes. The ictal onset, which was masked by muscle artifact activity, becomes visible in the BSS-CCA processed ictal EEG recording.

5.7.3 Conclusion

The muscle artifact removal technique was easy to implement, fast and user-friendly in a clinical environment, and improved the interpretation of ictal EEG in a clinically significant way in around 40% of patients. We are currently conducting the same study with two blinded EEG readers and a larger sample of ictal EEGs.

5.8 Conclusion

In this chapter a new method was proposed based on canonical correlation analysis as a blind source separation technique for muscle artifact removal. The performance was tested on both synthetic data and ictal EEG. In both cases the method outperformed the low-pass filter and an ICA based technique for muscle artifact removal. Moreover, the fast computational time and the ordering of the CCA components make the proposed method applicable in clinical practice. The first preliminary results of a clinical study on 26 ictal EEGs of patients with refractory epilepsy showed that the removal of muscle artifact results in a better interpretation of the ictal EEG, leading to an earlier detection of the seizure onset and a better localization of the seizures onset zone. These findings make the current method indispensable for every Epilepsy Monitoring Unit.

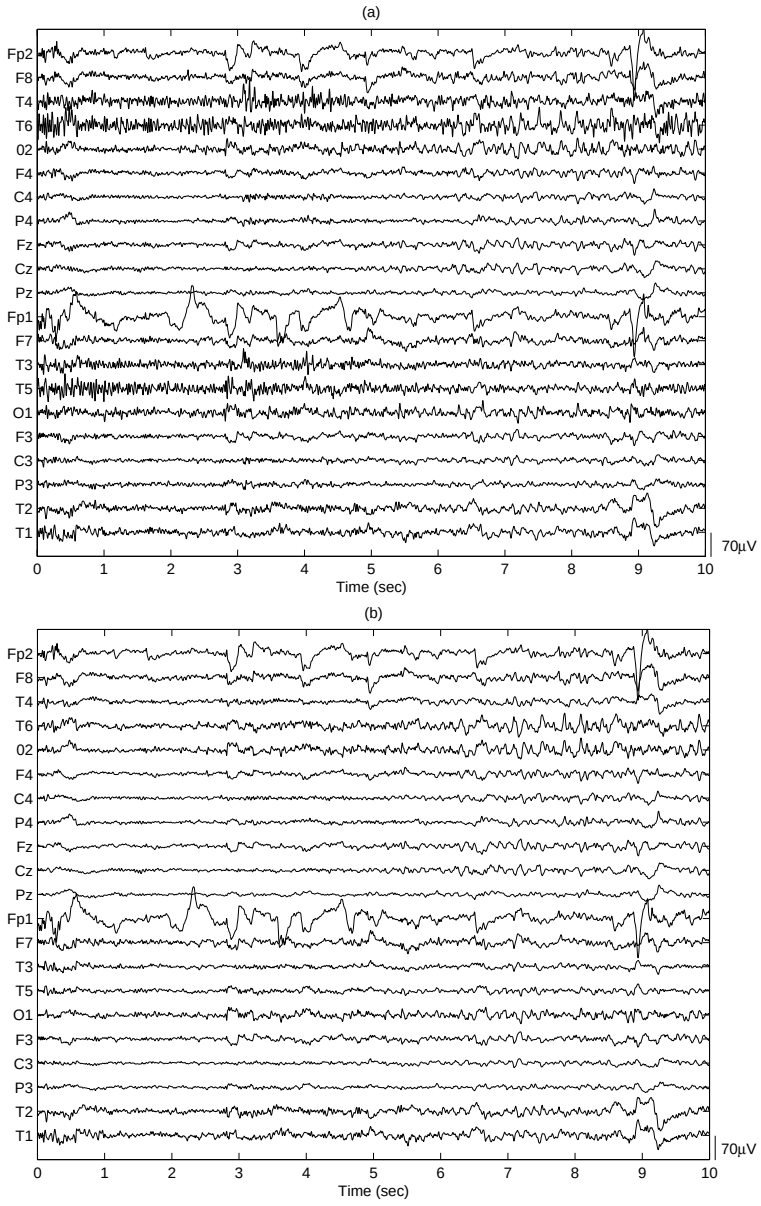

Figure 5.9: *(a) Band pass (0.3-35 Hz) filtered ictal EEG epoch of 10 s; (b) ictal EEG epoch after muscle artifact removal by BSS-CCA.*

Chapter 6

Conclusions and further research

In this final chapter, findings and conclusions of the presented work are summarized and some directions for further research are pointed out.

Seizure prediction on scalp EEG signals

Based on a data set of 12 patients with MTLE, we tried to replicate the findings reported in [74] and to detect a pre-ictal state preceding MTLE seizures using the similarity index of scalp EEG recordings. We were unable to replicate the work of Le Van Quyen et al. The similarity index was unable to detect pre-ictal changes in the scalp EEG recordings of all 12 patients with MTLE. However, in the scalp EEG recording of the patient with NPS the similarity index identified a pre-ictal state. The detection of the pre-ictal state in the patient with NPS ensured that the similarity method was correctly implemented and had the potential to identify a pre-ictal state in scalp EEG recordings. These findings were reported in [21, 19]. With these publications, our group was the first group to report on the inability to reproduce the results of one of the studies reporting on seizure prediction. After our negative results, many other studies reported on the low ability of nonlinear measures to predict seizures, confirming our findings [2, 87, 72, 71, 111]. Furthermore, we have illustrated that the similarity analysis of scalp EEG recordings would benefit from an additional preprocessing of the scalp EEG signals, in which artifacts like eye blinks and muscle artifacts are removed. As a consequence, our research was focused on artifact removal in scalp EEG recordings. The presence of artifacts might mask the brain activity related to the pre-ictal state in the scalp EEG recordings. If we want to have any success in predicting seizures from scalp EEG electrodes, we first need to remove the artifacts contaminating it. Further research on this topic should include a similarity analysis of the scalp EEG recordings after removing artifacts with the

preprocessing techniques presented in this work. The following steps need to be conducted in order to be able to perform this analysis:

- Seizure prediction methods are applied to continuous long term EEG recordings. As a consequence, automatic artifact removal techniques will be needed for the preprocessing of these long term EEG recordings. The artifact removal techniques presented in this work have proven their ability to remove artifacts. However, they are not yet fully automated and efforts should be made to automate the preprocessing methods.
- We have illustrated the sensitivity of the similarity index to the presence of eye blinks. As a consequence, these artifacts will need to be removed in order to obtain a correct analysis. In the present work, however, no research has been done on the removal of ocular artifacts. In literature, ICA was already successfully applied to ocular artifact removal [63, 99]. When applying ICA, a manual selection of the obtained independent components is required. Further research should be conducted on incorporating temporal and spatial prior knowledge into selection rules for the automatic selection of independent components related to the ocular artifacts.

Modelling the common dynamics

A new subspace-based method for modelling the common dynamics was introduced in the biomedical signal processing world in general and EEG signal processing world in particular. The method was applied for the removal of artifacts and background EEG from multichannel interictal and ictal EEG. The method was evaluated on synthetic data and interictal and ictal EEG. In all cases the proposed method removed successfully the artifact and background activity and performed better than PCA. These findings illustrated that modelling the common dynamics in multichannel EEG recordings opens new perspectives to removing artifacts and background EEG from interictal and ictal EEG. Further research is needed to address some specific issues:

- In this work the method was illustrated as a proof-of-concept on a limited number of real-life EEGs. However, in order to fully prove the quality of the method a full clinical study is necessary with a large number of EEG epochs.
- In order to fully assess the potential and limitations of this new method a thorough comparison with other artifact and noise removal techniques described in literature should be performed. Next to the comparison with PCA, performed in this work, a comparison with frequency filtering, adaptive filtering, regression methods and various ICA algorithms needs to be performed.
- If one wants to automate the proposed method one must keep in mind that the EDS model becomes ineffective when the signals of interest are not

yet started at the onset (n=0) of the selected time window. Consequently, further efforts should be made on the adaptive segmentation of EEG recordings.

- The method can be applied to other biomedical signals where there is a need to find the common information within a set of signals (e.g.[82, 96]).

Muscle artifact removal

The problem of muscle artifact removal was concerned. In this work a new method was proposed based on canonical correlation analysis as a blind source separation technique for muscle artifact removal. The performance was tested on both synthetic data and ictal EEG. In both cases the method outperformed the low-pass filter and an ICA based technique for muscle artifact removal. Moreover, the fast computational time and the ordering of the CCA components make the proposed method applicable in clinical practice. Furthermore, the method does not have the adverse effects of the existing filtering methods and removes the muscle artifact without altering the underlying brain activity (and thus without removing the interesting information). Heavily EMG contaminated recordings, that could not be interpreted with the existing filtering methods, can be correctly interpreted with the current method. Since the muscle artifact is one of the most common artifacts in scalp EEG recordings, every digital EEG acquisition station could benefit from incorporating this method.

The method is particularly suitable in an Epilepsy Monitoring Unit as at the onset of epileptic seizures the patients tend to bite, generating muscle artifacts which previously hampered the interpretation of clinical interesting EEG. We have demonstrated that the muscle artifact was successfully removed by the method without altering the underlying clinical relevant EEG. The method is now being evaluated on a group of 44 patients with different types of epilepsy. The first preliminary results on a subset of 26 ictal EEGs showed that the removal of muscle artifact results in a better interpretation of the ictal EEG, leading to an earlier detection of the seizure onset and a better localization of the seizures onset zone. These findings make the current method indispensable for every Epilepsy Monitoring Unit. Further research can be performed on the following topics:

- In this thesis, we presented the first preliminary results of a clinical study evaluating the potential clinical relevance of the method on the readability of 26 ictal EEGs. We are currently conducting the same study with two blinded EEG readers and a larger sample of ictal EEGs. The aims of this study are: (1) to study the impact of muscle artifact on the readability of ictal EEG, (2) to study the impact of our new muscle artifact removal algorithm to the readability of ictal EEG, (3) to study the improvement of the new method compared to the existing algorithms available for muscle artifact removal.

- In the presented work, we have established a semi-automatic removal of muscle artifacts based on a scrolling system. In this way, the method becomes practical for people without experience in the field of BSS and avoids manual selection of a fairly large set of components as in ICA. Further research will indicate whether thresholding on the autocorrelation index will be sufficient to remove muscle artifact automatically in a large subject group.

- As described above, the proposed EMG removal technique can be used to clean the EEG resulting in a better visual interpretation. The technique can also be used as a preprocessing step to improve the performance of further EEG signal processing tools. For example, as the muscle artifacts give rise to false positives in current seizure detection methods [119], preprocessing the EEG with CCA could improve the sensitivity and specificity of the detectors. As illustrated in this work, muscle artifacts obscure the interpretation of nonlinear measures when looking for a pre-ictal state in scalp EEG recordings [21]. Removing the artifacts could again improve the performance of the nonlinear measures. Furthermore, ictal dipole source localization would benefit considerably when muscle artifacts were removed. In the domain of the event related potentials, heavily EMG contaminated epochs will no longer need to be rejected. This could lead to a better interpretability of the ERP, especially in cases where a small number of epochs is available, as for example in complex memory tasks.

- The method could also be applied to MEG recordings. In MEG recordings the number of channels is usually much larger than in EEG. As a consequence, the number of components derived by ICA is also much larger and the selection of the artifactual ICA components on visual inspection becomes even more demanding than in EEG. For this reason, the ordered CCA components, could be of major use to MEG signals too.

- A previous pilot study has demonstrated that BSS-CCA can be used for separating ocular artifacts that are introduced in background EEG by an artificial mixing process [67]. It is for now, not clear yet whether BSS-CCA will outperform ICA on eye-blink removal from the EEG. Therefore, a study needs to be undertaken in which the performance of the eye blink removal based on BSS-CCA is compared with the performance of ICA on a large data set containing EEG recordings with eye blinks. Furthermore, it is not clear whether BSS-CCA will be the method of choice in separation of EEG brain signals in their underlying sources.

Appendix A

Parameter settings of the similarity index

In this appendix the effect of varying the parameter settings of the similarity index is studied.

A.1 Standard parameter settings

The standard parameter settings of the similarity index as described in [73] are:

- embedding dimension $m = 16$;
- SVD dimension reduction to embedding dimension $m = 4$;
- distance r equal to 30% of the cumulative distribution of pairwise Euclidean distances between the vectors of the reference set;
- delay time $\tau = 1$.

A.2 Distance

In the present application, the distance r is defined typically at 30% of the cumulative distribution of pairwise Euclidean distances between the vectors of the reference set. In this subsection we describe the effect of changing the distance r to the time course of the similarity index when it is applied on the same EEG channel.

The analysis of the similarity index was done for different values of r on the $O1$ EEG channel of the patient with NPS (patient 13, cf. Table 3.1). During this analysis, the values of the other parameters are equal to the parameter settings

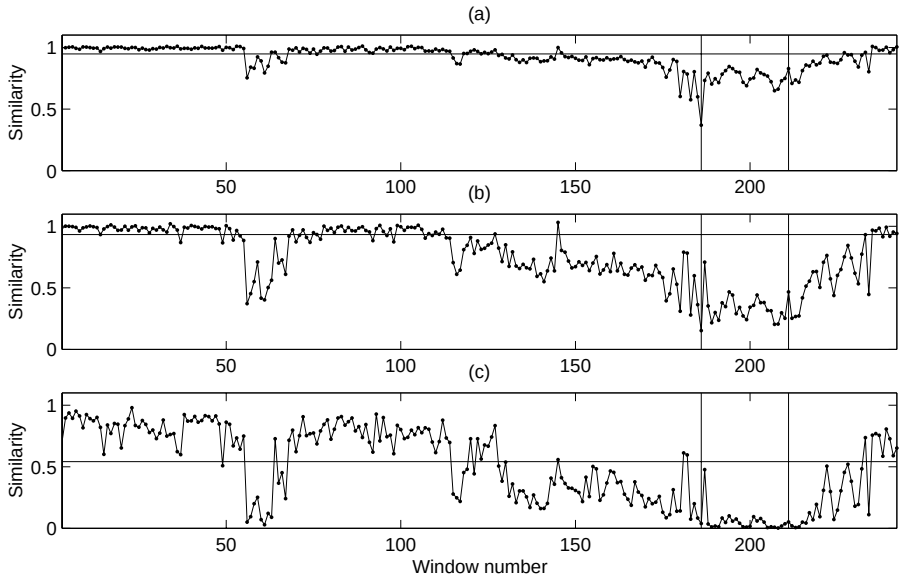

Figure A.1: *(a-c) The time course of the similarity index for r equal to (a) 50%, (b) 30% and (c) 10% of the cumulative distribution. The reference state was chosen from window number 1 to 10. Several seizures occurred between window numbers 186-211. The threshold is represented by the horizontal line. The large deviation of the similarity index between window number 60-70 was caused by artifacts.*

defined in section A.1 and remain unchanged. Fig. A.1 (a-c) shows the time course of the similarity index for r equal to 50%, 30% and 10% of the cumulative distribution, respectively. Decreasing the r value increases the sensitivity of the similarity index to dynamical changes. A lower r results in more pronounced drops in the time course of the similarity index. However, the standard deviation of the similarity index during the reference period (window 1 to 10) also increases. As a consequence, the threshold value of 5 standard deviations increases. Fig. A.2 shows the similarity analysis of channel $O1$ of patient 13 for different r values; the window numbers that drop below the threshold are colored in black. The pre-ictal state, defined as a sustained deviation below the threshold up to the seizure onset, is not detected when r is chosen to low.
We analyzed the scalp EEG recordings of all 12 patients with mTLCPS (cf. Table 3.1) with different r values ranging from 10% to 60% of the cumulative distribution. A sustained deviation below the statistical threshold up to the onset of the seizure was never observed.

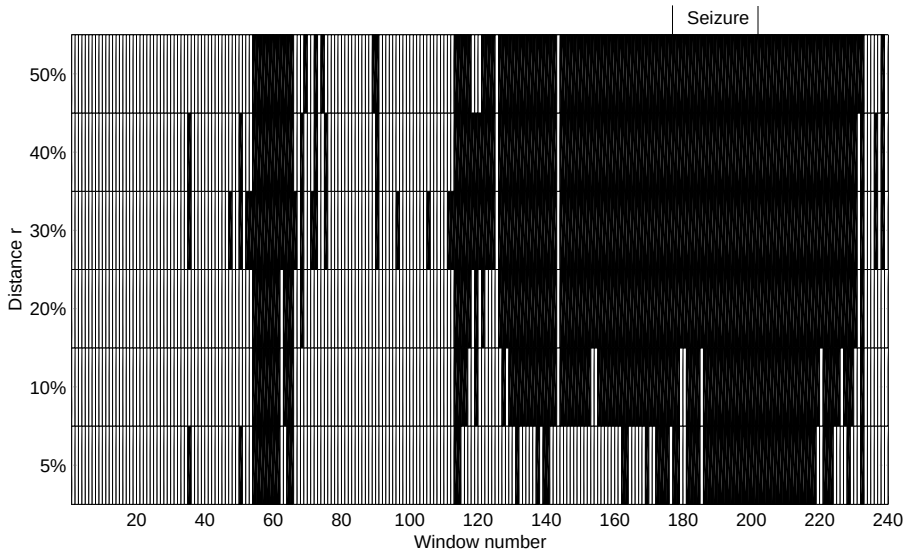

Figure A.2: *Similarity analysis of channel $O1$ of patient 13 for different r values. The window numbers that drop below the threshold are colored in black.*

A.3 Dimension reduction by SVD truncation

In order to further improve the dynamical reconstruction and reduce the noise level, a singular value decomposition of the 16-dimensional embedding space was applied, identifying the optimal space that contains the trajectory. The 16-dimensional reconstruction of the window W_t, $\mathbf{A}(W_t)$, is projected on the principal axes of the reference dynamics

$$\mathbf{X}(W_t) = \mathbf{A}(W_t) \cdot \mathbf{V}, \tag{A.1}$$

where $\mathbf{V}$ is the eigenvector matrix of the reference window. In order to retain the main components of the dynamics and to reduce the noise level, the embedding dimension was reduced to $m = 4$ by truncation of $\mathbf{V}$. In this subsection the effect of changing the truncation of $\mathbf{V}$ on the time course of the similarity index was studied.

The analysis of the similarity index was done on the $O1$ EEG channel of patient 13 for different truncations of $\mathbf{V}$. During this analysis, the values of the other parameters are equal to the parameter settings defined in section A.1 and remain unchanged. Fig. A.3 (a-c) shows the time course of the similarity index for a dimension reduction to m equal to 4, 8 and 12, respectively. The higher the dimension reduction, the less noisy the time profile of the similarity index and the more pronounced the pre-ictal state. Fig. A.4 shows the similarity analysis of

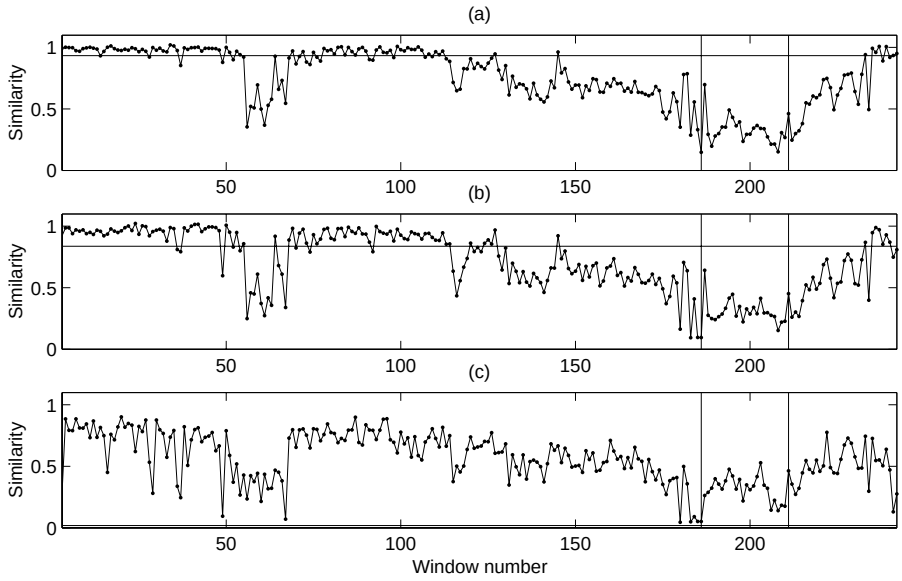

Figure A.3: *(a-c) The time course of the similarity index for a dimension reduction to (a) m=4, (b) m=8 and (c) m=12. The reference state was chosen from window number 1 to 10. Several seizures occurred between window numbers 186-211. The threshold is represented by the horizontal line. The large deviation of the similarity index between window number 60-70 was caused by artifacts.*

channel $O1$ of patient 13 for different dimension reductions; the window numbers that drop below the threshold are colored in black. A dimension reduction to $m \leq 8$ is necessary to detect the pre-ictal state on this EEG channel.
We analyzed the scalp EEG recordings of all 12 patients with mTLCPS (cf. Table 3.1) with different dimension reductions ranging from $m = 2$ to $m = 10$. A sustained deviation below the statistical threshold up to the onset of the seizure was never observed.

A.4 Embedding dimension

The analysis of the similarity index was done for different values of the embedding dimension m on the $O1$ EEG channel of the patient with NPS (patient 13, cf. Table 3.1). During this analysis, the values of the other parameters are equal to the parameter settings defined in section A.1 and remain unchanged. Fig. A.5 (a-c) shows the time course of the similarity index for an embedding dimension equal to 4, 16 and 24. A higher embedding dimension leads to a more pronounced pre-ictal dimension drop, while the standard deviation of the reference state remains more or less unaltered.

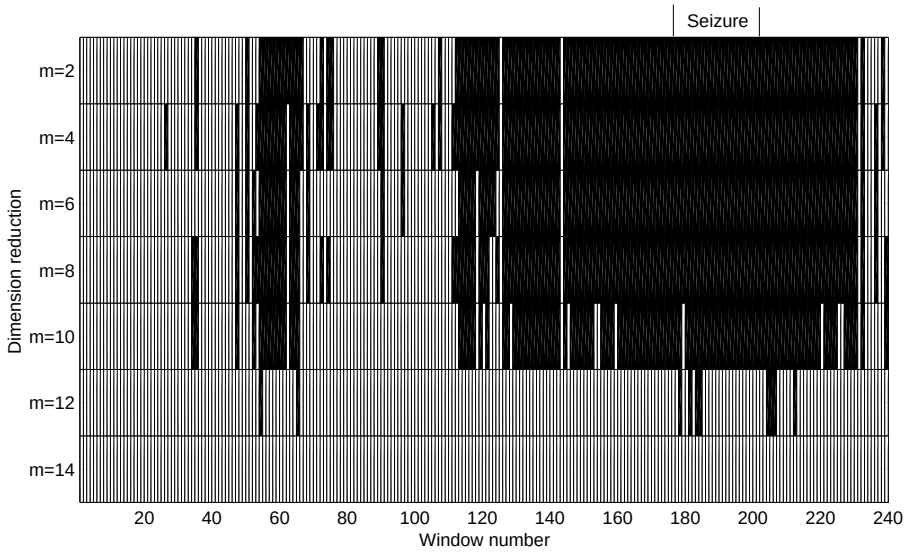

Figure A.4: *Similarity analysis of channel $O1$ of patient 13 for different dimension reductions. The window numbers that drop below the threshold are colored in black.*

We analyzed the scalp EEG recordings of all 12 patients with mTLCPS (cf. Table 3.1) with different embedding dimension ranging from $m = 4$ to $m = 24$. A sustained deviation below the statistical threshold up to the onset of the seizure was never observed.

A.5 Delay time

The analysis of the similarity index was done for different values of τ on the $O1$ EEG channel of the patient with NPS (patient 13, cf. Table 3.1). During this analysis, the values of the other parameters are equal to the parameter settings defined in section A.1 and remain unchanged. Fig. A.6 (a-c) shows the time course of the similarity index for a time delay τ equal to 1, 5 and 7, respectively. Increasing the τ value has no significant effect on the time course of the similarity profile.

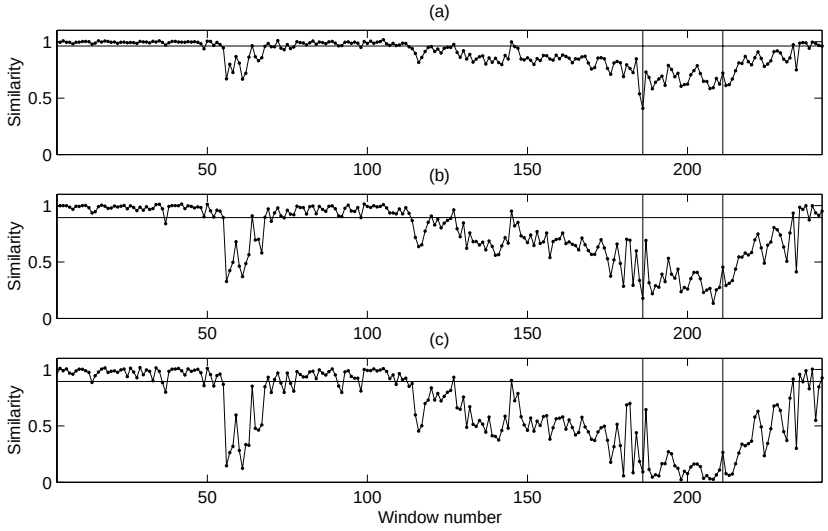

Figure A.5: *(a-c) The time course of the similarity index for an embedding dimension equal to (a) m=4, (b) m=16 and (c) m=24. The reference state was chosen from window number 1 to 10. Several seizures occurred between window numbers 186-211. The threshold is represented by the horizontal line. The large deviation of the similarity index between window number 60-70 was caused by artifacts.*

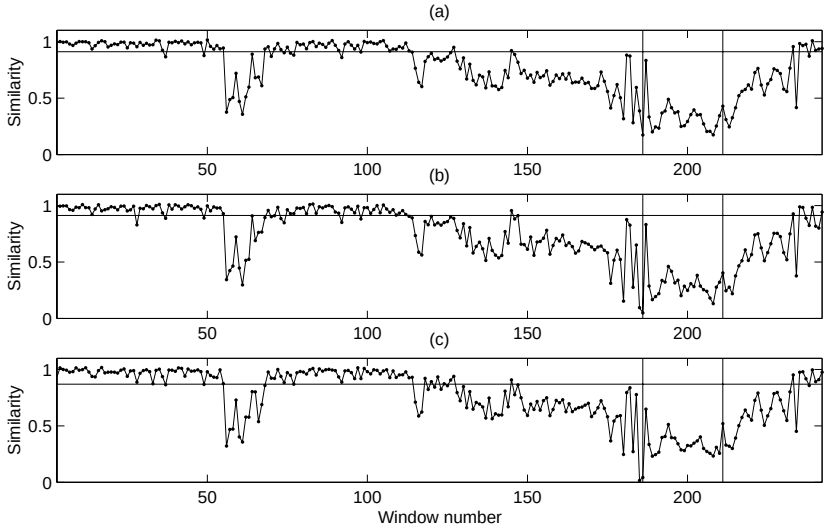

Figure A.6: *(a-c) The time course of the similarity index for a delay time equal to (a) $\tau = 1$, (b) $\tau = 5$ and (c) $\tau = 7$. The reference state was chosen from window number 1 to 10. Several seizures occurred between window numbers 186-211. The threshold is represented by the horizontal line. The large deviation of the similarity index between window number 60-70 was caused by artifacts.*

Appendix B

Mean phase coherence as a measure for phase synchronization and its application to the scalp EEG of patients with MTLE

The exact mechanisms leading to the occurrence of epileptic seizures in humans are still poorly understood. It is widely accepted, however, that the process of seizure generation is closely associated with abnormal synchronization of neurons. In order to investigate this process, the phase synchronization between different regions of the brain is measured using intracranial EEG recordings [93, 92, 70, 76, 77]. In [93, 92] it is shown that a large majority of analyzed seizures are preceded by a decrease in mean phase coherence as a measure for phase synchronization between the EEG signals recorded simultaneously from different locations in the brain. The pre-ictal state could be discriminated from the interictal state, which makes the method a promising concept for prospective seizure anticipation. In this appendix we will describe the method of mean phase coherence in detail and apply the method to scalp EEG recordings of patients with MTLE.

B.1 Hilbert transform

The Hilbert transform will be used to determine the instantaneous phase and amplitude of the original signal. Given a measurement $s(t)$ we define the analytic signal

$$Z(t) = s(t) + i\tilde{s}(t) = A(t)e^{i\phi(t)}, \tag{B.1}$$

where the function $\tilde{s}(t)$ is the Hilbert transform of $s(t)$:

$$\tilde{s}(t) = \frac{1}{\pi} P \int_{-\infty}^{+\infty} \frac{s(\tau)}{t-\tau} d\tau. \tag{B.2}$$

P indicates that the integral is taken in the sense of Cauchy principal value. The instantaneous phase angle of the input sequence $s(t)$ is the angle of the analytic signal given by:

$$\phi(t) = \arctan \frac{\tilde{s}(t)}{s(t)} \tag{B.3}$$

The instantaneous amplitude of $s(t)$ is given by $A(t)$.

B.2 Mean phase coherence

Phase synchronization is usually defined as locking of the phases of two oscillators a and b:

$$\phi_{n,m}(t) = n\phi_a(t) - m\phi_b(t) = const. \tag{B.4}$$

In brief, for studying phase synchronization two steps are needed:

1. estimate the instantaneous phase of each signal; and
2. provide a statistical criterion to quantify the degree of phase locking.

The instantaneous phase is estimated by the Hilbert transform. Since our aim is to measure the synchronization between time series that are obtained from the same physiological system (i.e. the brain), we consider it most likely to encounter synchronization at a phase locking ratio of $n : m = 1 : 1$ [93, 76]. Thus restricting ourselves to the case $n = m = 1$, we employ as a statistical measure for synchronization the *mean phase coherence* of an angular distribution [93] defined as

$$R = \left| \frac{1}{N} \sum_{j=0}^{N-1} e^{i\phi_{1,1}(j\Delta t)} \right|, \tag{B.5}$$

where $1/\Delta t$ is the sampling rate of the discrete time series. By construction, R will be zero if the phases are not synchronized at all and will be one when the phase difference is constant (perfect synchronization). This becomes evident by

the use of Euler's formula that turns R into

$$R = \left(\left[\frac{1}{N} \sum_{j=0}^{N-1} sin(\phi_{1,1}(j\Delta t)) \right]^2 + \left[\frac{1}{N} \sum_{j=0}^{N-1} cos(\phi_{1,1}(j\Delta t)) \right]^2 \right)^{1/2} . \quad \text{(B.6)}$$

The analysis of phase synchronization is usually done around a certain frequency value. A frequency range is defined around the chosen frequency (e.g. $\pm 2Hz$) and the signals are filtered with a bandpass filter corresponding to the particular frequency band.

B.3 Phase synchronization analysis of the scalp EEG of patients with MTLE

In this study scalp EEG recordings from 12 patients with MTLE were used (see Table 3.1 in chapter 3 for a full description of the materials). In order to find characteristic differences between interictal and ictal recordings, the phase synchronization between every possible combination of electrode contacts is evaluated in different frequency bands using the moving window technique. The analysis was performed in the following way: first the signals were filtered with a bandpass filter corresponding to a particular frequency band. Next, the filtered time series were divided into segments of 1250 sampling points each, corresponding to a window length of 5 sec; the windows did not overlap. Then the instantaneous phase of each filtered window is extracted by means of the Hilbert transform. Finally, the phase locking was characterized by the mean phase coherence. In order to leave the phase of the signal unaltered, the data was filtered with a Finite Impulse Response (FIR) filter.

In most of the analyzed scalp EEG recordings we observed an increased synchronization between several electrode pairs during the seizure, mostly in the theta ($4-8$Hz) and/or delta ($1-4$Hz) frequency band. As an example, the time course of the phase synchronization in the theta frequency range between channel $T4$ and channel $T6$ of patient 7 (cf. Table 3.1) is shown in Fig. B.1 (b). The ictal period is between the two vertical lines. For the interictal recording the synchronization is quite stable at a low constant level. During the ictal period an increased level of synchronization between the two channels in the theta band is observed. Fig. B.1 (a) shows the seizure onset as recorded on the $T4$ and $T6$ electrodes. The same rhythmic 5Hz epileptic activity appears on both channels, resulting in a high phase synchronization in the theta frequency band.

In Fig.B.2 the phase synchronization in the theta ($4-8$Hz) frequency band of channel $T2$ with all other EEG channels of patient 5 (cf. Table 3.1) is shown.

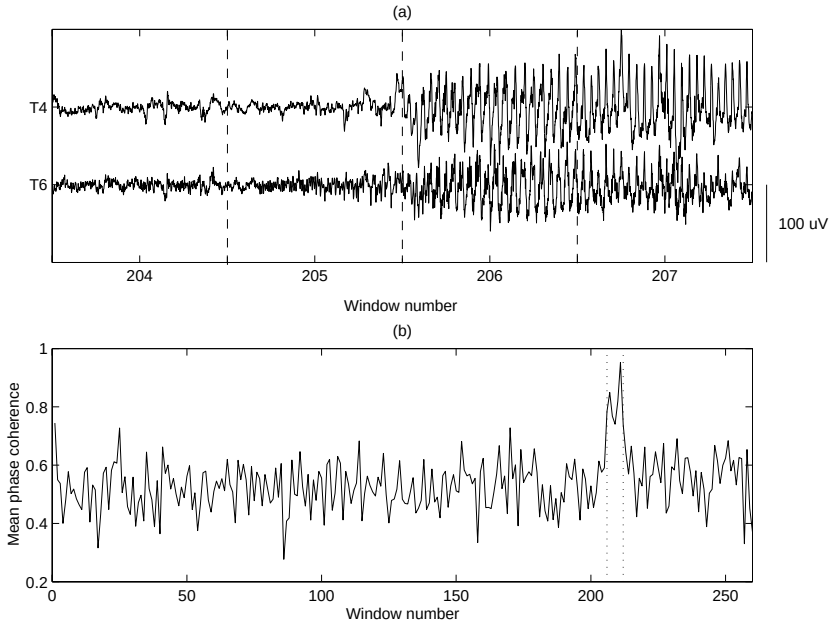

Figure B.1: *(a) The seizure onset as recorded on electrodes $T4$ and $T6$. The seizure starts in the beginning of window 206. (b) The mean phase coherence in the theta (4-8Hz) frequency band between channel $T4$ and channel $T6$. The seizure lasted from window number 206 to 212 (between vertical dotted lines). An increased level of synchronization is observed during the seizure.*

The ictal period is between the vertical lines. An increased synchronization of $T2$ with mainly the right frontal and temporal electrodes $F8$, $T4$ and $T6$ is observed during the ictal period. As for this patient the epileptic focus is located in the right temporal lobe, the epileptic waveform is the dominant activity on those electrodes resulting in an increased level of synchronization. For all other channels the epileptic waveform is mixed with background activity or below the noise level, resulting in a moderate increase or an unchanged level of synchronization of those electrodes with electrode $T2$.

In contrast to the use of the mean phase coherence on intracranial recordings, no pre-ictal decrease in synchronization was observed in any of the analyzed seizures. In the intracranial studies [93, 92] the phase synchronization is evaluated between the EEG signals recorded simultaneously from different locations in the brain. As discussed in section 2.3.3, the scalp EEG can not be used to measure such localized activity in the brain and consequently the pre-ictal decrease in synchronization is not observed when analyzing scalp EEG signals. What can be observed is an increased level of synchronization between different electrode pairs

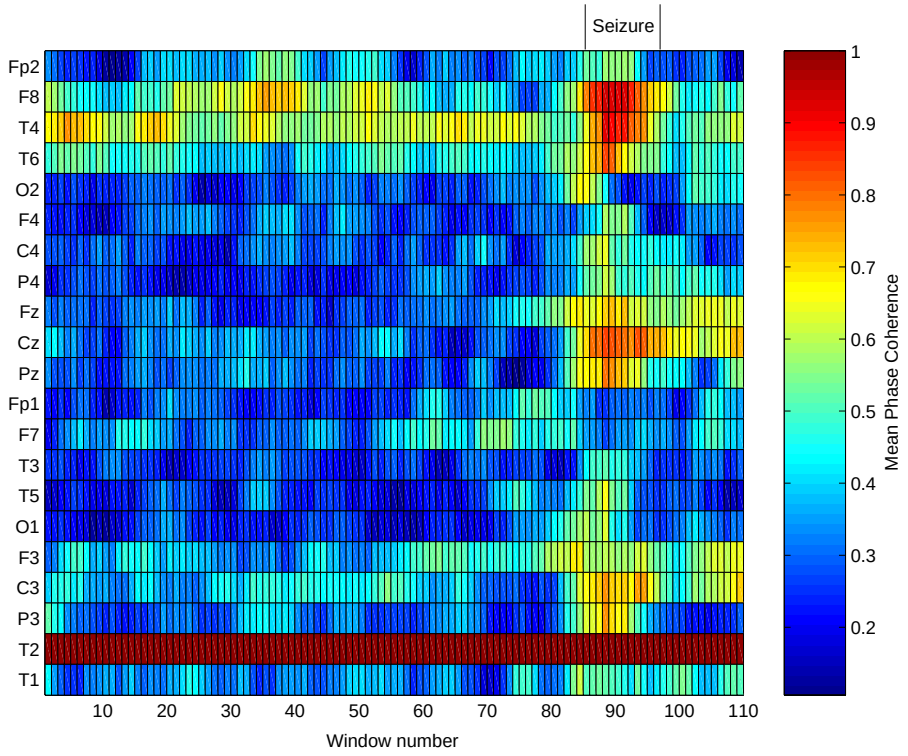

Figure B.2: *Synchronization between channel $T2$ and all other channels of the scalp EEG recording of patient 5. The ictal period is between the vertical lines. An increased synchronization of $T2$ with mainly the right frontal and temporal electrodes $F8$, $T4$ and $T6$ is observed during the ictal period. An average reference montage was used.*

during an epileptic seizures, due to the same epileptic waveform appearing on different scalp EEG channels. Which subset of electrodes becomes synchronized depends on the location and the corresponding field distribution of the epileptic focal source.

With the aim of constructing a fast analysis tool for characterizing interictal and ictal scalp EEG signals, three other measures were derived from the Hilbert transform. The Hilbert transform was used to define the instantaneous amplitude, frequency and rhythmicity of the scalp EEG recordings. The definition of these measures and their application to scalp EEG signals are fully described in [20].

Appendix C

Analyzing multichannel scalp EEG signals of patients with epilepsy using exponential data modelling

An epileptic seizure is a clinical manifestation due to an excessive and synchronized discharge of a group of neurons in the brain (cf. Chapter 2). Because of this excessive discharge the rhythmic epileptic waveform becomes the dominant waveform on all EEG channels during generalized and secondarily generalized seizures. This results in a high degree of common information in the different EEG channels. The interictal period, however, is characterized by a less orderly state of relatively low neuronal synchrony resulting in EEG signals of high complexity with multiple frequencies and a low degree of common activity in the different EEG channels [6]. In this appendix a multichannel analysis based on the subspace based pole estimation method HTLS (Hankel Total Least Squares) [131] was performed on the scalp EEG signals of patients with generalized and secondarily generalized seizures. The aim was to detect the decreased complexity and increased level of common information of the seizure EEG. Several measures were derived which allowed to make the distinction between three types of EEG recordings containing awake, sleep and epileptic seizure activity in all patients studied. The information can be useful for automatic scoring of EEG or an automated detection system for generalized and secondarily generalized seizures and sleep EEG. More research has to be conducted to determine the sensitivity and specificity of the derived measures on long term EEG recordings of a larger patient group. This study was published as a conference proceedings paper [22].

Patient	Age	Gender	Type of seizure	Number of seizures
P1	38	F	GS	2
P2	24	M	GS	1
P3	14	M	GS	6
P4	36	F	SGS	1
P5	26	M	SGS	1

Table C.1: Patients information.

C.1 Materials

The EEGs of 5 patients with epilepsy were evaluated. The EEG recordings were performed on a 21-channel OSG EEG recorder. The electrodes were placed according to the extended international 10-20 System [107]. The scalp potentials were sampled at 250 Hz. For the analysis of the signals a reference montage was used. The data were filtered between 1 and 30 Hz with a bandpass filter (finite impulse response). Three patients had Generalized Seizures (GS) and two patients had Complex Partial Seizures (CPS) evolving to Secondarily Generalized Seizures (SGS). Clinical seizure onset and end were determined by an epileptologist electroencephalographer. Table C.1 gives an overview of the age, gender, type of seizure and, number of seizures applied for each patient. In this study we used three EEG recordings to explore the behavior of the proposed measures derived in the methods section. The three EEGs studied are shown in Fig. C.1. In (a) the onset of a generalized seizure is presented. The seizure starts around t = 4.5 s. Recording (b) shows a normal awake EEG, recording (c) is an EEG recorded during sleep. All EEG recordings are from patient P3 (cf. Table C.1). In the generalized seizure EEG (recording (a) from t = 4.5 s to t = 10 s) we observe that most of the scalp EEG channels are represented by the same periodic signals of low complexity.

C.2 Methods

C.2.1 Subspace based pole estimation methods

A way to analyze EEG signals is to quantify them directly in the time domain by means of model-based (or parametric) methods. We used a method, called HTLS [131], where the EEG signal is modelled as a sum of K exponentially damped

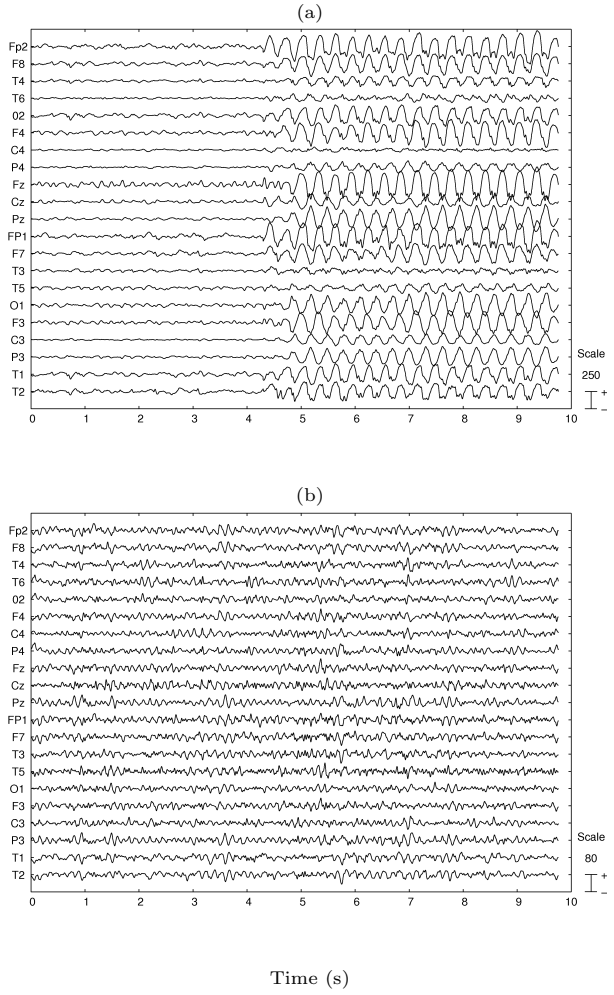

Figure C.1: *(a) shows an EEG recording of the onset of a generalized seizure, starting at $t = 4.5$ s. Recording (b) shows a normal awake EEG. The unit used on the Y-axis is μV.*

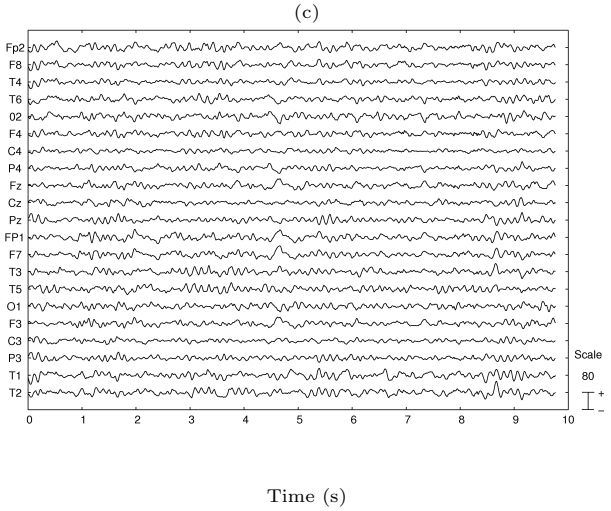

Figure C.1: *(c) Represents an EEG recorded during sleep. The unit used on the Y-axis is μV.*

sinusoids:

$$\begin{aligned} \overline{y}(n) &= \sum_{k=1}^{K} a_k e^{j\phi_k} e^{(-d_k + j2\pi f_k)n\Delta t}, \\ &= \sum_{k=1}^{K} c_k z_k^n, \\ n &= 0, 1, \ldots, N-1; \end{aligned} \tag{C.1}$$

with complex amplitudes

$$c_k = a_k e^{j\phi_k}, \tag{C.2}$$

and signal poles

$$z_k = e^{(-d_k + j2\pi f_k)\Delta t}. \tag{C.3}$$

$\overline{y}(n)$ represents the n-th modeled data point and Δt the constant sample interval between consecutive data points. The parameters to be determined are the frequencies f_k, dampings d_k, amplitudes a_k and phases ϕ_k. The model is a good approximation of the signal if the model order *(K)*, which is twice the number of frequency components, is chosen correctly. HTLS allows quantifying the frequencies more accurately with fewer data points than non-parametric methods such as the FFT (Fast Fourier Transform) [96]. Therefore, the method is better

suited for non-stationary signals (like EEG signals). An interesting generalization is HTLSstack [134], which allows to model the dynamics of the different EEG channels at the same time. In this case the data from each EEG channel are arranged in separate Hankel matrices and these are stacked together in one block matrix. HTLS is applied to this matrix in order to extract common frequencies and dampings (signal poles). Once these parameters are identified, the corresponding amplitudes and phases are determined separately for each channel. More details about the algorithm and some applications can be found in [134, 96, 133].

C.2.2 Measures based on the energy distribution of the common signal poles

First, the time series were divided into segments of 250 sampling points each, corresponding to a window length of 1 sec. The windows did not overlap. To get an idea of the dynamics in all EEG channels the channels were modelled with HTLSstack [134] and the energy distribution of the common signal poles was calculated. Equation C.4 gives the multichannel model function; all EEG channels are modelled with common frequencies f_k and dampings d_k (signal poles z_k) but different amplitudes $a_k^{y_i}$ and phases $\phi_k^{y_i}$:

$$\begin{aligned} \overline{y}_i(n) &= \sum_{k=1}^{K} a_k^{y_i} e^{j\phi_k^{y_i}} e^{(-d_k+j2\pi f_k)n\Delta t}, \\ &= \sum_{k=1}^{K} c_k^{y_i} z_k^n, \\ n &= 0, 1, \ldots, N-1; \\ i &= 1, 2, \ldots, I; \end{aligned} \tag{C.4}$$

with I equal to the number of EEG channels and N equal to the number of data points in a time window. Once the parameters are determined the energy of a signal pole z_k in channel i is computed as follows:

$$\begin{aligned} E(i,k) &= \sum_{n=0}^{N-1} |a_k^{y_i} e^{j\phi_k^{y_i}} e^{(-d_k+j2\pi f_k)n\Delta t}|^2, \\ n &= 0, 1, \ldots, N-1; \\ k &= 1, 2, \ldots, K; \\ i &= 1, 2, \ldots, I. \end{aligned} \tag{C.5}$$

To avoid that channels with a higher amplitude have a larger influence, equation C.5 is divided by the total energy of the channel. The relative energy contribution

of signal pole z_k to channel i is given by :

$$\begin{aligned} E_r^{channel}(i,k) &= \frac{E(i,k)}{\sum_{n=0}^{N-1} \mid \overline{y}_i(n) \mid^2}, \\ i &= 1,2,\ldots,I; \\ k &= 1,2,\ldots,K. \end{aligned} \tag{C.6}$$

The relative contribution of each signal pole to the total multichannel energy is determined as follows:

$$E_r^{multichannel}(k) = \frac{\sum_{i=1}^{I} E_r^{channel}(i,k)}{\sum_{k=1}^{K}\sum_{i=1}^{I} E_r^{channel}(i,k)}, \tag{C.7}$$

$$k = 1,2,\ldots,K.$$

Equation C.7 represents the energy distribution of the common signal poles. In Fig. C.2 the distribution of $E_r^{multichannel}(k)$ for the 15 first signal poles is shown for a seizure (a), awake (b) and sleep (c) EEG time window of 1 second. In this figure we see that for the seizure epoch more than 80% of the total energy is present in one signal pole indicating that one frequency component is dominant in many channels reflecting the increased neuronal synchrony during the generalized seizure. In the awake and sleep EEG epoch the energy is more evenly distributed among the various signal poles. For each distribution a vertical line is plotted at the 90% energy level. The signal poles on the right hand side of this line account for 90% of the total multichannel energy. A lower number of signal poles necessary to represent 90% of the energy indicates that the complexity of the multichannel EEG is lower. Again the complexity of the seizure EEG recording is lower because of the increased neuronal synchrony. The findings above have motivated us to define the following measures:

Most Active Signal Pole and $\mathbf{E}_{MASP}$. The Most Active Signal Pole (MASP) is defined as the signal pole with the highest $E_r^{multichannel}(k)$:

$$E_{MASP} = max_k(E_r^{multichannel}(k)). \tag{C.8}$$

E_{MASP} represents the amount of energy that the most active signal pole contributes to the total energy. The higher the energy contribution of the most active signal pole to the total multichannel energy the more important this signal pole.

Frequency$_{MASP}$. The frequency of the most active signal pole is called frequency$_{MASP}$.

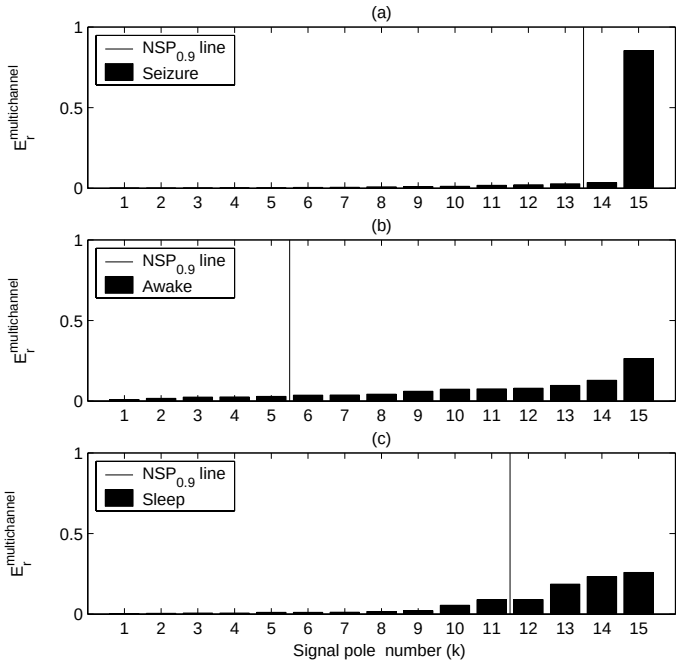

Figure C.2: *Distribution of the $E_r^{multichannel}(k)$ for (a) a generalized seizure, (b) awake and (c) sleep segment of 1 second (patient P3) is shown. A vertical line is plotted at the 90% energy level. The signal poles on the right hand side of this line represent 90% of the total multichannel energy.*

Multiplicity$_{MASP}$. The number of channels where the most active signal pole has the maximum energy contribution of all signal poles for that channel, divided by the total number of channels, is defined as multiplicity$_{MASP}$. If the MASP is the dominant signal pole in all EEG channels then the multiplicity$_{MASP}$ is equal to 1.

NSP$_{0.9}$. The Number of Signal Poles needed to represent 90% of the total multichannel energy is defined as NSP$_{0.9}$. A lower NSP$_{0.9}$ indicates that the complexity of the multichannel EEG epoch is lower.

C.3 Results

First we will explore the behavior of the above defined measures on the three EEG recordings shown in figure C.1. Subsequently the time evolution of the measures

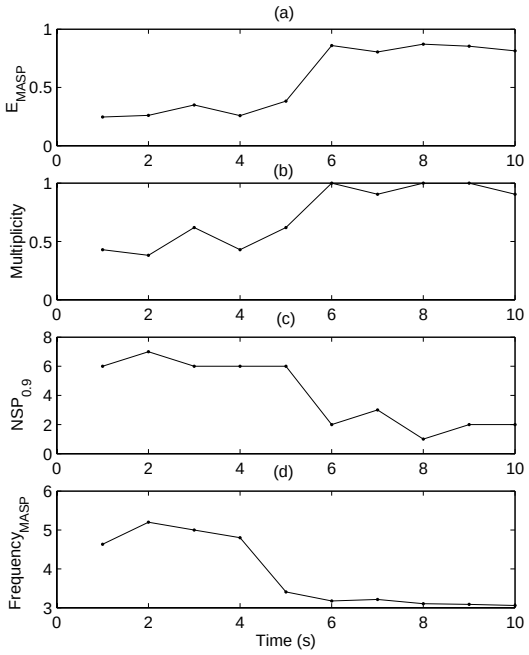

Figure C.3: *Time course is shown of (a) E_{MASP}, (b) multiplicity$_{MASP}$, (c) $NSP_{0.9}$ and (d) frequency$_{MASP}$ of the EEG containing the generalized seizure onset (recording (a) shown in Fig. C.1).*

is evaluated on long term EEG recordings of all patients. These EEG recordings contain periods with normal awake, epileptic seizure and, sleep activity.

C.3.1 Case studies

Fig. C.3 shows the time course of the measures of recording (a) in Fig. C.1. Because of the increased neuronal synchrony there is a strong increase in the energy and the multiplicity of the most active signal pole at seizure onset (t = 4.5 s). The energy of the MASP increases from ~ 0.3 to ~ 0.8 at seizure onset. The multiplicity$_{MASP}$ increases from ~ 0.5 to ~ 1. These findings reflect the fact that the same frequency component becomes dominant in all channels during the seizure because of the increased neuronal synchronization. The number of signal poles needed to account for 90% of the total energy drops at seizure onset from $\sim$ 7 signal poles to $\sim$2 signal poles indicating that the complexity of seizure EEG is lower. The frequency of the most active signal pole drops from 5 Hz before seizure onset to 3 Hz during the seizure (corresponding to the frequency of the epileptic activity). Fig. C.4 illustrates the time courses of the E$_{MASP}$, multiplicity$_{MASP}$,

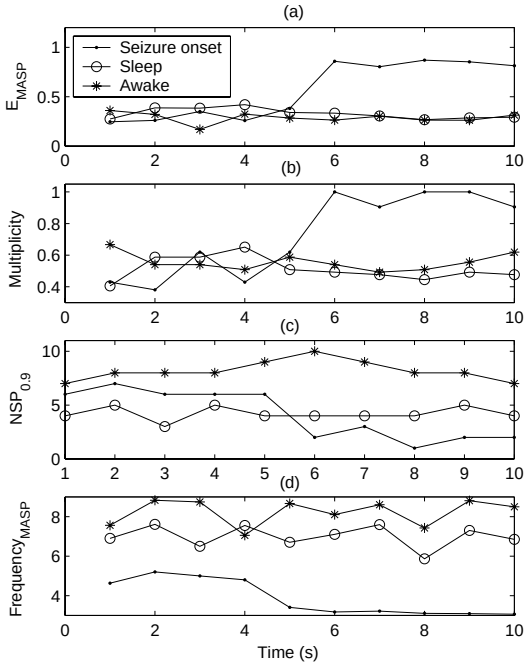

Figure C.4: *(a) E_{MASP}, (b) $multiplicity_{MASP}$, (c) $NSP_{0.9}$ and (d) $frequency_{MASP}$ are shown for the three EEG recordings (i.e. seizure onset, awake and sleep) shown in Fig. C.1.*

$NSP_{0.9}$ and $frequency_{MASP}$ for the three different recordings (i.e. seizure, awake, sleep) shown in Fig. C.1. The energy and the multiplicity of the most active signal pole is higher for the seizure EEG than for the sleep and awake EEG recordings (Fig. C.4 (a) and (b)). In the awake and sleep EEGs the energy is more evenly distributed than in the seizure EEG resulting in a lower E_{MASP}. The E_{MASP} and $multiplicity_{MASP}$ of the awake EEG and sleep EEG are almost equal. The number of signal poles necessary to account for 90% of the total multichannel energy is lower for the seizure and sleep EEG recordings than for the awake EEG recording as shown in Fig. C.4 (c) and Fig. C.2. This analysis indicates that awake EEG epochs are of greater complexity than generalized seizures and sleep epochs.

As shown in Fig. C.4 (d) the frequency of the most active signal pole in the awake EEG recording is around 8.5 Hz representing alpha activity. In the sleep recording the frequency of the MASP is around 7 Hz (theta activity). In the seizure onset recording the frequency of the most active signal pole drops from 5 Hz before seizure onset to 3 Hz during the seizure.

C.3.2 Long term EEG recordings

We applied the defined measures on EEG recordings of all patients containing periods with normal awake, epileptic seizure and sleep activity. We will discuss the results in two separate subsections depending on the type of seizure of the patient.

Generalized seizures. Fig. C.5 shows the time course of the E_{MASP}, multiplicity$_{MASP}$ and NSP$_{0.9}$ of patient P2 (cf. Table C.1). As shown the generalized seizure is characterized by a more active MASP (a higher E_{MASP}, multiplicity$_{MASP}$) compared to the awake and sleep EEG. The sleep period is distinguished from the awake and seizure EEG because the NSP$_{0.9}$ is lower than the awake NSP$_{0.9}$ and the E_{MASP} is lower than the seizure E_{MASP}. Based on these findings we can conclude that the measures are able to distinguish three types of EEGs (i.e. awake, seizure and sleep). These conclusions can be generalized for all other patients with generalized seizures (i.e. patients P1, P2 and P3).

Secondarily generalized seizures. Fig. C.6 shows the time course of the E_{MASP}, multiplicity$_{MASP}$ and NSP$_{0.9}$ for patient P4 with complex partial secondarily generalized seizures (cf. Table C.1). The end of the seizure is characterized by a more active MASP (a higher E_{MASP}, multiplicity$_{MASP}$) compared to the awake and sleep EEG. This is the part where the seizure activity spreads out to the majority of the EEG channels. The sleep period is distinguished from the awake and ictal EEG because the NSP$_{0.9}$ is lower than the awake NSP$_{0.9}$ and the E_{MASP} (multiplicity$_{MASP}$) is lower than the ictal E_{MASP} (multiplicity$_{MASP}$). The E_{MASP} and multiplicity$_{MASP}$ do not increase during the first part of the seizure because the epileptic activity is only present in 3 out of 21 EEG channels. These measures do only increase when the same epileptic frequency is present in a large part of the 21 channels; this happens when the seizure activity spreads out to the majority of the EEG channels. The same results were obtained for patient P5. These findings indicate that the measures can not be used for detection of partial seizures which do not evolve to secondarily generalized seizures.

C.4 Discussion and Conclusion

It was the aim of this study to investigate whether the HTLSstack method, which is often used in NMR spectroscopy, could detect the increased level of neuronal synchronization in the scalp EEG recordings of patients with (secondarily) generalized seizures. HTLSstack allowed modelling the dynamics of the different EEG signals. Based on the energy distribution of the common signal poles several measures were derived which allowed to make the distinction between three types of EEG recordings containing awake, sleep and epileptic seizure activity in all patients studied. The information can be useful for automatic scoring of EEG or an automated detection system for generalized and secondarily generalized seizures

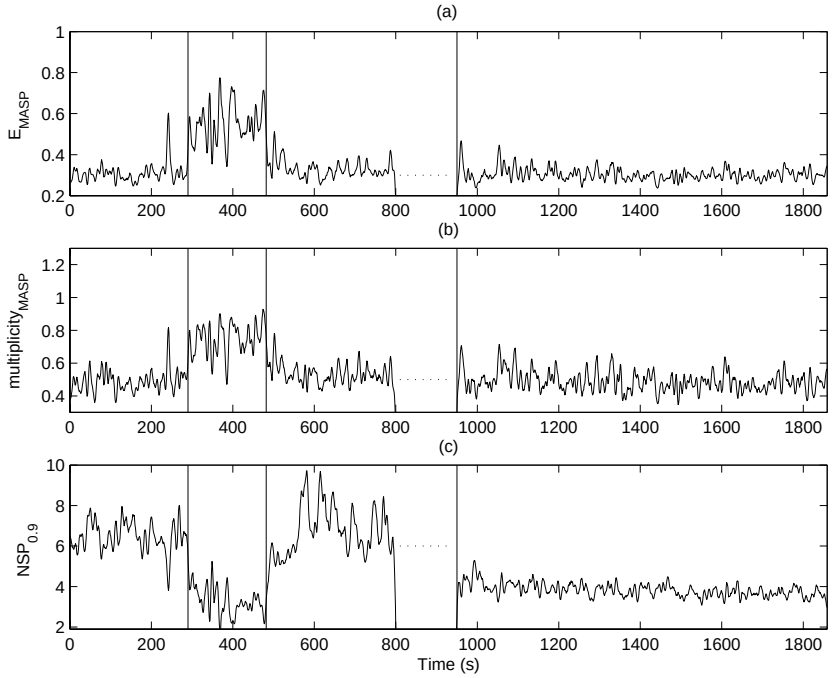

Figure C.5: *Time course is shown of (a) E_{MASP}, (b) multiplicity$_{MASP}$ and (c) $NSP_{0.9}$ for the analyzed EEG of patient P2. The generalized seizure is between the first two vertical lines. The horizontal dashed line represents 3 hour and 5 minutes of EEG. The sleep period starts from the third vertical line. A 3-point moving average filter has been applied for graphical display.*

and sleep EEG. More research has to be conducted to determine the sensitivity and specificity of the derived measures on long term EEG recordings of a larger patient group. It has to be mentioned that the method does not detect complex partial seizures for which the epileptic activity does not spread out to the majority of EEG channels.

As discussed in section 4.5 (Chapter 4) the EDS model becomes ineffective when there are transients with their origin not coinciding with the start of the selected time window. Taking this sensitivity of the model into account by an adaptive segmentation or by incorporating a time delay parameter in the complex damped exponential model function could improve the defined measures.

A comparison with existing multichannel methods [44] can be the subject of further research. Compared to the autoregressive method presented in [44], the proposed method provides additional information contained in the different parameters of the exponentially damped sinusoids.

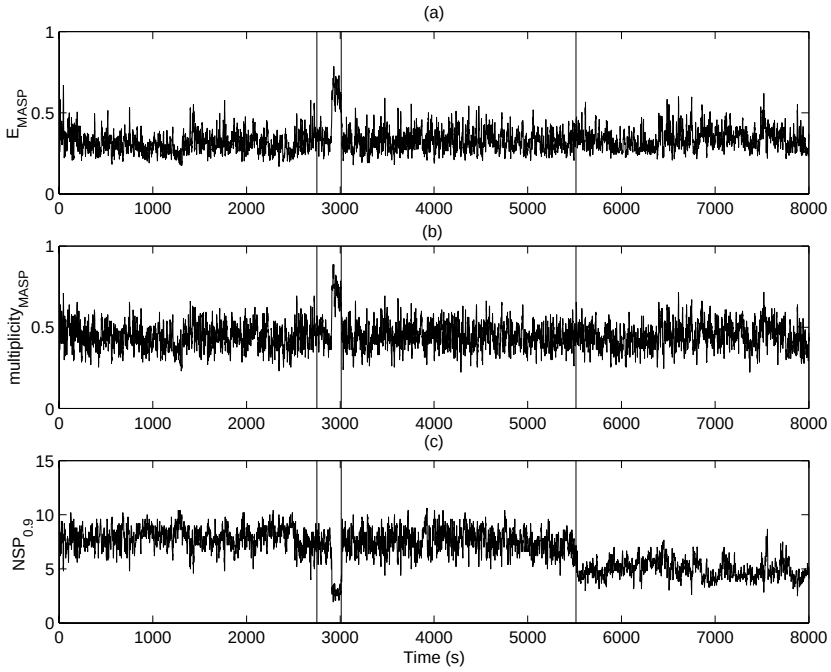

Figure C.6: *Time course is shown of (a) E_{MASP}, (b) multiplicity$_{MASP}$ and (c) $NSP_{0.9}$ for the analyzed EEG of patient P4. The seizure period is between the first two vertical lines. The sleep period starts from the third vertical line. A 3-point moving average filter has been applied for graphical display.*

Bibliography

[1] A.M Albano, J. Muench, C. Swartz, and et al. An automated drug delivery system for focal epilepsy. *Phys Rev Lett*, 78:3017–3027, 1988.

[2] R. Aschenbrenner-Scheibe, T. Maiwald, M. Winterhalter, H.U. Voss, J. Timmer, and A. Schulze-Bonhaege. How well can epileptic seizures be predicted? an evaluation of a nonlinear method. *Brain*, 126:1–11, 2003.

[3] M.F. Bear, B.W. Conners, and M.A. Paradiso. *Neuroscience: exploring the brain*. Lippincott Williams & Wilkins, Baltimore, second edition, 2001.

[4] A. Belouchrani, K. Abed-Meraim, J.-F. Cardoso, and E. Moulines. A blind source separation technique usingsecond order statictics. *IEEE Trans. Signal Processing*, 45:434–444, 1997.

[5] E. Ben-Menachem. Vagus-nerve stimulation for the treatment of epilepsy. *Lancet Neurology*, 1:477–782, 2002.

[6] G.K. Bergey and P.J. Franaszczuk. Epileptic seizures are characterized by changing signal complexity. *Clinical Neurophysiology*, 112:241–249, 2001.

[7] M. Borga and H. Knutsson. A canonical correlation approach to blind source separation. Technical Report LiU-IMT-EX-0062, Dept. of Biomedical Engineering, Linköping University, Sweden, 2001.

[8] R.J. Broughton. Polysomnography: principals and applications in sleep and arousal disorders. In E. Niedermeyer and F. Lopes da Silva, editors, *Electroencephalography: Basic Principels, Clinical Applications and Related Fields*, chapter 44. Urban and Swarzenberg, Baltimore, second edition, 1987.

[9] D. Buck, G.A. Baker, A. Jacoby, D.F. Smith, and D.W. Chadwick. Patients' experiences of injury as a reult of epilepsy. *Epilepsia*, 38:439–444, 1997.

[10] A.J. Cadzow. Signal enhancement-a composite property mapping algorithm. *IEEE Trans. Acoust., Speech, Signal Processing*, 36(1):49–62, 1988.

[11] J.-F. Cardoso. Higher-order contrast for independent component analysis. *Neural Comput*, 11:157–192, 1999.

[12] G.D. Cascino. Advances in neuroimaging: surgical localization. *Epilepsia*, 42:3–12, 2001.

[13] G.D. Cascino. Video-eeg monitoring in adults. *Epilepsia*, 43(Suppl.3):80–93, 2002.

[14] G.G. Celesia. Visual Evoked Potentials. In E. Niedermeyer and F. Lopes da Silva, editors, *Electroencephalography: Basic Principels, Clinical Applications and Related Fields*, chapter 47. Urban and Swarzenberg, Baltimore, second edition, 1987.

[15] G.G. Celesia and M.H. Grigg. Auditory Evoked Potentials. In E. Niedermeyer and F. Lopes da Silva, editors, *Electroencephalography: Basic Principels, Clinical Applications and Related Fields*, chapter 48. Urban and Swarzenberg, Baltimore, second edition, 1987.

[16] O.C. Cockerell, A.L. Johnson, J.W. Sander, Y.M. Hart, D.M. Goodbridge, and S.D Shorvon. Mortaility from epilepsy: results from a prospective population-based study. *Lancet*, 344:918–921, 1994.

[17] R.J. Croft and R.J. Barry. EOG correction: Which regression should we use? *Psychophysiology*, 37:123–125, 2000.

[18] B.N. Cuffin, D. Cohen, K. Ynokuchi, R. Maniewski, C. Purcell, G.R. Cosgrove, J. Ives, J. Kennedy, and D. Schomer. Tests of EEG localization accuracy using implanted sources in the human brain. *Ann. Neurol.*, 29:132–138, 1991.

[19] W. De Clercq, P. Lemmerling, S. Van Huffel, and W. Van Paesschen. Evaluation of methods for determining a pre-ictal state in scalp-EEG measurements. In *Conference Proceedings of 2nd European Medical and Biological Engineering Conference (EMBEC'02)*, pages 446–447, 2002.

[20] W. De Clercq, P. Lemmerling, S. Van Huffel, and W. Van Paesschen. Characterization of interictal and ictal scalp EEG signals with the Hilbert transform. In *Conference Proceedings of 25th annual international conference of the IEEE Engineering in Medicine and Biology Society (IEEE-EMBS)*, pages 2459–2462, 2003.

[21] W. De Clercq, P. Lemmerling, S. Van Huffel, and W. Van Paesschen. Correspondence : Anticipation of epileptic seizures from standard EEG recordings. *The Lancet*, 361:970–971, 2003.

[22] W. De Clercq, P. Lemmerling, B. Vanrumste, W. Van Paesschen, and S. Van Huffel. Analyzing multichannel scalp electroencephalograms of patients with epilepsy using exponential data modelling. In *Conference Proceedings of 2nd International Conference on Advances in Medical Signal and Information Processing (MEDSIP2004)*, pages 104–109, 2004.

[23] W. De Clercq, B. Vanrumste, J.-M. Papy, A. Vergult S. Van Huffel, and W. Van Paesschen. Removing artifacts and background in multichannel electroencephalograms by enhancing common activity. In *Proceedings of the 27th annual international conference of the IEEE Engineering in Medicine and Biology Society (IEEE-EMBS), invited paper submitted for publication*, 2005.

[24] W. De Clercq, B. Vanrumste, J.-M. Papy, W. Van Paesschen, and S. Van Huffel. Moddeling common dynamics in multichannel signals with application to artifact and background removal in EEG recordings. *accepted for publication in IEEE Trans. Biomed. Eng.*, 2005.

[25] W. De Clercq, A. Vergult, W. Van Paesschen, and S. Van Huffel. Muscle artifact removal from encephalograms, Patent Number GB0500180.5, January 2005.

[26] W. De Clercq, A. Vergult, B. Vanrumste, S. Van Huffel, J. Van Hees, A. Palmini, and W. Van Paesschen. A new muscle artifact removal technique to improve the interpretation of the ictal scalp electroencephalogram. In *Proceedings of the 27th annual international conference of the IEEE Engineering in Medicine and Biology Society (IEEE-EMBS), invited paper submitted for publication*, 2005.

[27] W. De Clercq, A. Vergult, B. Vanrumste, S. Van Huffel, M. Kokarakis, J. Van Hees, A. Palmini, and W. Van Paesschen. Improving the interpretation of the ictal scalp electroencephalogram: a new muscle artifact removal technique. *Epilepsia, submitted for publication*, 2005.

[28] W. De Clercq, A. Vergult, B. Vanrumste, W. Van Paesschen, and S. Van Huffel. Canonical correlation analysis applied to remove muscle artifacts from the electroencephalogram. *IEEE Trans. Biomed. Eng., submitted for publication*, 2005.

[29] J.C. de Munck, B.W. van Dijk, and H. Spereijse. Mathematical dipoles are adequate to describe realistic generators of human brain activity. *IEEE Trans. Biomed. Eng.*, 35:960–966, 1988.

[30] M.R. DeLucci, B. Garoutte, and R.B. Aird. The scalp as an electroencephalographic averager. *Electroencephalogr. Clin. Neurophysiol.*, 14:191–196, 1962.

[31] I. Dologlou and G. Carayannis. Physical interpretation of signal reconstruction from reduced rank matrices. *IEEE Trans. Signal Processing*, 39:1681–1682, 1991.

[32] C.W. Erwin, M.P. Rozear, R.A. Radtke, and A.C Erwin. Somatosensory Evoked Potentials. In E. Niedermeyer and F. Lopes da Silva, editors,

Electroencephalography: Basic Principels, Clinical Applications and Related Fields, chapter 48. Urban and Swarzenberg, Baltimore, second edition, 1987.

[33] B.J. Fisch. Artifacts. In *Fisch and Spelhmann's EEG Primer*, chapter 6, pages 107–121. Elsevier, third edition, 1999.

[34] B.J. Fisch. Classification of seizures. In *Fisch and Spelhmann's EEG Primer*, chapter 16, pages 245–259. Elsevier, third edition, 1999.

[35] B.J. Fisch. Digital and analog EEG instruments: parts and functions. In *Fisch and Spelhmann's EEG Primer*, chapter 3, pages 35–72. Elsevier, third edition, 1999.

[36] B.J. Fisch. Generalized epileptiform patterns. In *Fisch and Spelhmann's EEG Primer*, chapter 18, pages 285–305. Elsevier, third edition, 1999.

[37] B.J. Fisch. Localized epileptiform patterns. In *Fisch and Spelhmann's EEG Primer*, chapter 17, pages 261–283. Elsevier, third edition, 1999.

[38] B.J. Fisch. The normal EEG of wakefull resting adults of 20-60 years of age. In *Fisch and Spelhmann's EEG Primer*, chapter 11, pages 185–198. Elsevier, third edition, 1999.

[39] B.J. Fisch. The normal sleep EEG adults over 20 years. In *Fisch and Spelhmann's EEG Primer*, chapter 11, pages 185–198. Elsevier, third edition, 1999.

[40] B.J. Fisch. Recording electrodes. In *Fisch and Spelhmann's EEG Primer*, chapter 2, pages 19–34. Elsevier, third edition, 1999.

[41] B.J. Fisch. The source of the EEG. In *Fisch and Spelhmann's EEG Primer*, chapter 1, pages 3–17. Elsevier, third edition, 1999.

[42] B.J. Fisch. Spatial analysis of the eeg. In *Fisch and Spelhmann's EEG Primer*, chapter 4, pages 73–106. Elsevier, third edition, 1999.

[43] D. Fish. Anticipation of epileptic seizures from standaard electroencephslographic recordings. *The Lancet*, 357:160–161, 2001.

[44] P.J. Franaszczuk and G.K. Bergey. An autoregressive method for the measurement of synchronization of interictal and ictal channels. *Biological Cybernetics*, 81:513–521, 1998.

[45] M. Franceschi, F. Triulzi, L. Ferini-Strambi, et al. Focal cerebral lesions found by magnetic reasonance imaging in cryptogenic non-refractory temporal lobe epilepsy patients. *Epilepsia*, 30:540–546, 1989.

[46] O. Friman. *Adaptive analysis of functional MRI Data*. PhD thesis, Linköpings University, Linköping, 2003.

[47] O. Friman, M. Borga, P. Lundberg, and H. Knutsson. Exploratory fMRI analysis by autocorrelation maximization. *NeuroImage*, 16(2):454–464, 2002.

[48] O. Friman, J. Cedefamn, P. Lundberg, M. Borga, and H. Knutsson. Detection of neural activity in functional MRI using canonical correlation analysis. *Magnetic Resonance in Medicine*, 45:323–330, 2001.

[49] P. Gloor. Neuronal generators and the problem of localization in electroencephalography: applications of volume conductur theory to electroencephalography. *J. Clin. Neurophysiol.*, 2:327–354, 1985.

[50] B.J. Gluckman, H. Nguyen, S.L. Weinstein, and et al. Adaptive electric control of epileptic seizures. *J Neurosci*, 21:590–600, 2001.

[51] G.H. Golub and W. Kahan. Calculating the singular values and pseudoinverse of a matrix. *SIAM J. Numer. Anal.*, 2:205–224, 1965.

[52] G.H. Golub and C F. Van Loan. *Matrix computations*. John Hopkins University Press, Baltimore, third edition, 1996.

[53] I.I. Goncharova, D.J. McFarland, T.M. Vaughan, and J.R. Wolpaw. EMG contamination of EEG: Spectral and topographical characteristics. *Clinical Neurophysiology*, 114:1580–1593, 2003.

[54] P.C. Hansen and S.H. Jensen. Fir filter representations of reduced-rank noise reduction. *IEEE Trans. Signal Processing*, 46(6):1737–1741, 1998.

[55] K. Hermus, W. Verhelst, P. Lemmerling, P. Wambacq, and S. Van Huffel. Perceptual audio modeling with exponentially damped sinusoids. *Signal Processing*, 2004. accepted for publication.

[56] H. Hotelling. Relations between two sets of variates. *Biometrika*, 28:321–377, 1936.

[57] L.D. Iasemidis, J.C. Sackellares, H.P. Zaveri, and W.J. Williams. Phase space topography and the Lyapunov exponent of electrocorticograms in partial seizures. *Brain Topogr*, 2:187–201, 1990.

[58] L.D. Iasemidis, J.C. Sackellares, H.P. Zaveri, and W.J. Williams. *The evolution with time of the spatial distribution of th elargest Lyapunov exponent on the human epileptic cortex*, pages 49–82. Measuring Chaos in the Human Brain. World Scientific, Singapore, 1991.

[59] L.D. Iasemidis, D.S. Shiau, W. Chaovalitwongse, J.C. Sackellares, P.M. Pardalos, J.C. Principe, P.R. Carney, A. Prasad, B. Veeramani, and K. Tsakalis. Adaptive epileptic seizure prediction system. *IEEE Trans Biomed Eng*, 50:616–627, 2003.

[60] C.J. James and J. Gibson. Temporally constrained ICA: An applicaton to artifact rejection in electromagnetic brain signal analysis. *IEEE Trans. Biomed. Eng.*, 50(9).

[61] C.J. James and D. Lowe. Extracting multisource brain activity from a single electromagnetic channel. *Artif. Intell. Med.*, 28:89–104, 2003.

[62] K.K. Jerger, R.I. Netoff, J. T. Francis, T. Sauer, L. Pecora, S.L. Weinstein, and S.J. Schiff. Early seizure detection. *J Clin Neurophysiol*, 18:259–268, 2001.

[63] T.-P Jung, C. Humphries, T. Lee, S. Makeig, M.J. McKeown, V. Iragui, and T.J. Sejnowski. Extended ICA removes artifacts from electroencephalographic recordings. *Advances in Neural Information Processing Systems*, 10:894–900, 1998.

[64] T.-P. Jung, S. Makeig, C. Humphries, T.-W. Lee, M. J. McKeown, V. Iragui, and T.J. Sejnowski. Removing electroencephalographic artifacts by blind source seperation. *Psychophysiology*, 37:163–178, 2000.

[65] H. Kantz and T. Schreiber. *Nonlinear time series analysis.* Cambridge University Press, 1997.

[66] A. Katz, D.A. Marks, G. McCarthy, and S.S. Spencer. Does interictal spiking rate change prior to seizure? *Electroencephalogr Clin Neurophysiol*, 79:153–156, 1991.

[67] J.N. Knight. Signal fraction analysis and artifact removal in EEG. M. Sc. thesis, Colorado State University, 2003.

[68] K. Kobayashi, C.J. James, T. Nakahori, T. Akiyama, and J. Gotman. Isolation of epileptiform discharges from unaveraged EEG by independent component analysis. *Clin. Neurophysiol.*, 110:1755–1763, 1999.

[69] Z.J. Koles, J.C. Lind, and A.C.K. Soong. Spatio-temporal decompositon of the EEG: a general approach to the isolation and localization of sources. *Electroenceph. Clin. Neurophysiol.*, 95.

[70] J. Lachaux, E. Rodriguez, J. Martinerie, and J. Varela. Measuring phase synchrony in brain signals. *Human Brain Mapping*, 8:194–208, 1999.

[71] Y.-C. Lai, M.A.F. Harrison, M.G. Frei, and I. Osorio. Inability of lyapunov exponents to predict epileptic seizures. *Phys Rev Lett.*, 91:068102–1–4, 2003.

[72] Y.-C. Lai, M.A.F. Harrison, Y-C. Lai, M.G. Frei, and I. Osorio. Controlled test for predictive power of lyapunov exponent: Their inability to predict epileptic seizures. *Chaos*, 14:630–642, 2004.

[73] M. Le Van Quyen, J. Martinerie, M. Baulac, and F. Varela. Anticipating epileptic seizures in real time by a non-linear analysis of similarity between eeg recordings. *Neuroreport*, 10:2149–2155, 1999.

[74] M. Le Van Quyen, J. Martinerie, J. Navarro, P. Boon, M. D'Have, C. Adam, B. Renault, F. Varela, and M. Baulac. Anticipation of epileptic seizures from standard EEG recordings. *The Lancet*, 357:183–188, 2001.

[75] M. Le Van Quyen, J. Martinerie, V. Navarro, M. Baulac, and F. Varela. Characterizing neurodynamic changes before seizures. *Brain*, 125:640–655, 2002.

[76] M. Le Van Quyen, J. Martinerie, V. Navarro, M. Baulac, and J. Varela. Characterizing neurodynamic changes before seizures. *J. Clin. Neurophysiol.*, 18:191–208, 2001.

[77] M. Le Van Quyen, J. Soss, V. Navarro, R. Robertson, M. Chavez, M. Baulac, and J. Martinerie. Preictal state identification by synchronization changes in long-term intracranial eeg recordings. *Clin. Neurophysiol.*, 116:559–568, 2005.

[78] K. Lehnertz, R.G. Andrzejak, J. Arnold, T. Kreuz, F. Mormann, C. Rieke, G. Widman, and C. E. Elger. Nonlinear eeg analysis in epilepsy: Its possible use for interictal focus localization, seizure anticipation and prevention. *J Clin Neurophysiol*, 18:209–222, 2001.

[79] K. Lehnertz and C.E. Elger. Spatio-temporal dynamics of the primary epoleptogenic area in temporal lobe epilepsy characterized by neuronal complexity loss. *Electroencephalogr Clin Neurophysiol*, 95:108–117, 1995.

[80] K. Lehnertz and C.E. Elger. Can epileptic seizures be predicted? *Phys Rev Lett*, 80:5019–5022, 1998.

[81] P. Lemmerling, N. Mastronardi, and S. Van Huffel. Efficient implementation of a structured total least squares based speech compression method. *Linear Algebra and its Applications*, pages 295–315, 2003.

[82] P. Lemmerling, L. Vanhamme, R. Romano, and S. Van Huffel. A subspace time-domain algorithm for automated NMR normalization. *J. Magn. Res.*, 157(2), 2002.

[83] B. Litt and J. Echauz. Prediction of epileptic seizures. *Lancet Neurol*, 1:22–30, 2002.

[84] B. Litt and K. Lehnertz. Seizure prediction and the preseizure period. *Curr Opin Neurol*, 15:209–222, 2002.

[85] F.H. Lopes da Silva. Event-Related Potentials: methodology and quantification. In E. Niedermeyer and F. Lopes da Silva, editors, *Electroencephalography: Basic Principels, Clinical Applications and Related Fields*, chapter 46. Urban and Swarzenberg, Baltimore, second edition, 1987.

[86] W. Lu and J.C. Rajapakse. ICA with reference. In *Proceedings 3rd In. Conf. Independent Component Analysis and Blind Signal Separation:ICA 2003*, pages 120–125, 2003.

[87] T. Maiwald, M. Winterhalter, R. Aschenbrenner-Scheibe, H.U. Voss, A. Schulze-Bonhaege, and J. Timmer. Comparison of three nonlinear seizure prediction methods by means of the seizure prediction charcteristic. *Physica D: Nonlinear Phenomena*, 194:357–368, 2004.

[88] J. Malmivuo and R. Plonsey. *Bioelectromagnetism: Principles and Applications of Bioelectric and Biomagnetic Fields*. Oxford University Press, New York, 1995.

[89] J. Martinerie, C. Adam, M. Le Van Quyen, M. Baulac, S. Clemencéau, B. Renault, and F. Varela. Epileptic seizures can be anticipated by nonlinear analysis. *Nat Med*, 4:1173–1176, 1998.

[90] P.E. McSharry, L.A. Smith, and L. Tarassenko. Comparison of predicability of epilpeptic seizures by a linear and a nonlinear method. *IEEE Trans Biomed Eng*, 50:628–633, 2003.

[91] P.E. McSharry, L.A. Smith, and L. Tarassenko. Prediction of epileptic seizures: are nonlinear methods relevant? *Nat Med*, 9:241–242, 2003.

[92] F. Mormann, T. Kreuz, R.G. Andrzejak, P. David, K. Lehnertz, and C.E. Elger. Epileptic seizures are preceded by a decrease in synchronization. *Epilepsy Research*, 53:173–185, 2003.

[93] F. Mormann, K. Lehnertz, P. David, and C.E. Elger. Mean phase coherence as a measure for pase synchronization and its application to the eeg of epilepsy patients. *Physica D*, 144:358–369, 2000.

[94] G. Morren. *Advanced signal processing applied ro in-vivo spectroscopy and heart rate variability*. PhD thesis, Katholieke Universiteit Leuven, Leuven, May 2004.

[95] G. Morren, P. Lemmerling, S. Van Huffel, G. Naulaers, H. Devlieger, and P. Casaer. Detection of autoregulation in the brain of premature infants using a novel subspace-based technique. In *Proceedings 23rd Annual International Conference IEEE Engineering in Medicine and Biology Society*, pages 2064– 2067, 2001.

[96] G. Morren, S. Van Huffel, I. Helon, G. Naulaers, H. Daniels, H. Devlieger, and P. Caesar. Effects of non-nutritive sucking on heart rate, respiration and oxygenation: a model-based signal processing approach. *Comp. Biochem. Physiol. A*, 132:97–106, 2002.

[97] S. Mozaffar and D.W. Petr. Artifact Extraction from EEG Data Using Independent Component Analysis. Technical Report ITTC-FY2003-TR-03050-02, Information Telecommunication and Technology Center, University of Kansas, Lawrence, KS, Dec. 2002.

[98] J. Murray. Coping with the uncertainty of uncontrolled epilepsy. *Seizure*, 2:167–178, 1993.

[99] H. Nam, T.-G. Yim, S.K. Han, J.-B. Oh, and S.K. Lee. Independent component analysis of ictal EEG in medial temporal lobe epilepsy. *Epilepsia*, 43(2):160–164, 2002.

[100] V. Navarro, J.Martinerie, M. Le Van Quyen, S. Clemencéau, C. Adam, M. Baulac, and F. Varela. Seizure anticipation in human neocortical partial epilepsy. *Brain*, 125:640–655, 2002.

[101] E. Niedermeyer. Abnormal EEG patterns (epileptic and paroxysmall). In E. Niedermeyer and F. Lopes da Silva, editors, *Electroencephalography: Basic Principels, Clinical Applications and Related Fields*, chapter 14. Urban and Swarzenberg, Baltimore, second edition, 1987.

[102] E. Niedermeyer. Depth electroencepalography. In E. Niedermeyer and F. Lopes da Silva, editors, *Electroencephalography: Basic Principels, Clinical Applications and Related Fields*, chapter 37. Urban and Swarzenberg, Baltimore, second edition, 1987.

[103] E. Niedermeyer. Epileptic seizure disorder. In E. Niedermeyer and F. Lopes da Silva, editors, *Electroencephalography: Basic Principels, Clinical Applications and Related Fields*, chapter 27. Urban and Swarzenberg, Baltimore, second edition, 1987.

[104] E. Niedermeyer. Sleep and EEG. In E. Niedermeyer and F. Lopes da Silva, editors, *Electroencephalography: Basic Principels, Clinical Applications and Related Fields*, chapter 10. Urban and Swarzenberg, Baltimore, second edition, 1987.

[105] E. Niedermeyer and F. Lopes da Silva. In E. Niedermeyer and F. Lopes da Silva, editors, *Electroencephalography: Basic Principels, Clinical Applications and Related Fields*. Urban and Swarzenberg, Baltimore, second edition, 1987.

[106] J. Nieuwenhuijse, R. Heusdens, and E.F. Deprettere. Robust exponential modeling of audio signals. In *Proc. of International Conference on Acoustic,*

Speech and Signal Processing (ICASSP 98), volume 6, pages 3581–3584, 1998.

[107] M.R. Nuwer, G.Comi, R. Emmerson, et al. IFCN standards for digital recording of clinical EEG. *Electroencephalogr Clin Neurophysiol*, 106:259–261, 1998.

[108] T.F. Oostendorp, J. Delbeke, and D.F. Stegeman. The conductivity of the human skull: Results of in vivo measurements. *IEEE Trans. Biomed. Eng.*, 47(11):1487–1492, 2000.

[109] I. Osorio, M. G. Frei, J. Giftakis, T. Peters, J. Ingram, and et al. Performance reassessment of a real time seizure-detection algorithm on long ECoG series. *Epilepsia*, 43:1522–1535, 2002.

[110] I. Osorio, M.G. Frei, and S.B. Wilkinson. Real-time automated detection and quantitative analysis of seizures and short-term prediction of clinical onset. *Epilepsia*, 39:615–627, 1998.

[111] I. Osorio, M.A.F. Harrison, Y-C. Lai, and M.G. Frei. Observations on the application of the correlation dimension and correlation integral to the prediction of seizures. *J Clin Neurophysiol*, 18:269–274, 2001.

[112] J.-M. Papy, L. De Lathauwer, and S. Van Huffel. A technique for common pole estimation in the multi-channel case. *accepted for publiction in Signal Processing*, 2005.

[113] R. Plonsey and D.B. Heppner. Considerations of quasistationarity in electrophysiological systems. *Bulletin of Mathematical Biophysics*, 29(4):657–664, 1967.

[114] J.G. Proakis and D.G. Manolakis. *Digital Signal Processing*. Prentice Hall, Upper Saddle River, New Jersey, third edition, 1996.

[115] H. Qu and J. Gotman. A seizure warning system for long term epilepsy monitoring. *Neurology*, 45:2250–2254, 1995.

[116] M.W. Risinger. *Eelctroencephalographic Strategies for determining the epileptogenic zone*, pages 337–347. Epilepsy Surgery. Raven Press, New York, 1991.

[117] Z. Rogowski, I. Gath, and E. Bental. On the prediction of epileptic seizures. *Biol Cybern*, 42:9–15, 1981.

[118] F. Rosenow and H. Luders. Presurgical evaluation of epilepsy. *Brain*, 124:1683–1700, 2001.

[119] M.E. Saab and J. Gotman. A system to detect the onset of epileptic seizures in scalp EEG. *Clinical Neurophysiology*, 116:427–442, 2005.

[120] Y. Salu, L.G. Cohen, D. Rose, S. Sato, C. Kufta, and M. Hallet. An improved method for localizing electric brain dipoles. *IEEE Trans. Biomed. Eng.*, 37(7):699–708, 1990.

[121] S.C. Schachter and C.B. Saper. Vagus nerve stimulation. *Epilepsia*, 39:677–687, 1998.

[122] S.J. Schiff. Forecasting brain storms. *Nat Med*, 4:1117–1118, 1998.

[123] D. Smith and D. Chadwick. The management of epilepsy. *J. Neurosurg. Psychiatry*, 70:ii15–ii17, 2001.

[124] E.L. So. Integration of EEG, MRI and SPECT in localizing the seizure focus for epilepsy surgery. *Epilepsia*, 41:S48–S54, 2000.

[125] S.S. Spencer, P.D. Williamson, S.L. Bridgers, R.H. Mattson, D.V. Cicchetti, and D.D Spencer. Reliability and accuracy of localization by scalp ictal EEG. *Neurology*, 30:1567–1575, 1985.

[126] M.M. Stecker. The effects of automatic artifact rejection on evoked potential recordings. *Computers in Biology and Medicine*, 32:247–259, 2002.

[127] A.G. Stein, H.G. Eder, D.E. Blum, A. Drachev, and R.S. Fischer. An automated drug delivery system for focal epilepsy. *Epilepsy Res*, 39:103–114, 2000.

[128] F. Takens. *Detecting strange attractors in turbulence*, pages 366–381. Lecture notes in mathematics. Springer-Verlag, Berlin, Germany, 1981.

[129] D.C. Taylor, D. McMackin, H. Staunton, N. Delanty, and J. Phillips. Patients' aims for epilepsy surgery: desires beyond seizure freedom. *Epilepsia*, 42:629–633, 2001.

[130] E. Urrestarazu, J. Iriarte, M. Alegre, M. Valencia, C. Viteri, and J. Artieda. Independent component analysis removing artifacts in ictal recordings. *Epilepsia*, 45(9):1071–1078, 2004.

[131] S. Van Huffel, H. Chen, C.P. Decanniere, and P. Van Hecke. Algorithm for time-domain NMR data fitting based on total least squares. *J. Magn. Res. A*, 110:228–237, 1994.

[132] S. Vandenplas, J.M. Papy, M. Wevers, and S. Van Huffel. Acoustic emission monitoring using a multimode optical fibre sensor. *Insight*, 46:203–209, 2004.

[133] L. Vanhamme. Advanced time-domain methods for Nuclear Magnetic Resonance spectroscopy data analysis. *pH.D.-Thesis, Dept. of electrical engineering, Katholieke Universiteit Leuven, Leuven, Belgium*, 1999.

[134] L. Vanhamme and S. Van Huffel. Multichannel quantification of biomedical Magnetic Resonance Spectroscopic signals. *Advanced Signal Processing Algorithms, Architectures and implementations VIII, (Eds) Luk FT, Proceedings of SPIE*, 3461:237–248, 1998.

[135] A. Vergult, W. De Clercq, B. Vanrumste, S. Van Huffel, and W. Van Paesschen. A blind source separation technique to remove muscle artifacts in the electroencephalogram without affecting beta activity. In *Conference Proceedings of 3th European Medical and Biological Engineering Conference (EMBEC'05), submitted for publication*, 2005.

[136] G.L. Wallstrom, R.E. Kass, A. Miller, J.F. Cohn, and N.A. Fox. Automatic correction of ocular artifacts in the EEG: A comparison of regression-based and component-based methods. *International Journal of Psychophysiology*, 53:105–119, 2004.

[137] G.A. Worell, E.L. So, J. Kazemi, T.J. O'Brien, R.K. Mosewich, G.D. Cascino, F.B. Meyer, and W.R. Marsh. Focal ictal beta discharge on scalp EEG predicts excellent outcome of frontal lobe epilepsy surgery. *Epilepsia*, 43(3):277–282, 2002.

List of publications

Publications in International Journals

- **W. De Clercq**, P. Lemmerling, S. Van Huffel and W. Van Paesschen , "Anticipation of epileptic seizures from standard EEG recordings", *The Lancet*, Vol. 361, p. 970-971, 2003.

- **W. De Clercq**, B. Vanrumste, J.-M. Papy, W. Van Paesschen and S. Van Huffel, "Modelling common dynamics in multichannel signals with application to artifact and background removal in EEG recordings", *IEEE Trans. Biomed. Eng.*, accepted for publication.

- **W. De Clercq**, A. Vergult, B. Vanrumste, W. Van Paesschen and S. Van Huffel, "Canonical correlation analysis applied to remove muscle artifacts from the electroencephalogram", *IEEE Trans. Biomed. Eng.*, submitted for publication.

- G. Neyens, D.L. Balabanski, D. Borremans, N. Coulier, R. Coussement, **W. De Clercq**, G. Georgiev, S. Teughels, K. Vyvey, "Nuclear magnetic and quadrupole moments of exotic isomeric states", *Acta Physica Polonica B*, Vol. 32(3), p.1061-1070, 2001

- D.L. Balabanski, K. Vyvey, G. Neyens, D. Almehed, P. Blaha , D. Borremans, S. Chmel, N. Coulier, R. Coussement, **W. De Clercq**, S. Frauendorf, G. Georgiev, H. Hubel, A. Lepine-Szily, M. Mineva , N. Nenoff, S. Pancholi, D. Rossbach, R. Schwengner, S. Teughels, P.M. Walke, "Quadrupole moments of high-spin isomers: test of the tilted-axis cranking model", *Acta Physica Polonica B*, Vol. 32(9), p. 2655-2660, 2001.

Patent Pending

- **W. De Clercq**, A. Vergult, W. Van Paesschen, S. Van Huffel, "Muscle artifact removal form encephalograms", Patent number GB 0500180.5, Filed 7 Jan. 2005.

Invited Publications on International Conferences

- **W. De Clercq**, A. Vergult, B. Vanrumste, J. Van Hees, A. Palmini and W. Van Paesschen, S. Van Huffel, "A new muscle artifact removal technique to improve the interpretation of the ictal scalp electroencephalogram", *Proceedings of the 27th annual international conference of the IEEE Engineering in Medicine and Biology Society (IEEE-EMBS)*, Shanghai, China, Sep. 2005, invited paper submitted for publication.

- **W. De Clercq**, B. Vanrumste, J.-M. Papy, A. Vergult W. Van Paesschen and S. Van Huffel, "Removing artifacts and background activity in multichannel electroencephalograms by enhancing common activity", *Proceedings of the 27th annual international conference of the IEEE Engineering in Medicine and Biology Society (IEEE-EMBS)*, Shanghai, China, Sep. 2005, invited paper submitted for publication.

Publications on International Conferences

- **W. De Clercq**, P. Lemmerling, S. Van Huffel and W. Van Paesschen, "Evaluation of methods for determining a pre-ictal state in scalp-EEG measurements", *Conference Proceedings of 2nd European Medical and Biological Engineering Conference (EMBEC'02)*, Vienna, Austria, Dec. 2002, p. 446-447.

- **W. De Clercq**, P. Lemmerling, W. Van Paesschen and S. Van Huffel, "Characterization of interictal and ictal scalp EEG signals with the Hilbert transform", *Proceedings of the 25th annual international conference of the IEEE Engineering in Medicine and Biology Society (IEEE-EMBS)*, Cancun, Mexico, Sep. 2003, p. 2459-2462.

- **W. De Clercq**, P. Lemmerling, B. Vanrumste, W. Van Paesschen and S. Van Huffel, "Analyzing multichannel scalp electroencephalograms of patients with epilepsy using exponential data modelling", *Proceedings of the 2nd International Conference on Advances in Medical Signal and Information Processing (MEDSIP2004)*, Sliema, Malta, Sep. 2004, p. 104-109.

- **W. De Clercq**, A. Vergult, B. Vanrumste, S. Van Huffel, M. Kokarakis, J. Van Hees, A. Palmini and W. Van Paesschen, "Improving the interpretation of the ictal scalp electroencephalogram: a new muscle artifact removal technique", *submitted for presentation at the 26th International Epilepsy Congress*, Paris, France, Aug. 2005.

- A. Vergult, **W. De Clercq**, B. Vanrumste, W. Van Paesschen and S. Van Huffel, "A blind source separation technique to remove muscle artifacts in the electroencephalogram without affecting beta activity", *Conference Proceedings of 3rd European Medical and Biological Engineering Conference*

(EMBEC'05), Prague, Czech Republic, Nov. 2005, submitted for publication.

- E. Huupponen, G. Herrero, K. Egiazarian, A. Saastamoinen, A. Värri, B. Vanrumste, A. Vergult, **W. De Clercq**, S. Van Huffel, W. Van Paesschen, "Bioprofile of sleep", *Conference Proceedings of the Second International Conference on Computational Intelligence in Medicine and Healthcare, The BIOPATTERN Conference (CIMED 2005)*, Lisbon, Portugal, Jun. 2005, submitted for publication.

- G. Gomez Herrero, E. Huupponen, A. Värri, K. Egiazarian, B. Vanrumste, A. Vergult, **W. De Clercq**, S. Van Huffel, W. Van Paesschen, "Independent component analysis of single trial evoked brain responses : is it reliable ?", *Conference Proceedings of the Second International Conference on Computational Intelligence in Medicine and Healthcare, The BIOPATTERN Conference (CIMED 2005)*, Lisbon, Portugal, Jun. 2005, submitted for publication.

- E. Huupponen, G. Herrero, A. Saastamoinen, K. Egiazarian, A. Värri, B. Vanrumste, A. Vergult, **W. De Clercq**, S. Van Huffel, W. Van Paesschen, J. Hasan, S.L. Himanen, "Dictionaries of waveforms for frequency analysis of simulated spindles", *Conference Proceedings of the Second International Conference on Computational Intelligence in Medicine and Healthcare, The BIOPATTERN Conference (CIMED 2005)*, Lisbon, Portugal, Jun. 2005, submitted for publication.

Curriculum Vitae

Wim De Clercq was born in Leuven on May 26, 1978. He received the M.Sc. degree in Physics from the Katholieke Universiteit Leuven in 2000. His main topic was Nuclear Physics and his Master's thesis under supervision of prof. G. Neyens was devoted to *'Experimentele verificatie van magnetische rotatie in neutron-arme Pb-kernen'*. In 2001 he started working as a researcher at the Electrical Engineering Department ESAT in the Lab of Signals, Identification, System Theory and Automation (SCD/SISTA) at the Katholieke Universiteit Leuven. During this period, he was supported by a grant of the Fonds voor Wetenschappelijk Onderzoek Vlaanderen (FWO).